COURSE 4

MAGNETOHYDRODYNAMIC TURBULENCE

Annick Pouquet

Observatoire de la Côte d'Azur,
06003 Nice, France
and
High Altitude Observatory/MMM,
National Center for Atmospheric Research,
Boulder, CO 80307, USA

J.-P. Zahn and J. Zinn-Justin, eds.
Les Houches, Session XLVII, 1987
Dynamique des fluides astrophysiques
Astrophysical fluid dynamics

Contents

1. Magnetohydrodynamic turbulence

1.1. Fundamental equations

1.1.1. Introduction

One of the earliest manifestations of the magnetic field of the Earth put to use by man is the compass, which was brought to Europe from China in the Middle Ages; the cause for which the needle was indicating to a good precision North under all circumstances was not known. The great phase of discovery of our planet by land and, above all, sea travel, together with the mapping of Earth, allowed the scholars of the seventeenth century to draw a map of the field and to realize that it behaves as a lodestone with a simple dipole structure. On the other hand, the field of the Earth is clearly weak, since no pull is felt when holding a small magnet in the hand; hence, unlike gravity, magnetism, which occurs only between special materials, has a reputation of mystery. Incidentally, the explanation of the Earth's magnetic field, $\boldsymbol{B}$, as that of a lodestone had to be dropped once it was realized that the core of the Earth is liquid and that at the temperature present in it, the magnetization is lost. However, in the source of the difficulty lies also the answer: it are the very motions in the core that are the source of the field.

So, the magnetic field of the Earth is, to first approximation, a dipole. No indication of a source nor of a sink, allows to write that:

$$\nabla \cdot \boldsymbol{B} = 0. \tag{1.1}$$

This law stands up to the present time: there is no conclusive observational evidence of magnetic monopoles; on the other hand, the equivalent equation for the electric field, $\boldsymbol{E}$, reads:

$$\nabla \cdot \boldsymbol{E} = \mathcal{V}/\epsilon. \tag{1.2}$$

The rationalized mksa system of units will be used here; for a discussion of the Gaussian system versus this one, see appendix 1 of Priest (1982). We will assume the usual constitutive laws $\boldsymbol{B} = \mu \boldsymbol{H}$ and $\boldsymbol{D} = \epsilon \boldsymbol{E}$, where μ and ϵ are, respectively, the magnetic permeability and the dielectric constant; they will be taken equal to their value in free space, i.e. $\mu_0 = 4\pi \times 10^{-7}$ H m^{-1} and $\epsilon_0 = 8.85 \times 10^{-12}$

$\mathrm{F\,m^{-1}}$, with $\mu_0\epsilon_0 c^2 = 1$, where c is the speed of light. $\boldsymbol{E}$ is the electric field, $\boldsymbol{D}$ the electric displacement, and $\mathcal{V}$ is the charge density, respectively in $\mathrm{V\,m^{-1}}$, $\mathrm{C\,m^{-2}}$, and $\mathrm{C\,m^{-3}}$; $\boldsymbol{H}$ is the magnetic field, in $\mathrm{A\,m^{-1}}$, and $\boldsymbol{B}$ the magnetic induction, in T (with $1\ \mathrm{T} = 10^4$ G).

Now, these two equations induce many comments. Because the electric field is made up by positive and negative particles, when taking the spatial average over a large enough region, it will cancel out, whereas no such cancellation can occur for the magnetic field. This is the fundamental reason why in large, and hence in many astrophysical, flows, magnetic fields are observed and furthermore are of dynamical importance. Now, why such a discrepancy? This is unexpected when one recalls that the $\boldsymbol{E}$ and $\boldsymbol{B}$ fields in fact, through their respective potentials, $\boldsymbol{A}$:

$$\boldsymbol{B} = \boldsymbol{\nabla} \times \boldsymbol{A}, \tag{1.3}$$

(to within a gauge transformation) and Φ:

$$\boldsymbol{E} = \boldsymbol{\nabla}\Phi, \tag{1.4}$$

are part of the same quadrivector; through a Lorentz transformation, the electric field may be zero in one frame of reference and not in another one; the transformation reads:

$$\boldsymbol{E}' = (\boldsymbol{E} + \boldsymbol{v} \times \boldsymbol{B})\gamma_v + (1 - \gamma_v)\frac{(\boldsymbol{v} \cdot \boldsymbol{E})}{v^2}\boldsymbol{v}, \tag{1.5}$$

$$\boldsymbol{B}' = (\boldsymbol{B} - \mu\epsilon\boldsymbol{v} \times \boldsymbol{E})\gamma_v + (1 - \gamma_v)\frac{(\boldsymbol{v} \cdot \boldsymbol{B})}{v^2}\boldsymbol{v}, \tag{1.6}$$

where $\boldsymbol{E}'$ and $\boldsymbol{B}'$ are measured in the frame of reference moving with the fluid velocity $\boldsymbol{v}$ (Landau and Lifshitz 1959), and where $\gamma_v = 1 - v^2/c^2$.

$\boldsymbol{E}'$ is called the effective electric field and $\boldsymbol{v} \times \boldsymbol{B}$ the induced electric field (induced by the motion of the plasma). The electric current density, $\boldsymbol{j}'$, is related to the electric field, $\boldsymbol{E}'$, in the frame moving with the fluid by a linear constitutive equation, Ohm's law (in the non-relativistic case):

$$\boldsymbol{j}' = \sigma\boldsymbol{E}', \tag{1.7}$$

where σ is the electrical conductivity, measured in $\Omega^{-1}\,\mathrm{m}^{-1}$. By analogy with the viscosity of a non-conducting fluid, it is convenient to introduce the magnetic diffusivity, η, measured in $\mathrm{m^2\,s^{-1}}$:

$$\eta = 1/\sigma\mu. \tag{1.8}$$

For a collision-dominated plasma, we have $\eta \sim 10^9 T^{-3/2}$ m^2 s^{-1} (Spitzer 1962), where T is the temperature. In the laboratory frame, Ohm's law thus reads:

$$\boldsymbol{j} = \sigma'(\boldsymbol{E} + \boldsymbol{v} \times \boldsymbol{B}). \tag{1.9}$$

Often, the electrical conductivity is large, although the current remains finite, so that eq. (1.9) reduces to $\boldsymbol{E} \simeq -\boldsymbol{v} \times \boldsymbol{B}$ and thus $\boldsymbol{B}' = \boldsymbol{B}$ to $\mathcal{O}(v^2/c^2)$ terms, consistent with Maxwell's equation, eq. (1.18) introduced below. Ohm's law describes the way by which the magnetic field is dissipated, via the current. A generalized Ohm's law can be introduced taking into account in particular the multi-fluid aspect (electrons, protons, neutrals) of the plasma, e.g. through the Hall conductivity associated with the drifting of charged particles across the magnetic field. Particularly worth mentioning is the phenomenon of ambipolar diffusion; it arises because the magnetic field lines are attached to the charged particles in the gas, which collide with the neutrals; this effect dominates that of Ohmic diffusion at low densities, such as those encountered in interstellar molecular clouds ($\sim 10^{-3}$ particles/m^3). For a discussion of the validity of Ohm's law in astrophysical plasmas, see section 4.6 in Parker (1979).

1.1.2. Coupling to the dynamics

It is a remarkable feature of Maxwell's equations, which we are about to write, that they are compatible with special relativity, which appeared much later historically (they can in fact be written in the general relativity framework). This may be related to the fact that in electromagnetism particle velocities may be close to the velocity of light, whereas in daily life mechanical velocities are much smaller. The coupling to the fluid velocity appears in the transformation (1.5) above; hence, we can now write the hydrodynamical equations for a compressible fluid, in which $\boldsymbol{\mathcal{F}}_i$ are the various body forces per unit mass that can come into play; Newton's law of motion (non-relativistic) for a continuum medium reads:

$$\rho \frac{\mathrm{D}\boldsymbol{v}}{\mathrm{D}t} = \rho \left(\frac{\partial \boldsymbol{v}}{\partial t} + \boldsymbol{v} \cdot \boldsymbol{\nabla} \boldsymbol{v} \right) = \rho \boldsymbol{\mathcal{F}}_i - \boldsymbol{\nabla} p + \frac{1}{3} \mu' \operatorname{grad} \operatorname{div} \boldsymbol{v} + \mu' \boldsymbol{\nabla}^2 \boldsymbol{v}, \tag{1.10}$$

where ρ is the density, p the pressure, $\mu' = \rho\nu$ the coefficient of viscosity, and ν the kinematic viscosity. The equation for the conservation of mass is:

$$\frac{\partial \rho}{\partial t} + \operatorname{div}(\rho \boldsymbol{v}) = 0. \tag{1.11}$$

The equation of motion is written in a frame that is not rotating (otherwise, one would add the Coriolis force, $\boldsymbol{\mathcal{F}}_c = 2\boldsymbol{\Omega} \times \boldsymbol{v}$, where $\boldsymbol{\Omega}$ is the instantaneous angular

velocity relative to an inertial frame, and Ω is assumed constant). The equation of state will be that for a perfect gas:

$$p = R'T/\rho, \tag{1.12}$$

where T is the temperature and R' the gas constant. The energy equation can take many forms. For adiabatic changes we have:

$$p/\rho^{\gamma} = \text{constant}, \tag{1.13}$$

where γ is the ratio of the specific heats at constant pressure and volume, respectively; it will suffice for our purpose. Otherwise, the energy equation should include (see Priest (1982), section 2.4) the heat loss from Ohmic dissipation, thermal conduction, and radiation, and also the heat gain from nuclear reactions.

Two body forces of importance for astrophysical flows are the gravitational force, giving rise to convection, and the force $\mathcal{F}_m$ exerted by an electromagnetic field on a solid conductor:

$$\mathcal{F}_m = \sigma E + j \times B. \tag{1.14}$$

Let us go back to the problem of the absence of magnetic monopoles. It is surprising on the basis of the similarity between the E and B fields; and in fact, in the process of unifying the forces of physics (a topic most certainly beyond the scope of these lectures), the need appears for the existence of monopoles at an early time in the universe. They have recently been sought for, in particular at the suggestion of Parker, who made an estimation of their presence in the galaxy; a discussion of this point can be found in his book (Parker 1979), but for the moment they have not been identified.

We will now write the remaining Maxwell's equations; they involve the curl of the E and B field and read:

$$\text{curl } H = j + \frac{\partial D}{\partial t}, \tag{1.15}$$

$$\text{curl } D = -\frac{1}{c^2}\frac{\partial H}{\partial t}, \tag{1.16}$$

or, equivalently:

$$\text{curl } B = \mu j + \frac{1}{c^2}\frac{\partial E}{\partial t}, \tag{1.17}$$

$$\text{curl } E = -\frac{\partial B}{\partial t}. \tag{1.18}$$

They show that from time variation of the magnetic field an electrical field arises, and inversely a current together with a time-varying electrical field give rise to a magnetic field. We will now see that, in the non-relativistic case, the former effects dominate.

1.2. The MHD approximation

1.2.1. The non-relativistic limit

In a conducting fluid, typical velocities range from 1 m s^{-1} in the laboratory (at best) to 1 km s^{-1}, e.g., in the solar photosphere. Hence, $v/c \ll 1$, and the above set of equations can be simplified further using this fact in a consistent way, yielding the MHD approximation. It was written soon after the second world war, when extensive studies of the terrestrial and solar environment were undertaken. Such an assumption naturally excludes relativistic, magnetized flows, since they occur, e.g., in some radio jets and in the magnetosphere of pulsars.

Let us evaluate the relative strength in eq. (1.17) of the displacement current to $\boldsymbol{B}$:

$$\frac{1}{c^2}\frac{\partial \boldsymbol{E}}{\partial t} \Big/ \operatorname{curl} \boldsymbol{B} \sim \frac{1}{c^2}\frac{\boldsymbol{E}}{t} \cdot \frac{l}{\boldsymbol{B}} \sim \frac{v^2}{c^2},$$

where $\boldsymbol{E} \sim \boldsymbol{v}\boldsymbol{B}$ has been used; therefore we can neglect the displacement current and write Ampère's law:

$$\operatorname{curl} \boldsymbol{B} = \mu \boldsymbol{j}. \tag{1.19}$$

Combining this with Ohm's law (eq. (1.9)) and eq. (1.18), we can eliminate the electric field and obtain:

$$\frac{\partial \boldsymbol{B}}{\partial t} = \operatorname{curl}(\boldsymbol{v} \times \boldsymbol{B}) + \eta \nabla^2 \boldsymbol{B}. \tag{1.20}$$

Note that, by dropping from Maxwell's equations terms of order v^2/c^2 and smaller, we filter out the familiar electromagnetic waves, so we can concentrate on fluid-type phenomena. As noted previously, by changing the frame of reference we have, again up to terms $\mathcal{O}(v^2/c^2)$:

$$\boldsymbol{B}' = \boldsymbol{B}, \tag{1.21}$$

and therefore, because of eq. (1.19):

$$\boldsymbol{j}' = \boldsymbol{j}. \tag{1.22}$$

In this approximation, the magnetic field is independent of the frame of reference in which it is measured, and the electric field is determined using Ohm's law once the velocity and the magnetic field are known:

$$\boldsymbol{E} = -\boldsymbol{v} \times \boldsymbol{B} + \eta \,\mathrm{curl}\, \boldsymbol{B}. \tag{1.23}$$

1.2.2. The parameters

The induction equation (1.20) is linear in the magnetic field; its right-hand side contains a term of stretching of magnetic field lines by velocity gradients, with characteristic time $\tau_{\mathrm{st}} \sim l_0/V_0$, and a term of Joule dissipation, which will become preponderant on small scales; the Ohmic diffusion time is $\tau_{\mathrm{J}} \sim l_0^2/\eta$; both times are computed at scale l_0, with velocity V_0. The ratio of these two times, which measures the relative strength of the related terms, defines the magnetic Reynolds number, R^{M} :

$$R^{\mathrm{M}} = \frac{\tau_{\mathrm{J}}}{\tau_{\mathrm{st}}} = \frac{V_0 l_0}{\eta}. \tag{1.24}$$

In the laboratory, typical magnetic Reynolds numbers are small: Roberts (1967) gives the example of a sphere of mercury of 1 m in diameter; when imparting to the mercury a velocity of 1 $\mathrm{m\,s^{-1}}$, $R^{\mathrm{M}} = 1$. Magnetic Reynolds numbers of the order of 30 can be achieved in the cooling circuit of liquid-metal breeder reactors. This situation is in sharp contrast with the values for R^{M} that are encountered in astrophysical flows, including in the magnetosphere, where they range from 10^3 to 10^{12}, be it only because of the astronomical distances involved. Because of the severe limitation on R^{M} for laboratory flows, numerical computations will be a privileged tool for the experimental approach to an understanding of MHD turbulent flows. This will be discussed later. Experiments with plasmas, on the other hand, are numerous, in particular in the context of fusion. Several devices, such as the reversed field pinch (RFP), can lead to a better understanding of MHD turbulence. One can also mention the experiments of Stenzel et al. (1983), with an argon plasma with density 10^{18} particles/m^3, with the electron and ion temperature respectively equal to 5 and 0.5 eV; the plasma is confined in a 2 m vessel by a radial magnetic field of 20 G. Clever graphical displays have helped the diagnostics of the flow and have yielded information in particular on the reconnection events; however, MHD-induced effects are but one aspect of such experiments, which appear to be dominated by whistler waves.

Finally, note that $|\mathcal{V}E/(\boldsymbol{j} \times \boldsymbol{B})| = \mathcal{O}(v^2/c^2)$, and thus can be neglected. We will therefore take for the Lorentz force:

$$\boldsymbol{\mathcal{F}}_{\mathrm{m}} = \boldsymbol{j} \times \boldsymbol{B}. \tag{1.25}$$

Several dimensionless parameters, besides the kinetic and magnetic Reynolds number, R^V and R^M, can be defined starting from the MHD equations for the velocity (1.10), with the Lorentz force (1.25), for the density (1.11) with the barotropic law (1.13), and for the induction (1.20) together with the divergence-free condition (1.1).

Linearizing them (see section 1.6) around a basic state with density ρ_0, pressure p_0, and induction B_0, two velocities naturally arise, that of sound, V_S:

$$V_S = \sqrt{\gamma \frac{p_0}{\rho_0}} \,. \tag{1.26}$$

and the Alfvén velocity:

$$V_A = B_0/\sqrt{\mu\rho_0} \,. \tag{1.27}$$

Finally, the magnetic Prandtl number, P^M:

$$P^M = \nu/\eta = \tau_J/\tau_{visc} \,, \tag{1.28}$$

measures the relative dissipation by Joule and viscous effects. We leave aside several other dimensionless numbers, to prevent the list from getting too long.

Let us give some idea of such numbers, including the Reynolds number $R^V = V_0 l_0/\nu$, ν being the viscosity. For example, in the core of the Earth $R^V \sim 10^6$ and $R^M \sim 10^3$ (with the velocity in the fluid core of iron and nickel of the order of a few mm s^{-1}). In a sunspot ($l_0 = 10^7$ m, $V_0 = 10^3$ m s^{-1}) $R^V \sim 10^{12}$ and $R^M \sim 10^7$, with subsonic velocities ($M_a = V_0/V_S = 0.05$), and even more so sub-Alfvénic ($M_{aa} = V_0/V_A \sim 4 \times 10^{-3}$), thus yielding a plasma $\beta = 2\mu\rho_0/B_0^2 \sim 10^{-3}$, with $B_0 \sim 10^3$ G. Finally, in a molecular cloud ($l_0 = 1$ pc $= 3 \times 10^{16}$ m, $V_0 = 10^3$ m s^{-1}, $T \sim 100$ K), Reynolds numbers can be estimated (with $\eta \sim 10^9 T^{-3/2}$, following relationships given by Spitzer) as 10^{13}, and the Mach number as $M_a \sim 4$, indicative of highly turbulent supersonic flows.

1.2.3. The incompressible case

Because they will be often used, the MHD equations in the incompressible limit are now given, for a velocity field $\boldsymbol{v}$ and for the Alfvén velocity $\boldsymbol{b} = \boldsymbol{B}/\sqrt{\mu\rho_0}$, where $\boldsymbol{B}$ is the induction and ρ_0 the uniform density; they read:

$$\frac{\partial \boldsymbol{v}}{\partial t} + \boldsymbol{v} \cdot \nabla \boldsymbol{v} = -\frac{1}{\rho_0} \nabla p + \nu \nabla^2 \boldsymbol{v} + \boldsymbol{j} \times \boldsymbol{b}. \tag{1.29a}$$

$$\frac{\partial \boldsymbol{b}}{\partial t} = \mathrm{curl}(\boldsymbol{v} \times \boldsymbol{b}) + \eta \nabla^2 \boldsymbol{b}. \tag{1.29b}$$

$$\nabla \cdot \boldsymbol{v} = 0. \tag{1.29c}$$

$$\nabla \cdot \boldsymbol{b} = 0. \tag{1.29d}$$

with here the current density being defined as $\boldsymbol{j} = \nabla \times \boldsymbol{b}$. Using the vector identity

$$\boldsymbol{a} \times (\boldsymbol{b} \times \boldsymbol{c}) = \boldsymbol{b}(\boldsymbol{a} \cdot \boldsymbol{c}) - \boldsymbol{c}(\boldsymbol{a} \cdot \boldsymbol{b})$$

specifically for the case where $\boldsymbol{a}$ is the ∇ operator, yields:

$$\text{curl}(\boldsymbol{v} \times \boldsymbol{b}) = (\text{div}\, \boldsymbol{b} + \boldsymbol{b} \cdot \nabla)\boldsymbol{v} - (\text{div}\, \boldsymbol{v} + \boldsymbol{v} \cdot \nabla)\boldsymbol{b}.$$

so that the induction equation can be written as:

$$\frac{\partial \boldsymbol{b}}{\partial t} + \boldsymbol{v} \cdot \nabla \boldsymbol{b} = \boldsymbol{b} \cdot \nabla \boldsymbol{v} + \eta \nabla^2 \boldsymbol{b}. \tag{1.30}$$

This shows that Ohm's law separates, in the incompressible case, into an advection term and a term of stretching of magnetic field lines by velocity gradients. Similarly, using:

$$(\text{curl}\, \boldsymbol{b}) \times \boldsymbol{b} = \boldsymbol{b} \cdot \nabla \boldsymbol{b} - \nabla(\tfrac{1}{2} b^2),$$

where $\nabla \cdot \boldsymbol{b} \equiv 0$ is taken into account, and where the relationship between the antisymmetric tensor ϵ_{ijl} and the Kronecker symbol δ_{ij},

$$\epsilon_{ijl}\, \epsilon_{imn} = \delta_{jm}\, \delta_{ln} - \delta_{jn}\, \delta_{lm},$$

can be found of some use, one can rewrite eq. (1.29a) as:

$$\frac{\partial \boldsymbol{v}}{\partial t} + \boldsymbol{v} \cdot \nabla \boldsymbol{v} = -\nabla(p + \tfrac{1}{2} b^2) + \nu \nabla^2 \boldsymbol{v} + \boldsymbol{b} \cdot \nabla \boldsymbol{b}. \tag{1.31}$$

The Lorentz force thus amounts to a magnetic pressure term $b^2/2\mu$ transverse to the lines of force and isotropic, and to a tension along the lines of force.

1.2.4. The Elsässer variables

An even more symmetrical form of the MHD equations in the incompressible case is readily seen to be, using the Elsässer variables (Elsässer 1950)

$$\boldsymbol{z}^{\pm} = \boldsymbol{v} \pm \boldsymbol{b}, \tag{1.32}$$

and defining the dissipation coefficients as $\nu_1 = \frac{1}{2}(\nu + \eta)$ and $\nu_2 = \frac{1}{2}(\nu - \eta)$:

$$\frac{\partial \boldsymbol{z}^+}{\partial t} + \boldsymbol{z}^- \cdot \nabla \boldsymbol{z}^+ = -\nabla p^* + \nu_1 \nabla^2 \boldsymbol{z}^+ + \nu_2 \nabla^2 \boldsymbol{z}^-, \tag{1.33a}$$

$$\frac{\partial z^-}{\partial t} + z^+ \cdot \nabla z^- = -\nabla p^* + \nu_1 \nabla^2 z^- + \nu_2 \nabla^2 z^+, \tag{1.33b}$$

with $p^* = p/\rho + \frac{1}{2}b^2$ the total pressure. These equations, found independently by Lundquist (1952), correspond in fact to the characteristic system of the MHD equations in the absence of pressure; the viscosity ν_2 can be negative for magnetic Prandtl numbers smaller than unity. This form of the equations will prove very useful in several instances; their symmetry under interchanging + and − allows one to write eq. (1.33b) directly from eq. (1.33a), and shows that the underlying mathematical structure only contains one type of non-linear vertex; indeed, only (z^+/z^-) interactions appear in eqs. (1.33a, b), and either (z^+/z^+) or (z^-/z^-) non-linear interactions are ruled out. An exact solution of the MHD equations in the incompressible case is thus readily found: when either $z^+ \equiv 0$ (corresponding to $v = -b$) or when $z^- \equiv 0$ (corresponding to $v = +b$), the non-linear terms cancel exactly and the temporal evolution is simply on the dissipative time scale, assumed to be very large in most astrophysical or geophysical situations. This solution does not require to linearize the MHD equations; it has a finite amplitude and was shown to be stable by Chandrasekhar (1961).

1.2.5. Discussion

Pertinent boundary conditions can be found in Roberts (1967). Let us simply mention here that the magnetic induction must decay at infinity ($r \to \infty$) as $B \sim 1/r^{2+\epsilon}$, because of the divergence-free condition; also we will write that on the boundary of the domain (surface of discontinuity) with its normal, n, oriented in the outward direction, $B \cdot n = 0$ (together with $v \cdot n = 0$).

Finally, let us mention two sub-sets of eqs. (1.29a–d) that are often found in the literature. One concerns the flow in a liquid metal, for which $R^M \ll 1$, embedded in a strong external magnetic field in the vertical direction. Balancing in the induction equation the Joule diffusion of magnetic fluctuations against the stretching of B_0, one finally ends up with the usual Navier–Stokes equation for the velocity field, in which an extra linear dissipation term appears, proportional to $B_0^2 \cos^2\theta$, where θ is the angle between B_0 and the wavevector k of a given Fourier mode $\tilde{u}(k, t)$. Thus, except for $\theta = \frac{1}{2}\pi$, the velocity modes are strongly damped. This is in fact used in the laboratory to produce two-dimensional fluid turbulence.

A different simplification of eqs. (1.29a–d) arises in the context of fusion; making use of the large aspect ratio in a tokamak, an ordering is taken whereby derivatives in the vertical z-direction (the length of the plasma the long way along the torus) are taken to be small compared to derivatives in the x- and y-direction (cross section of the torus), and also the magnetic induction in the z-direction is dominating the other two components (Strauss 1976). The resulting two, scalar, three-dimensional equations for the (orthogonal) vorticity and the flux (z-component of the magnetic potential) have been used extensively, in particular in numerical stud-

ies, because of the substantial reduction in storage that they imply (scalar instead of vector equations for the general three-dimensional problem).

1.3. Joule dissipation

The simplest form of the induction equation, assuming $\boldsymbol{v} \equiv 0$,

$$\frac{\partial \boldsymbol{B}}{\partial t} = \eta \nabla^2 \boldsymbol{B}, \tag{1.34}$$

is easily solved by writing $\boldsymbol{B} = \boldsymbol{B}(0,t)\exp(i\boldsymbol{k}\cdot\boldsymbol{x})$, from which follows that $\boldsymbol{B}(t) = \boldsymbol{B}(0)\exp(i\boldsymbol{k}\cdot\boldsymbol{x} - \eta k^2 t)$. The Joule dissipation time, $\tau_J \sim l_0^2/\eta$, for the Sun ($l_0 = 10^9$ m, $T = 10^4$ K) is $\tau_J \sim 10^{15}$ s or 3×10^7 yr; it is very long indeed, unless some other process can hasten the decay of the field, through turbulent transport to the small scales. From eq. (1.34) we can also write the equation for the decay of magnetic energy:

$$\frac{\partial E^M}{\partial t} = -\eta\langle j^2\rangle + \eta\sigma \iint_S \mathrm{d}\boldsymbol{S}\cdot(\boldsymbol{B}\times\boldsymbol{E}), \tag{1.35}$$

using $\boldsymbol{j} = \sigma\boldsymbol{E}$ when $v \equiv 0$. The first term corresponds to Joule heating by the current in the conductor (here, the loss is due to the mechanical displacement of the fluid, not to radiation) and the second term is the Poynting flux of energy flowing through the surface of the conductor into it; if zero, the field decays on the Ohmic time scale, τ_J.

1.4. Large magnetic Reynolds number

1.4.1. The frozen field

Let us now suppose that R^M is so large that we can neglect Ohmic losses altogether; then, the induction equation reads:

$$\frac{\partial \boldsymbol{B}}{\partial t} = \mathrm{curl}(\boldsymbol{v}\times\boldsymbol{B}), \tag{1.36a}$$

or equivalently, for the Lagrangian derivative of $\boldsymbol{B}/\rho$:

$$\frac{\mathrm{D}}{\mathrm{D}t}\left(\frac{\boldsymbol{B}}{\rho}\right) = \left(\frac{\boldsymbol{B}}{\rho}\cdot\nabla\right)\boldsymbol{v}. \tag{1.36b}$$

Equation (1.36b) indicates that lines of constant $\boldsymbol{B}/\rho$ are permanently attached to the fluid (lines of $\boldsymbol{B}$ in the incompressible case). This is not unexpected if one recalls that the vorticity equation for a Navier–Stokes fluid reads:

$$\frac{\partial \boldsymbol{\omega}}{\partial t} = \mathrm{curl}(\boldsymbol{v}\times\boldsymbol{\omega}), \tag{1.37}$$

and thus the vorticity, ω, and the magnetic field, B (when weak, so that we can neglect the Lorentz force in eq. (1.37)) evolve similarly. This analogy will be used again in section 3 when looking at the invariants of the equations. We can then derive the analogue of the Kelvin–Helmholtz theorem: the zero-divergence equation $\nabla \cdot B = 0$, in integral form $\iint_S B \cdot \mathrm{d}S = 0$, states that the magnetic flux through a closed surface is zero. By taking for S the surface enclosed by the closed curve C_1 at time t, using the surface swept by C_1 in time δt, and taking the surface enclosed by $C_1(t + \delta t) = C_2$, we can write:

$$\iint_{C_2} B(t + \delta t) \cdot \mathrm{d}S_2 + \oint_{C_1} B(t) \cdot \mathrm{d}s \times v \, \mathrm{d}t - \iint_{C_1} B(t) \cdot \mathrm{d}S_1 = 0,$$

where $\mathrm{d}s$ is a linear element on contour C_1 and $\mathrm{d}S \times V \, \delta t$ is the surface swept by C_1 during time δt.

Thus, the change of flux through a given contour, following the motion, is:

$$\delta\Phi = \delta t \iint_{C_1} \mathrm{d}S \cdot \left(\frac{\partial B}{\partial t}\right) - \oint_{C_1} \delta t \, \mathrm{d}s \cdot (v \times B) = 0.$$

Recalling eq. (1.36a) and using Stokes' theorem, we arrive at the desired result: the magnetic flux through any closed contour moving with the fluid is constant.

1.4.2. Hamiltonian dynamics

Let us recall that a magnetic field line is at any point tangent to the direction of B, and thus obeys, in Cartesian coordinates:

$$\mathrm{d}x/B_x = \mathrm{d}y/B_y = \mathrm{d}z/B_z. \tag{1.38}$$

Note that $\nabla \cdot B = 0$ does not necessarily imply that magnetic field lines are closed. In fact, they can terminate at singular points or they can be ergodic: take the simple example (Elsässer 1956) of two wires carrying currents i_1 and i_2, with i_1 flowing along the vertical axis and i_2 flowing in a loop in the horizontal plane; a magnetic field line encircling the loop will not close upon itself, except for a set of values of i_1/i_2 of zero measure and linked to the safety factor, in tokamak terminology (a field line wrapped around a torus n times the large way and m times the small way around, will close upon itself for $m = a'n$, $a' \in \mathcal{N}$). This has far-reaching consequences and is linked to the definition of magnetic surfaces and to the underlying Hamiltonian dynamics. For example (Tsinganos et al. 1984) in the case of a magnetic field around an O-type neutral point (i.e. a point at which B vanishes, with nested magnetic surfaces around that point), the field due to the current $J = (0, 0, 2a)$, with $a = B_0/\Gamma_0$, is simply $B = (-ay, ax, c)$, with c an arbitrary constant. Take for the phase variables, p and q, of the Hamiltonian, $\mathcal{H}$,

$p \equiv y$ and $q \equiv x$, and for the pseudo-time variable $\tau = z/b$, and write $\mathrm{d}f/\mathrm{d}\tau = \dot{f}$; then, defining:

$$\mathcal{H} = \tfrac{1}{2}a(p^2 + q^2),$$

you can check that the usual Hamiltonian dynamics, $\partial\mathcal{H}/\partial p = \dot{q}$ together with $\partial\mathcal{H}/\partial q = -\dot{p}$, is equivalent to eq. (1.38) for the magnetic field lines. These equations of motion are those for a classical harmonic oscillator, and its one-dimensional phase portrait coincides with the magnetic field lines around an O-type neutral point. The X-type neutral point can be treated similarly by writing now $\boldsymbol{B} = (ay, ax, c)$, and the Hamiltonian, with the same change of variables, reads:

$$\mathcal{H} = \tfrac{1}{2}a(p^2 - q^2);$$

it now corresponds to the phase portrait of an unstable one-dimensional Hamiltonian system.

1.4.3. Flux tubes

A magnetic flux tube is a volume enclosed by a set of field lines. Then, taking a flux tube with infinitesimally small cross-section, we see that the lines of force, in the absence of dissipation, move with the fluid: the magnetic field is said to be frozen-in. However, one must recall that the dissipation term, $\eta\,\boldsymbol{\nabla}^2\boldsymbol{B}$, is omitted in the preceding derivation: at sufficiently small scales it will become relevant, and field lines will be able to change topology and reconnect.

The strength of a flux tube is defined as $\Phi = \iint_S \boldsymbol{B} \cdot \mathrm{d}\boldsymbol{S}$, i.e. as the amount of flux going through its cross section (no flux goes through the walls of a flux tube for which $\boldsymbol{B} \cdot \boldsymbol{n} = 0$). In a molecular cloud contracting under the action of self-gravity, both the magnetic flux, yielding $B \sim r^{-2}$, and the mass is conserved, yielding $\rho \sim r^{-3}$; thus $B \sim \rho^{2/3}$, a relationship not too far from being verified, although numerical simulations in the magnetostatic case seem to indicate that $B \sim \rho^n$ with $\frac{1}{3} < n < \frac{1}{2}$ (Mouschovias 1980). The conservation of flux also tells us that the larger the cross section of a flux tube of given strength Φ, the weaker the field: strong-$\boldsymbol{B}$ regions have field lines packed together. In a compressible fluid, eq. (1.36b) indicates that where $\boldsymbol{B}$ is weak, ρ is weak, and conversely.

1.5. Magnetohydrodynamical waves

When linearizing the MHD equations, several types of waves are found; see e.g. Van Kampen and Felderhof (1967), whose derivation of the properties of the waves is sketched below, or Jeffrey and Taniuti (1964) for an extended treatment of shocks, or Roberts (1984) for the inhomogeneous case.

Let us write as the unperturbed solution, in the static case:

$$\rho = \rho^0 = \text{constant}, \quad p = p^0, \quad \boldsymbol{b} = \boldsymbol{b}^0, \quad \boldsymbol{v}^0 \equiv 0,$$

and let us perturb it in the following way:

$$\rho = \rho^0 + \cdots, \tag{1.39a}$$

$$p = p^0 + p^1, \tag{1.39b}$$

$$\boldsymbol{v} = \boldsymbol{v}^1, \tag{1.39c}$$

$$\boldsymbol{b} = \boldsymbol{b}^0 + \boldsymbol{b}^1, \tag{1.39d}$$

where p^1, $\boldsymbol{v}^1$, and $\boldsymbol{b}^1$ are small. It is straightforward to write:

$$\nabla \cdot \boldsymbol{v}^1 = 0,$$

$$\nabla \cdot \boldsymbol{b}^1 = 0,$$

$$\rho^0 \frac{\partial \boldsymbol{v}^1}{\partial t} = -\nabla p^1 + \frac{1}{\mu}(\nabla \times \boldsymbol{b}^1) \times \boldsymbol{b}^0,$$

$$\frac{\partial \boldsymbol{b}^1}{\partial t} = \operatorname{curl}(\boldsymbol{v}^1 \times \boldsymbol{b}^0).$$

This system is linear, homogeneous, with constant coefficients; by expanding the perturbation f^1 in plane waves (where f stands for either p^1, $\boldsymbol{v}^1$, or $\boldsymbol{b}^1$) we obtain:

$$f^1 = f_k \exp(\mathrm{i}\boldsymbol{k} \cdot \boldsymbol{r} - \mathrm{i}\omega t),$$

where the wavevector $\boldsymbol{k}$, the frequency ω, and the amplitudes f_k are constant. We now have:

$$\boldsymbol{k} \cdot \boldsymbol{v}_k = 0. \tag{1.40a}$$

$$\boldsymbol{k} \cdot \boldsymbol{b}_k = 0. \tag{1.40b}$$

$$-\omega \rho^0 \boldsymbol{v}_k = -\boldsymbol{k} p_k + \frac{1}{\mu}(\boldsymbol{k} \times \boldsymbol{b}_k) \times \boldsymbol{b}^0, \tag{1.40c}$$

$$-\omega b_k = \boldsymbol{k} \times (\boldsymbol{v}_k \times \boldsymbol{b}^0) = \boldsymbol{v}_k(\boldsymbol{k} \cdot \boldsymbol{b}^0). \tag{1.40d}$$

From the eight equations (1.40a–d) above, the divergence-free condition for the magnetic field can be deduced from eq. (1.40b); thus we have to solve a system of seven linear homogeneous equations for seven unknown; the condition $\Delta \equiv 0$.

where Δ is the determinant, yields the dispersion relation. Equation (1.40a) indicates that the wave propagates transversely to the wavevector: the stretching by velocity gradients is counteracted by the tension of the lines of force. Equation (1.40d) shows that v_k and b_k are parallel. The dispersion relation is:

$$\omega^2 = \frac{(\boldsymbol{k} \cdot \boldsymbol{b}^0)^2}{\rho^0 \mu} = (\boldsymbol{k} \cdot \boldsymbol{V}_\mathrm{A})^2, \tag{1.41}$$

where $\boldsymbol{V}_\mathrm{A}$ is the Alfvén velocity. The phase velocity of the Alfvén wave is $\omega/k = V_\mathrm{A} \cos(\boldsymbol{k}, \boldsymbol{b}^0)$; the Alfvén wave is anisotropic ($\omega_\mathrm{A} = 0$ for $\boldsymbol{k} \perp \boldsymbol{b}^0$); its group velocity, $\mathrm{d}\omega/\mathrm{d}k = \omega/k$, shows that it is non-dispersive. In the simplest case ($\boldsymbol{k} \parallel \boldsymbol{b}^0$), the wave propagates along the magnetic field, stretching the field lines transversely; averaged over one period, $b_k^2 = \rho^0 v_k^2$, i.e. there is equipartition of energy, corresponding to equipartition between potential and kinetic energy in the harmonic oscillator.

In the presence of dissipation, the dispersion relation becomes:

$$k^2 V_\mathrm{A}^2 = (\omega + \mathrm{i}\eta k^2)(\omega + \mathrm{i}\nu k^2), \tag{1.42}$$

which induces both dispersion and penetration of the wave, on a length scale $l_\mathrm{h} = V_\mathrm{A}/\sqrt{\nu\eta}$, which is called the Hartmann layer.

In the compressible case, the analysis carries along as before, with now $\rho = \rho^0 + \rho^1$, with as perturbation of the density $\rho^1 = \rho_k \exp(\mathrm{i}\boldsymbol{k} \cdot \boldsymbol{r} - \mathrm{i}\omega t)$. Writing $p = f(\rho)$ and $V_\mathrm{S} = \sqrt{f'(\rho)}$, the dispersion law in the general case reads:

$$\omega^4 - \omega^2 k^2 (V_\mathrm{S}^2 + V_\mathrm{A}^2) + k^2 \kappa^2 V_\mathrm{S}^2 = 0, \tag{1.43}$$

where $\kappa = \boldsymbol{k} \cdot \boldsymbol{V}_\mathrm{A}$. Three modes are now found: one is the transverse Alfvén wave as before, with no pressure variation ($\rho_k = 0$) and with $\omega = \boldsymbol{k} \cdot \boldsymbol{V}_\mathrm{A}$. Assuming $\omega \neq 0$, two new, longitudinal modes arise, corresponding to the two solutions of eq. (1.43): the fast magnetoacoustic mode (with $V_\mathrm{f} > V_\mathrm{A}$) and the slow mode (with $V_\mathrm{sl} < V_\mathrm{A}$); like the Alfvén wave, the slow mode cannot propagate along field lines, in sharp contrast to the fast mode.

When $\boldsymbol{b}^0 \parallel \boldsymbol{k}$, we have $\kappa = kV_\mathrm{A}$ and $\omega^2 = k^2 V_\mathrm{S}^2$; this represents an ordinary sound wave propagating along the magnetic field line. It is not affected by the magnetic field because it moves parallel to it ($b^1 \equiv 0$). When $\boldsymbol{b}^0 \perp \boldsymbol{k}$, the phase velocity is $\omega/k = \sqrt{V_\mathrm{S}^2 + V_\mathrm{A}^2}$; it is a compression wave propagating across the field at a speed associated with the total kinetic plus magnetic pressure.

1.6. Discussion

The topic of waves has many ramifications. For the description of waves in an inhomogeneous medium, see Roberts (1984) and Campos (1987) for a general review. The damping of MHD waves by diffusion in a non-uniform atmosphere can

provide part of the energy needed to heat the solar corona from 5×10^3 K at the photospheric level to 10^6 K in the chromosphere (Nocera et al. 1986) by phase mixing, or by resonant absorption linked to the discrete (instead of continuous) sets of modes when the magnetic diffusivity is non-zero (Reidel 1986). When the waves grow to finite amplitudes, they couple together and they steepen, giving rise to magnetized shocks (see, e.g., Jeffrey and Taniuti (1964)). In the simplest case, when the magnetic field is parallel to the shock front, one simply modifies the Rankine–Hugoniot relations by adding the magnetic pressure, $B_i^2/2\mu$ ($i = 1, 2$ referring to each side of the shock), and the magnetic momentum, $B_i^2 V_i/2\mu$, to the corresponding equations, together with a continuity equation for the magnetic flux across the shock $[B_i V_i] = 0$ (where the brackets indicate jump conditions). In the general case, fast, intermediate (Alfvén), and slow waves give rise to fast, intermediate, and slow shocks. Transport of energetic particles in a magnetized medium by diffusion can be considerably enhanced in the presence of shocks by a process referred to as first-order Fermi acceleration (see, e.g., Drury (1987) for a review): one solves through the shock the diffusion equation (in the shock frame) for the particle distribution function $f(\boldsymbol{p}, \boldsymbol{x}, t)$, where $\boldsymbol{p} = \rho \boldsymbol{V}$ is the momentum, with $\boldsymbol{V}$ the velocity of the particle. Notating by V_1 and V_2 the upstream and downstream velocities of the medium, with $V \gg V_2$, the probability that the particle escapes to infinity as opposed to being scattered by collisions, is $P_{\text{esc}} \sim V_2/V$. By crossing the shock many times back and forth, particles can gain momentum, with $\Delta p/p \sim V_2/V$. The resulting distribution function, $f(p)$, is the power-law $f(p) \sim (p/p_0)^{\alpha}$, with $\alpha = 3/(j_c - 1)$, where $j_c = V_2/V_1$ is the compression jump ($j_c = 4$ is a typical number in a strong shock, leading to a -2 energy spectrum). This mechanism seems to give reasonable agreement for the cosmic-ray spectrum below 10^{15} eV.

This is not the place to discuss the interaction of magnetic fields and rotation (see Chandrasekhar (1961) or Acheson and Hide (1973)). Let us simply mention that in the case of aligned velocity and magnetic fields, as measured relative to the rotating frame, i.e. when $\boldsymbol{B} = C\boldsymbol{U}\sqrt{\mu\rho}$, the potential-vorticity theorem still holds, where the potential vorticity is now defined as $\omega + 2\Omega/(1 - C^2)$, with $\omega = \operatorname{curl} \boldsymbol{v}$ and Ω the angular velocity. In fact, Hide (1983) has shown that there is a magnetic analogue of Ertel's potential-vorticity theorem: starting from eq. (1.36b) for $\boldsymbol{B}/\rho$ and from an equation for a Lagrangian scalar invariant, Λ, such as entropy:

$$\frac{\mathrm{D}\Lambda}{\mathrm{D}t} = 0,$$

the quantity

$$\Gamma = \rho^{-1} \boldsymbol{B} \cdot \boldsymbol{\nabla} \Lambda \tag{1.44}$$

is also conserved for each fluid element; Hide proposed to call Γ the potential magnetic field, although this may induce some confusion with the widely studied configurations where B is potential (no current).

2. Observations and phenomenology

2.1. *Introduction*

Magnetic fields are widespread in the Universe and a review of relevant observations is far beyond the scope of these lectures. The following sections are thus a totally biased sample of what is presently known, from numerous observations, about magnetic fields. The reader is referred to basic books, and to the many reviews devoted to the several components of this subject. However, a brief glance is given below to set the scene of action.

2.2. *Methods of observation*

2.2.1. *The Zeeman effect*

A magnetic field lifts the degeneracy of the atomic line emission associated with angular momentum, and in the simplest case of a singlet, the line is split up in three components. Two circularly polarized σ components are symmetrically shifted on the blue and red side of the basic frequency ν_0 by $\delta\nu$; the shift is directly proportional to the magnetic field and also depends on the quantum numbers L and S. When viewed in directions perpendicular to the field, a non-shifted linearly polarized π component, parallel to the field's direction, is also present. In a more general case, the shift is:

$$\delta\nu \sim gB, \tag{2.1}$$

where

$$g = 1 + \frac{J(J+1) + S(S+1) - L(L+1)}{2J(J+1)}$$

is the Landé factor. For the iron line Fe 5250, for which the natural line width is 0.1 Å, one has $\delta\nu = 4 \times 10^{-5}$ Å/G. When the field is so weak that the line splitting is smaller than the natural line width, one can use a differential effect between the two wings of the line, because of the difference in sign of the circular polarization; this is the basis of the Babcock magnetograph. Note that a possible selection effect is due to the fact that there are other sources of broadening, such as rotation and micro-turbulence.

2.2.2. Polarization observations

In radioastronomy, the most widely used method of measurement of a magnetic field is Faraday rotation (Gardner and Whiteoak 1966). It gives the $B_{\parallel}$ component through the rotation measure R_M:

$$R_M = 0.81 \int N_e B_{\parallel} \, dl, \tag{2.2}$$

where R_M is in rad/m^2, the line element, dl, in parsec, the parallel (to the line of sight) component of the magnetic field, $B_{\parallel}$, in μG, and N_e is the electron density in m^{-3}. The rotation of the direction of polarization by scattering on irregularities in the electron density is over an angle $\psi = R_M \lambda^2$, where λ is the wavelength, and where 2π ambiguities are removed by measuring at several wavelengths. Note that, to have access to the induction, one must know the electron density, which is unfortunately quite often not the case. As a last resource, one can evaluate the magnetic field from equipartition arguments with the dynamic, the gas, or the cosmic-ray pressure.

2.3. The Earth as a planet

From paleomagnetism, knowledge of the Earth's magnetic field goes back to 10^9 yr. It is quite weak: its mean value is 0.3 G at the equator, with the dipole axis tilted 11° from the axis of rotation, and with a quadrupole component of about 0.15 times the value of the total field (unlike Jupiter, where it is much stronger). It extends to ten Earth radii, where it is finally stopped by the solar-wind pressure in the solar direction. In the anti-solar direction it is drawn out to a long tail. A reversal of the field has occurred at random intervals of 10^5–10^7 yr, and happens abruptly, in less than 10^3 yr. The field is due to the motions in the liquid core of iron and nickel at 4000 K; with $\eta = 1$ m^2 s^{-1}, and with a westward drift of inhomogeneities of 3×10^{-4} m s^{-1}, the magnetic Reynolds number is of the order of 10^3 and the Joule diffusion time of the order of 10^5 yr.

In situ measurements by satellite provide data on other planets and on the solar wind. In the latter case, the mean field is 60 μG, with fluctuations of the same order of magnitude, a velocity of 4×10^5 m s^{-1} and an Alfvén velocity of 6×10^4 m s^{-1}; the wind is viewed as an ensemble of Alfvén waves propagating outwards from the Sun, probably generated by supergranulation, and of discontinuities and shocks. The Voyager-2 data, averaged every 10 s, indicate that the spectra of the energy, of the correlation $\langle \boldsymbol{v} \cdot \boldsymbol{b} \rangle$, and of the magnetic helicity $\langle \boldsymbol{a} \cdot \boldsymbol{b} \rangle$ are well developed over several decades of wavenumbers (Matthaeus and Goldstein 1982, Matthaeus et al. 1983, Smith et al. 1983); the spectral index m of the energy spectrum, $E(k) \sim k^{-m}$, seems in good agreement with the Kolmogorov $-\frac{5}{3}$ law; the correlation spectrum sometimes changes sign rapidly on the small scales, which may be due

to an early development of turbulence in that case (see section 7.3), whereas the magnetic helicity remains to have the same sign and is between 2 and 5 au (1 au $\approx$ 10^{11} m). The correlation between the three components of the velocity and of the magnetic field is high in periods of 24 h (Belcher and Davis 1971); the ratio of kinetic to magnetic energy on the small scales is within a factor two equal to unity, and in general (but not always) smaller than one; finally, the characteristic length, λ_t, defined as:

$$\lambda_t = 2\pi E^t \int kE^t(k)\,\mathrm{d}k,$$

is greater by a factor five for the magnetic helicity spectrum,

$$\lambda_{H^M} = 1.2 \times 10^{10}\ \mathrm{m}, \tag{2.3a}$$

than for the magnetic energy,

$$\lambda_{E^M} = 10^9\ \mathrm{m}. \tag{2.3b}$$

2.4. *The Sun as a star*

The mean field of the Sun is weak, of the order of 1 G, whereas in stars it ranges from 100 G (the detection limit) to 20 000 G. Sunspots, barely visible to the naked eye, have been observed in ancient China, and starspots covering large portions of the stellar surface, are now being identified by the temporal modulation of the light curves of the stars. The solar cycle of 22 yr – which corresponds to a large-scale circulation, with $L = 10^9$ m and $V = 10\ \mathrm{m\,s^{-1}}$ – is now known to be typical of stars of the same spectral type (Wilson 1978), although stars close in the H–R diagram may have cycles differing by almost a factor of three: three years as opposed to eight (S. Baliunas, private communication). A detailed investigation of these stars, to find their intrinsic characteristics (mass and radius), is certainly needed!

Other manifestations of stellar magnetic activity, like their coronae, studied with X-ray measurements, and the inference of the existence of stellar winds complete this description (Cram 1983, Marcy 1983). It is not clear, however, whether the X-ray activity is transient or corresponds to continual flaring (Montmerle et al. 1983). For a brief review of theoretical aspects of magnetic activity in stars, see Spruit (1983).

On the Sun, moreover, a lot of small-scale activity is routinely observed: isolated flux tubes, with a strength of 1 kG, spicules in the chromosphere, and loops

in the corona, made visible by density and temperature inhomogeneities. The motions of some of these features are probably linked to the underlying large-scale convection and circulation. Sunspots, e.g., may be attributed, following Parker (1979), to the emerging part of toroidal flux tubes, because of magnetic buoyancy: a flux tube is in pressure equilibrium with its surroundings:

$$p_e = p_i + \frac{B_i^2}{2\mu}, \tag{2.4}$$

where e stands for the exterior of the tube and i for its interior. Using

$$p = \rho kT/m,$$

we can write:

$$\rho_e = \rho_i + \frac{B_i^2}{2\mu}\frac{m}{kT}.$$

The flux tube is thus less dense than the medium in which it is embedded, and it feels a buoyancy force $(\rho_e - \rho_i)g$ per unit volume; the tube will rise as long as the restoring force due to magnetic tension in the stretched field lines, is negligible; defining $\Lambda = kT/mg$ as the scale height, we get:

$$g(\rho_e - \rho_i) > \frac{B_i^2}{\mu}\frac{1}{L}, \tag{2.5}$$

the right-hand side being an estimate of the Lorentz force, and L being the size of the tube. It is estimated that, at 1000 km below the photosphere, the residual force, $\delta\rho/\rho$, is 4×10^{-3}, for an external density $\rho_e = 8 \times 10^{-6}$, with $T = 1.5 \times 10^4$ and $B = 10^{-1}$ G.

2.5. Beyond the Sun

Magnetic fields in the interstellar medium are estimated to be in the 1–100 μG range. Using flux conservation, $\int \boldsymbol{B} \cdot \mathrm{dS}$ = constant, and mass conservation:

$$\iiint \rho \, \mathrm{d}^3\boldsymbol{r} = \text{constant},$$

one obtains:

$$B \sim \rho^{2/3}. \tag{2.6}$$

Note that scaling down from the Sun to a white dwarf with radius 10 km, one predicts for the latter a field of 10^{10} G. However, when applied to a field of 1 μG in an interstellar cloud, with a density of 100 particles m^{-3}, this also gives a field of 10^{10} G for the Sun. Probably, the law (2.6) has to be modified; Mouschovias (1980) suggests:

$$B \sim \rho^k,$$

with $\frac{1}{3} < k < \frac{1}{2}$, on the basis of numerical simulations of the evolution in the magnetostatic case.

The Joule dissipation time of interstellar fields is very large: for $L = 0.1$ pc, $T = 10$ K, and using Spitzer's evaluation of the magnetic diffusivity, one arrives at $\tau_J \sim 10^{16}$ yr. Other diffusion mechanisms, such as ambipolar diffusion, possibly have to be invoked in very dense clouds where the degree of ionization falls below 10^8 (Mestel 1983).

The magnetic field of external galaxies is known only in a few cases, mostly for spirals (Beck 1986, Sofue et al. 1986). The field lines of $B_\perp$ seem aligned with the spiral arms, although the same data may also be fitted with a field twisted out of the galaxy plane. It is either a circular configuration or a bi-symmetrical one, and more observations clearly need to be made. The magnetic fluctuations, $\Delta B/B$, are of order one, and the intensity of $B_\parallel$, measured from Faraday rotation and assuming a density of 3×10^{-8}, is found to be 2.2 ± 0.4 μG, with irregularities of the field on scales of 50 pc.

2.6. *Radio jets*

Extremely well collimated radio jets have now been observed to find their magnetic structures (Königl 1987). The central engine may be active galactic nuclei (AGN). In several cases, the magnetic field is first aligned with the axis of the jet and then switches to the perpendicular direction. This can be understood by assuming (i) flux conservation and (ii) constancy of velocity; if R is the radius of the jet, these yield:

$$B_\parallel R^2 = \text{constant}$$

and

$$B_\perp 2\pi R V \, dt = \text{constant}.$$

Hence, the scaling with radius of the magnetic field along the axis (and along the line of sight, because they are superluminal in many instances) and across it, is different:

$$B_\parallel / B_\perp \sim R^{-1}. \tag{2.7}$$

When looking in detail at the magnetic structures within radio lobes, e.g. in Cygnus A, using the resolution of VLA (Very Large Array), small eddies appear, and the magnetic flow takes a turbulent appearance (Perley 1987).

2.7. A phenomenological analysis of MHD turbulence

Dealing with turbulent flows, can one apply the classical Kolmogorov phenomenology, or should it be modified for conducting fluids? One essential difference in MHD is the presence of Alfvén waves with a characteristic time $\tau_A = (kB_0)^{-1}$ at wavenumber k. Such coherent motions, or a mixture of them traveling along the large-scale field B_0 in opposite directions, are slowing down the transfer of energy to small scales (Iroshnikov 1963, Kraichnan 1965), since such eddies interact only while they collide. Writing now that the transfer time, τ_{tr}, is the eddy turn-over time, τ_{NL}, modified by the fractional collision time, i.e. τ_{NL}/τ_A, where

$$\tau_A < \tau_{NL},$$

one obtains for the transfer time:

$$\tau_{tr} = \tau_{NL}^2/\tau_A; \tag{2.8}$$

thus, one can write for the rate of energy transfer, ϵ, assumed independent of wavenumber, as for the classical Kolmogorov range:

$$\epsilon = \frac{dE}{dt} \sim \frac{E}{\tau_{tr}} = \frac{kE(k)}{\tau_{NL}^2/\tau_A} = \frac{k^3E^2(k)}{B_0}. \tag{2.9}$$

Constancy of flux then implies

$$E(k) \sim (\epsilon B_0)^{1/2}k^{-3/2}. \tag{2.10}$$

Following Kraichnan and Nagarajan (1967), one can envisage that, in the transistory period – provided a dynamo mechanism is at work – when $b \ll v$, and assuming $\eta \gg \nu$, the energy spectrum will contain several regions, as depicted in fig. 1.

In region 1, as long as the eddy turn-over time is shorter than the local Alfvén time, the Kolmogorov $-\frac{5}{3}$ range will prevail. When these two times become equal, at wavenumber $k_1 = \epsilon/B_0^3$, for energy injected at a rate ϵ at wavenumber $k_0 = 1$, the $-\frac{3}{2}$ range takes over, with equipartition between velocity and magnetic field (region 2). The range ends when Joule dissipation prevails over transfer, at

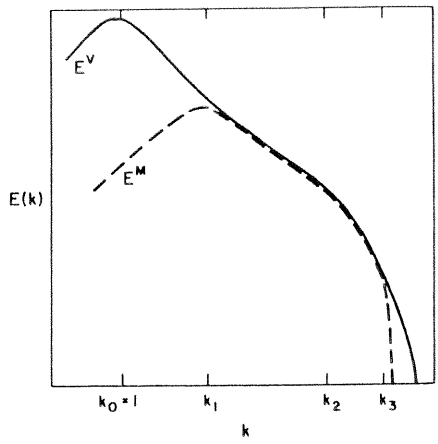

Fig. 1. Kinetic (solid line) and magnetic (dashed line) energy spectra for different regimes (see text).

wavenumber $k_2 = (\epsilon B_0^{-1}/\eta^2)^{1/3}$, obtained by equating τ_{tr} and τ_J (region 3). Note that equipartition will stop when $\tau_A > \tau_J$, i.e. in the range of wavenumbers

$$k > k_3 = B_0/\eta.$$

In that latter range, equating advection, $\boldsymbol{B}_0 \cdot \boldsymbol{\nabla} \boldsymbol{b}$, and diffusion, $\eta \boldsymbol{\nabla}^2 \boldsymbol{b}$, indicates that

$$E^M(k)/E^V(k) \sim k^{-2}.$$

Temporal spectra can also be assessed with the same type of phenomenology (and I am thankful to A. Brandeburg for having asked this question). Following Von Weissäcker, one writes that

$$\epsilon \sim \omega E(\omega)/\omega^{-1} = \omega^2 E(\omega)$$

is independent of frequency, ω, thus leading to:

$$E(\omega) \sim \omega^{-2}.$$

When taking again into account the effect of Alfvén waves, what happens? We can now write:

$$\epsilon \sim \frac{\omega E(\omega)}{\tau_{tr}}.$$

with as before $\tau_{tr} = \tau_{NL}^2/\tau_A$. Using $\omega_{NL} = \omega$, we have:

$$\epsilon \sim \omega^3 E(\omega)\tau_A \sim \frac{\omega^3 E(\omega)}{B_0}[E(\omega)\omega^{-1}]^{1/2}.$$

Writing $E(\omega) \sim \omega^{-5/3}$, constancy of flux requires $m = \frac{5}{3}$, and the temporal spectrum now reads:

$$E(\omega) \sim (\epsilon B_0)^{2/3}\omega^{-5/3}, \tag{2.11}$$

not to be mixed up with the Kolmogorov law.

The inertial-range spectral indices can be further modified to take into account the discrepancy between z^+ and z^- eddies when the flow is strongly correlated. This point will be discussed further in the last section.

3. Large-scale behavior

3.1. The invariants of the MHD equations

In the absence of dissipative processes ($\nu \equiv 0$, $\eta \equiv 0$), the MHD equations conserve several global invariants: the total energy

$$E^T = \tfrac{1}{2}\int_V (v^2 + b^2)\,dV, \tag{3.1}$$

and the cross-correlation

$$E^C = \tfrac{1}{2}\int_V \boldsymbol{v}\cdot\boldsymbol{b}\,dV, \tag{3.2}$$

which does not require the stating of an equation of state.

Alternatively, in Elsässer variables, we have:

$$E^{\pm} = \tfrac{1}{2}\int_V (z^{\pm})^2\,dV. \tag{3.3}$$

Moreover, in three dimensions the magnetic helicity is conserved:

$$H^M = \int_V (\boldsymbol{a}\cdot\boldsymbol{b})\,d^3\boldsymbol{r}, \tag{3.4}$$

whereas, in two dimensions it is the vector potential which is conserved, and in particular its variance:

$$E^a = \int_V a^2 \, \mathrm{d}^2 \boldsymbol{r}. \tag{3.5}$$

These two invariants depend solely on the induction equation and are therefore conserved also for viscous flows, as long as $\eta \equiv 0$. This strongly restricts the non-linear coupling between the velocity and the magnetic field. One useful identity in obtaining these conservation laws is:

$$\int \boldsymbol{v} \cdot \mathrm{curl}(\boldsymbol{w}) \, \mathrm{d}^3 \boldsymbol{r} = \int \boldsymbol{w} \cdot \mathrm{curl}(\boldsymbol{v}) \, \mathrm{d}^3 \boldsymbol{r}, \tag{3.6}$$

assuming the boundary terms to be zero. From the analogy between the vorticity and the magnetic field, we can in fact deduce that the kinetic helicity invariant $H^V = \int \langle \boldsymbol{v} \cdot \boldsymbol{\omega} \rangle \, \mathrm{d}^3 \boldsymbol{r}$ carries on to MHD as either the correlation $E^C = \langle \boldsymbol{v} \cdot \boldsymbol{b} \rangle$ or as magnetic helicity, with $\boldsymbol{\omega} \sim \boldsymbol{b}$ and now $\boldsymbol{v} = \mathrm{curl}^{-1} \boldsymbol{\omega} \sim \boldsymbol{a}$. Other types of analogies between fluid mechanics and magnetohydrodynamics are utilized in Shercliff (1979).

To these invariants one should add those valid in the dissipative case as well, like mass:

$$M^0 = \int_V \rho \, \mathrm{d}V, \tag{3.7}$$

and those stemming from symmetry considerations, namely invariance under translation (momentum) and under rotation, i.e. angular momentum:

$$M^X = \int_V (\boldsymbol{l} \times \boldsymbol{r} \cdot \rho \boldsymbol{v}) \, \mathrm{d}V, \tag{3.8a}$$

$$M^Y = \int_V (\boldsymbol{m} \times \boldsymbol{r} \cdot \rho \boldsymbol{v}) \, \mathrm{d}V, \tag{3.8b}$$

$$M^Z = \int_V (\boldsymbol{n} \times \boldsymbol{r} \cdot \rho \boldsymbol{v}) \, \mathrm{d}V, \tag{3.8c}$$

where $\boldsymbol{l}$, $\boldsymbol{m}$, and $\boldsymbol{n}$ are unit vectors in Cartesian geometry.

3.2. An MHD fluid as a mechanical system

Lacking a general theory, one can look at familiar physics to try to describe the flow. Here, we will draw from classical mechanics, and in section 3.6 statistical

mechanics will be used. In classical mechanics, the state of most stable equilibrium is one which minimizes the energy while being compatible with a set of given constraints. Following Woltjer (1958), we will, therefore, minimize the energy of an MHD fluid, assuming it is being dissipated by viscous and/or resistive processes, while constraining the flow, to conserve the other quadratic invariants. One must be a little careful here: in a two-dimensional neutral fluid, one should rather minimize enstrophy while maintaining energy. This is linked to the concept of cascade, as opposed to inverse cascade, and will be mentioned later. But in MHD energy minimization will work fine, both in two and in three dimensions. Let us first work out a simple example where the magnetic helicity is maintained constant over the whole volume. Assuming $\boldsymbol{b} \cdot \boldsymbol{n} = 0$ and $\boldsymbol{v} \cdot \boldsymbol{n} = 0$ on the boundary of the vessel, we can write, using a Lagrange multiplier, α:

$$\delta E^{\mathrm{T}} + \alpha\, \delta H^{\mathrm{M}} = 0,$$

leading to:

$$\boldsymbol{v} \cdot \delta\boldsymbol{v} + \boldsymbol{b} \cdot \delta(\operatorname{curl} \boldsymbol{a}) - \tfrac{1}{2}\alpha \boldsymbol{a} \cdot \delta(\operatorname{curl} \boldsymbol{a}) - \tfrac{1}{2}\alpha \boldsymbol{b} \cdot \delta\boldsymbol{a} = 0,$$

where $\delta \boldsymbol{X}$ implies independent and arbitrary variation of $\boldsymbol{X}$; using, as a consequence of eq. (3.6):

$$\boldsymbol{a} \cdot \delta\boldsymbol{b} = \boldsymbol{b} \cdot \delta\boldsymbol{a}$$

and working directly with the magnetic potential, which will preserve the $\operatorname{div} \boldsymbol{b} = 0$ condition, we readily obtain:

$$\boldsymbol{v} \equiv 0,$$

and

$$\boldsymbol{j} \equiv \operatorname{curl} \boldsymbol{b} = \alpha\, \boldsymbol{b}. \tag{3.9a}$$

Thus, the minimization of energy constrained to the sole conservation of magnetic helicity, yields a force-free field, or fff, i.e. one for which the Lorentz force is zero. Such fields appear time and again, and we will now give a few examples of them. This particular minimization, a subset of the general case treated by Woltjer (1958), has been studied at length in the context of fusion problems (Taylor 1974, 1986) because of its ability to predict current profiles in reversed field pinch experiments; it can be further refined by reintroducing other invariants, or by looking at a maximal entropy condition (see Hameiri and Hammer (1982) for a finite-pressure compressible equilibrium). But this would take us far afield. When the

conservation of magnetic helicity is imposed on the whole volume, the Lagrange multiplier α is constant; this minimization procedure can, however, be generalized to cases where H^M is conserved on individual flux tubes, in which case α becomes space-dependent,

$$\boldsymbol{j} \equiv \operatorname{curl} \boldsymbol{b} = \alpha(\boldsymbol{r})\, \boldsymbol{b}, \tag{3.9b}$$

and the fff is no longer linear.

Equation (3.9b) is very hard to solve. However, in the linear case for eq. (3.9a), there are several known solutions for the fff condition; e.g. $\boldsymbol{b} \equiv 0$, or $\boldsymbol{j} \equiv 0$ almost everywhere except where $\boldsymbol{b} \equiv 0$ (current sheet), or, more general, a parallel field and current. Let us restrict ourselves to the latter. Writing $\boldsymbol{\nabla} \cdot \boldsymbol{j} = 0$, we obtain:

$$(\boldsymbol{b} \cdot \boldsymbol{\nabla})\alpha = 0, \tag{3.10}$$

i.e. the magnetic field lines lie on surfaces of constant α (or α is constant per flux tube).

Note that a simple fff stays force-free; assuming a stationary flow ($\boldsymbol{v} \equiv 0$), and taking α constant, we obtain, taking the curl of eq. (3.9):

$$\alpha^2 \boldsymbol{b} = -\boldsymbol{\nabla}^2 \boldsymbol{b},$$

hence, the induction equation becomes:

$$\frac{\partial \boldsymbol{b}}{\partial t} = -\eta \alpha^2 \boldsymbol{b}.$$

Therefore, $\boldsymbol{b}(t) = \boldsymbol{b}_0 \, \mathrm{e}^{-\eta\alpha^2 t}$ and $\boldsymbol{j}(t) = \boldsymbol{j}_0 \, \mathrm{e}^{-\eta\alpha^2 t}$, and thus field and current remain parallel.

As an example of an fff, take:

$$(b_0 \sin kz, b_0 \cos kz, 0).$$

This field is constant in each $z = z_0$ plane, with its direction changing periodically with z, left-handedly for $k > 0$. This field has $\boldsymbol{j} = k\boldsymbol{b}$, and $\boldsymbol{a} = k^{-1}\boldsymbol{b}$. It thus has maximal magnetic helicity, i.e. the equality in

$$\langle \boldsymbol{a} \cdot \boldsymbol{b} \rangle \leqslant \langle \boldsymbol{a}^2 \rangle^{1/2} \langle \boldsymbol{b}^2 \rangle^{1/2}$$

is fulfilled. This will generally be the case for fff since a relative minimal $\boldsymbol{j} \times \boldsymbol{b}$ for non-zero fields implies maximal $\boldsymbol{j} \cdot \boldsymbol{b}$, which is directly related, in Cartesian

geometry, to the magnetic helicity, by a factor k^{-2}. Another example of an fff helical field is the ABC flow (Arnold 1965), with components:

$$\boldsymbol{D} : (A \sin \alpha z + C \cos \alpha y,\ B \sin \alpha x + A \cos \alpha z,\ C \sin \alpha y + B \cos \alpha x). \tag{3.11}$$

This field is solenoidal (div $\boldsymbol{D} = 0$), and is a Beltrami flow. Define $\boldsymbol{\xi}$ and $\boldsymbol{F}$ as: $\boldsymbol{\xi} = \operatorname{curl} \boldsymbol{D} = -\alpha \boldsymbol{D}$ and $\boldsymbol{D} = \operatorname{curl} \boldsymbol{F}$, $\boldsymbol{F} = -\boldsymbol{D}/\alpha$. Thus, either the kinetic helicity, if $\boldsymbol{D}$ is a velocity field, or the magnetic helicity, if $\boldsymbol{D}$ is a magnetic field, is maximal. When $ABC \neq 0$, the field lines of $\boldsymbol{D}$ are chaotic (Hénon 1966, Dombre et al. 1986). This flow has been studied in connection with the kinematic dynamo (Galloway and Frisch (1984, 1986), see also Roberts' Lectures). In that context, it is interesting to mention that a necessary condition for chaos in stationary solutions (and stationarity is important) of Euler flows is that it is a Beltrami – maximal helical – flow; indeed:

$$\boldsymbol{v} \cdot \left[\nabla \left(\frac{p}{\rho} + \frac{1}{2} v^2 \right) + \boldsymbol{v} \times \boldsymbol{\omega} \right] = 0; \tag{3.12}$$

hence, the velocity lies on lines of constant total pressure, unless $\boldsymbol{v} \times \boldsymbol{\omega} = 0$; moreover, in this case, $\boldsymbol{\omega} = \lambda \boldsymbol{v}$ with λ constant (otherwise the velocity would lie on lines of constant λ). The emergence of chaos and/or magnetic fields are related problems.

Another example of a pressure-balanced field (but stricto sensu no longer fff) is that of the θ-pinch: take, in cylindrical coordinates (z, r, θ), a field in the z-direction: $\boldsymbol{b} = b(r)\, \hat{\boldsymbol{e}}_z$; its current, $\boldsymbol{j} = -(\mathrm{d}b/\mathrm{d}r)\, \hat{\boldsymbol{e}}_\theta$ is only in the θ-direction (hence the name "θ"-pinch). The Lorentz force then only amounts to a pressure $-(\mathrm{d}b^2(r)/2\mu \mathrm{d}r)\, \hat{\boldsymbol{e}}_r$ in the radial direction, pinching the flow towards the axis.

The stability, or lack thereof, of force-free fields is briefly discussed in section 4.3.

3.3. The general state of minimal energy

Returning to the minimization procedure in the general case of a barotropic flow ($p = f(\rho)$), and taking now for the total energy:

$$E^{\mathrm{T}} = \int_V \left(\frac{1}{2} \rho [v^2] + \frac{b^2}{2\mu} + \rho U + q \rho \Phi \right) \mathrm{d}V, \tag{3.13}$$

where U is the internal energy per unit mass and where Φ is a gravitational potential ($\nabla \Phi = 4\pi G \rho$), with $q = 1$ (respectively $\frac{1}{2}$) for an external (respectively self-gravitating) potential, we have in the three-dimensional case (Woltjer 1958):

$$\delta E^{\mathrm{T}} + \alpha\, \delta H^{\mathrm{M}} + \beta\, \delta E^{\mathrm{C}} + \gamma_X\, \delta M^X + \gamma_Y\, \delta M^Y + \gamma_Z\, \delta M^Z + \gamma_0\, \delta M^0 = 0,$$

thus leading to:

$$\text{curl}\, \boldsymbol{b} = \alpha \boldsymbol{b} + \beta \boldsymbol{\omega}, \tag{3.14a}$$

$$\rho(\boldsymbol{v} - \boldsymbol{L} \times \boldsymbol{r}) = \beta \boldsymbol{b}, \tag{3.14b}$$

$$\frac{1}{2}[v^2] - \boldsymbol{L} \times \boldsymbol{r} \cdot \boldsymbol{v} = \frac{\mathrm{d}(U\rho)}{\mathrm{d}\rho} = \gamma_0, \tag{3.14c}$$

where

$$\boldsymbol{L} = \gamma_X \boldsymbol{l} + \gamma_Y \boldsymbol{m} + \gamma_Z \boldsymbol{n} \tag{3.14d}$$

and where β and the γ's are again Lagrange multipliers. Note that when $\beta \neq 0$, i.e. for non-zero cross correlations, and when the density goes to zero, $\boldsymbol{b} \rightarrow 0$ (this can be seen as a consequence of the conservation of $\boldsymbol{b}/\rho$ along the motion). Also, taking the divergence of eq. (3.14a) yields $\boldsymbol{b} \cdot \boldsymbol{\nabla}\alpha + \boldsymbol{\omega} \cdot \boldsymbol{\nabla}\beta = 0$; assuming incompressibility, eq. (3.14b) yields:

$$\boldsymbol{b} \cdot \boldsymbol{\nabla}\beta = -\boldsymbol{r} \cdot \text{curl}\, \boldsymbol{L}.$$

The most studied subset of eqs. (3.14a–c) above is one for which $\gamma_i = 0$, $\forall i$; we then have:

$$\boldsymbol{j} = \text{curl}\, \boldsymbol{b} = \alpha \boldsymbol{b} + \beta \boldsymbol{\omega}, \tag{3.15a}$$

$$\boldsymbol{v} = \beta \boldsymbol{b}. \tag{3.15b}$$

For constant β, we again have an fff when $\beta^2 \neq 1$:

$$\boldsymbol{j} = \frac{\alpha}{1 - \beta^2} \boldsymbol{b}, \tag{3.16}$$

but with non-zero velocity proportional to the magnetic field. The solutions mentioned by Tsinganos (1981) fall in this category, but in fact are more general, since the third components of the fields are not necessarily proportional (B.C. Low, private communication).

The solution for $\beta = \pm 1$ is one with pure Alfvén waves:

$$\boldsymbol{v} = \pm \boldsymbol{b}, \tag{3.17}$$

with maximal correlation E^C; it also corresponds to $\alpha \equiv 0$; note that it does not give information on what range of scales, or equivalently of wavenumbers, the solution sets in, contrary to the case of eq. (3.16). This will be discussed further in

section 7.5. Also note that, when $\beta = 0$, we always obtain an fff, whatever the other constraints that are imposed. When $\beta \neq 0$, however, and taking into account the angular momentum invariants, which are bound to play a role, e.g., in the collapse of a molecular cloud, the solution is no longer force-free.

3.4. The two-dimensional case

The magnetic helicity invariant may now be replaced by the squared magnetic potential, and only one invariant for the angular momentum remains, say in the z-direction. The general equations for the equilibrium with minimal energy are the same as in the three-dimensional case, except the one involving the magnetic variable, which now reads:

$$\boldsymbol{j} = \alpha \boldsymbol{a} + \beta \boldsymbol{\omega}; \tag{3.18}$$

all three variables are scalar, along z, and eq. (3.18) is thus the equivalent of the force-free condition in the two-dimensional case, for which clearly $\boldsymbol{j}$ and $\boldsymbol{b}$ cannot be parallel. Taking again the incompressible limit, with $\rho = \rho_0 =$ constant, the system now reduces to:

$$\boldsymbol{v} - \boldsymbol{L} \times \boldsymbol{r} = \beta \boldsymbol{b}, \tag{3.19}$$

together with eq. (3.18); here $\boldsymbol{L} = \gamma \hat{\boldsymbol{e}}_z$. For zero angular momentum, $\boldsymbol{v}$ and $\boldsymbol{b}$ are aligned.

$$\boldsymbol{v} = \beta \boldsymbol{b} \tag{3.20}$$

and

$$j = \frac{\alpha}{1 - \beta^2} a = -\nabla^2 a, \tag{3.21}$$

for constant β, a solution similar to the one in the three-dimensional case. In Fourier space this determines the wavenumber for which the solution sets it. Again, the fully correlated Alfvénic state for which $\beta = \pm 1$, with j undetermined ($\alpha a = 0$), appears as a special case. In the general case, taking the curl of eq. (3.19) yields, assuming $\partial_z \equiv 0$:

$$\omega - (2 + \boldsymbol{r} \cdot \nabla)\gamma = \beta j.$$

For constant γ and for $\beta^2 \neq 1$, we obtain:

$$\omega = \frac{\alpha \beta}{1 - \beta^2} a + \frac{2\gamma}{1 - \beta^2}. \tag{3.22}$$

a generalization of eq. (3.21) for $\gamma \neq 0$. When $\beta = \pm 1$, it is the velocity, corrected by a contribution stemming from angular-momentum conservation, which is aligned with the magnetic field, with now $\alpha a = \mp 2\gamma$. For zero angular momentum, the competition between conservation of magnetic anastrophy, E^{a}, and of correlation, E^{C}, is examined further in section 7.6.

3.5. *Oscillations in a radio jet*

Observations indicate that the apparent width of a jet oscillates with increasing distance from the AGN core. The degree of linear polarization oscillates as well with angular distance from the core, with a wavelength $\lambda_0 \sim 2.5R$, where R is the jet radius, whereas the ridge line of the jet shows an oscillation with $\lambda_{\mathrm{r}} = 5R$. A possible explanation for such oscillations comes from the minimum-energy principle just described. The argument is as follows (Königl and Choudhuri 1985, Königl 1987). Using the condition for a linear force-free field, i.e. $\nabla \times B = \mu B$ with μ constant, associated with constant global magnetic helicity, H^{M}, and with $B_r(R) = 0$, the minimum-energy configuration in cylindrical coordinates is given by a linear superposition of the $m = 0$ and $m = 1$ modes, involving the Bessel functions of the first kind $J_0(y)$ and $J_1(y)$, where the argument is $y = (\mu^2 - k^2)^{1/2} r$ and where $m\theta + kz$ is the phase. The point made by Königl and Choudhuri is that the axisymmetric $m = 0$ mode is the lowest-energy configuration for:

$$\mu R < 3.11.$$

Above that value, the non-axisymmetric $m = 1$ mode is energetically favorable, with $\mu R = 3.11$ and $kR = 1.23$, corresponding to a wavelength $\lambda \simeq 5R$, as observed in NGC 6251; but see the discussion in the aforementioned papers for other possibilities, taking more constraints into consideration to account for the observations of 3C 219, or for the braided field configuration in emission knot A of the M 87 jet.

3.6. *Statistical mechanics of truncated systems*

The minimization of energy while preserving other invariants, may receive further support from statistical mechanics. In the simplest case, in the absence of dissipative processes, an assembly of coupled modes evolves, for long times, towards a state of equipartition of the energy among the modes, $U(k) = \text{constant}$.

In three dimensions, the energy spectrum, summing over spherical shells, is $E(k) = 4\pi k^2 U(k)$, thus leading to an ultraviolet catastrophe, the accumulation of energy in the high-wavenumber region; this UV catastrophe in fact sometimes happens in numerical simulations with insufficient dissipation through either viscosity or artificial viscosity. As already noted by Onsager (1949), however, when

the dynamics of a system which can be seen as an assembly of coupled oscillators, preserves more than one invariant, the resulting equilibrium may be of a very different nature; the distribution now depends on two effective temperatures, associated with the two invariants, and in some cases the resulting spectra will peak at low wavenumber: this is the case for both the two-dimensional MHD problem (Montgomery et al. 1979, Kraichnan and Montgomery 1980) and the three-dimensional one (Frisch et al. 1974): non-linear interactions tend to redistribute the excitation among the available modes both to smaller and to larger wavenumbers. When dissipation is switched on, it is unlikely to affect the large scales very much, at least within a few eddy turn-over times, so that indeed one can predict the onset of inverse cascade towards large scales. This formalism can be rewritten in terms of maximal entropy in plasmas, see Montgomery (1985).

3.7. Self-organization of flows

The system of dual cascades towards both small scales and large scales, with the subsequent formation, by non-linear mode coupling, of both a small-scale chaotic excitation, probably spatially intermittent, and large-scale coherent structures, long-lived (although also presenting some chaos, as will be discussed in section 4.4), is a rather common occurrence in fluid and plasma physics (see the review of Hasegawa (1985)). In isentropic 3D flows, the kinetic helicity is still an invariant (Gaffet 1985), and it thus may lead to an inverse cascade again; instability has in fact been demonstrated (Moiseev et al. 1982) in the linear case.

4. Topology of magnetic field lines

4.1. Knots are vital

Let us first divert our attention to biology, a field in which the theory of knots plays an important role (Frank-Kamenetski and Vologodski 1981) in understanding the properties of DNA – desoxyribonucleic acid. As is well known, it is structured as a double helix, but, like any piece of string, it can be open-ended (OE) or closed in a circular fashion (CC). Moreover, it can be knotted and/or twisted, and several of such strings can be linked. The same can be said for magnetic field lines, and the question now is: does it matter? It seems that it does, and I strongly encourage you to read the afore-mentioned paper.

Although the topology of ribbons of DNA can change in time, evolving to a configuration with lower energy through interactions with enzymes, it is of interest at some time to identify and classify the different configurations of DNA strands that are observed, and in particular to be able to decide which ones are

equivalent. This problem – fundamental to knot theory – can be tackled, on the one hand, observationally, by measuring the amount of "supercoiling" in the DNA (op. cit.), and, on the other hand, one can resort to the theory of knots and linkages (Crowell and Fox 1963). In particular, invariants can be attributed to knots belonging to the same class of isotopy (obtained from one another by continuous isotopic deformation), with the standard form of a knot being the one with the minimal number of crossings when projected onto a plane (note that topology is intrinsically three-dimensional: knottedness is the property of how a curve is embedded in three-dimensional space). Having defined a sense of rotation along the knot, by numbering the different segments between each crossing and by assigning ± 1 to each according to whether the crossing is a top one or a bottom one, one can define an Alexander polynomial for each knot, hopefully different for different knots. However, the polynomials for the trefoil knot and for its mirror-image, depicted in fig. 2, are equal, although such knots are not equivalent. However, new types of polynomials have been recently devised that do distinguish between them (Jones 1986). Let us finally mention that most of what is known on knots is for tamed knots; the wild ones, where there is loss of analyticity, e.g. because of self-similarity (Trotter 1963), are less amenable to treatment.

Many properties of CC-DNA differ from the OE form, because of topological restrictions. Moreover, the stress in the DNA ribbons induced by coiling, twisting, and knotting weakens it: CC-DNA can be more easily modified by mutagens and by carcinogens. Furthermore, a knotted ribbon, when duplicated by cutting along it, gives rise to two linked ribbons (or sometimes one long one, as in the case of the Moebius strip), which clearly defies the required properties for reproduction and give rise to problems. Thus, knots are of vital importance.

4.2. *Magnetic helicity and linkage of field lines*

Take two flux tubes, ϕ_1 and ϕ_2; a simple way to distinguish between a configuration where these tubes are free, from one where they are linked (see fig. 3), is to compute the amount of magnetic flux piercing any surface S with oriented normal N, sustained by the curve C_1 (or equivalently C_2).

Let us now evaluate the magnetic helicity, $H^{\mathrm{M}} = \langle \boldsymbol{a} \cdot \boldsymbol{b} \rangle$, of the two configurations depicted in fig. 3. In the unlinked case it is zero, since no flux passes through S; in the simple linked case, using Stokes' theorem, one finds:

$$H^{\mathrm{M}} = -2\phi_1\phi_2; \tag{4.1}$$

the factor two comes from computing the flux through both surfaces S_1 and S_2, and the sign is positive for the right-hand screw rule and negative otherwise.

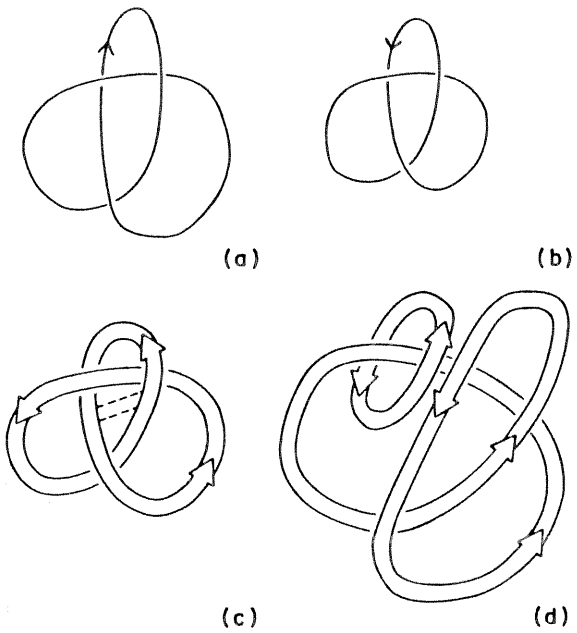

Fig. 2. The right-handed (a) and left-handed (b) trefoil knot (each other's mirror image); its decomposition by insertion of a flux tube (c) into linked flux tubes (d), one of which is twisted.

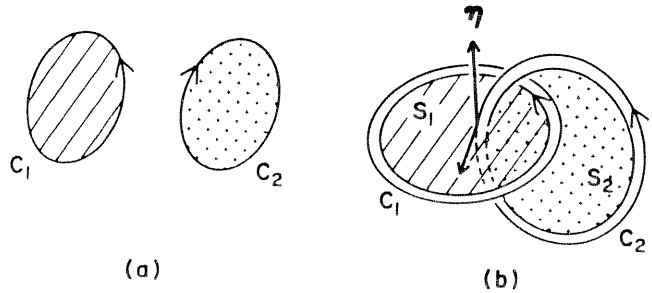

Fig. 3. Two flux tubes that are disjointed (a), leading to zero magnetic helicity, or linked (b).

The integral of eq. (4.1) is gauge-invariant, and can be computed for simply connected volumes; it is also a non-local quantity and depends – through the potential – on the whole flow.

In the same way, the kinetic helicity, $\langle v \cdot \omega \rangle$, measures the degree of knottedness

of vortex lines and the cross correlation, $\langle \boldsymbol{v} \cdot \boldsymbol{b} \rangle$, the mutual linkage of the velocity and the magnetic field (Moffatt 1969, Zeldovich et al. 1983).

In the case of the trefoil knot, the computation of its helicity is best done by arranging it as two linked loops by an auxiliary flux tube of the same strength, ϕ, and in this case, the helicity is in fact $-3\phi^2$, because the large loop (see fig. 2c) has a twist in it (Berger and Field 1984). For some configurations, though, such as the Borromean rings, in which no two rings are linked, but three are, the helicity is zero and some other (third-order?) integral constraint should be devised.

Also note that zero total helicity does not mean that there is no linkage of field lines, but that $\pm$ linkages have canceled exactly.

In a continuous magnetic fluid, the field lines do not have such a simple structure as that depicted in fig. 3. We saw in previous sections that they can in fact be chaotic; remember, Arnold showed that for inviscid stationary incompressible fluids only Beltrami flows can be chaotic (see eq. (3.12)).

Examples of axisymmetric helical flows are given in Moffatt (1969); taking a steady blob of vorticity confined to a sphere with $R < a$, and writing, in cylindrical polar coordinates (x, r, ϕ),

$$\boldsymbol{v} = \left(\frac{1}{r} \frac{\partial \psi}{\partial r}, -\frac{1}{r} \frac{\partial \psi}{\partial x}, w \right). \tag{4.2}$$

with $\psi = \psi(x, r; t)$, for a steady flow:

$$w = C(\psi)/r$$

and

$$p/\rho + \tfrac{1}{2} v^2 = H(\psi),$$

where $v^2 = \boldsymbol{v} \cdot \boldsymbol{v}$ and where p is the pressure. A family of solutions is given by:

$$H = H_0 + \lambda \psi, \qquad C = \pm \alpha \psi, \tag{4.3}$$

where H_0, λ, and α are constants. Note that eq. (4.2) is an extension of the Hill (1894) vortex, for which $w \equiv 0$ and which therefore is strictly non-helical. In spherical polar coordinates (R, θ, ϕ) we have:

$$\psi = R^2 \sin^2 \theta \left[\frac{\lambda}{\alpha^2} + A \left(\frac{\alpha}{R} \right)^{3/2} \mathcal{J}_{3/2}(\alpha R) \right], \tag{4.4}$$

where A is constant and $\mathcal{J}$ denotes a Bessel function. These solutions contain as particular cases that of Chandrasekhar (1956) for a Beltrami flow and that of

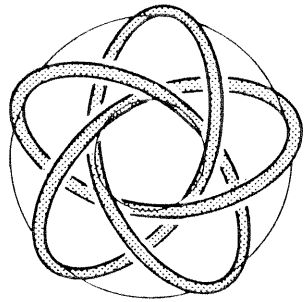

Fig. 4. A (3; 5) torus knot: one of many exact solutions to the MHD equations; this represents the field lines, with $\boldsymbol{v} = \pm\boldsymbol{b}$.

Prendergast (1957) for an equilibrium star. The surfaces ψ = constant consist of a family of nested tori for $R < a$.

They close when their pitch, p_i, is such that $p_i = 2\pi m/n$, where the line goes m times around the large side of the torus and n times around the small side. For example, for the self-knotted structure in fig. 4 $m = 3$ and $n = 5$, and for the trefoil knot $m = 2$ and $n = 3$. To see this, pack the lines either close to the central hole, giving m, or close together around the donut, giving n (Neuwirth 1979). The toric knots, which are all classified, will appear again as topological solitons (section 4.5).

4.3. Magnetostatic equilibrium

4.3.1. The derivation

I will here follow a paper by Moffatt (1985) concerning the emergence of such equilibria and their stability. The point is to consider again a structure as depicted in fig. 3b and look at the dynamical consequences. In the presence of viscosity, the total (kinetic plus magnetic) energy of the configuration will decay, but because of the non-trivial topology of the magnetic field, which cannot change in the absence of resistivity, the energy will reach a non-zero lower bound. This can be written directly using Schwarz's inequality:

$$E^{\mathrm{M}} \geqslant (H^{\mathrm{M}})^2/\langle a^2 \rangle. \tag{4.5}$$

The use of topological constraints to demonstrate the existence of non-zero energy solutions is found in gauge field theories since Polyakov (1974) and 't Hooft (1974). Pictorially, one can imagine that, because of flux conservation, as the energy gets smaller, the flux tubes in fig. 3b grow bigger and at some time they touch

and the energy can no longer decrease; by the way, in the process a current sheet is likely to form; the minimum energy is attained when one of the flux tubes wraps itself around the other one reaching an axisymmetric configuration, or vice-versa (no unicity of the solution).

The end result of this process of relaxation is one with $\boldsymbol{v} \equiv 0$ and a magnetostatic equilibrium field $\boldsymbol{B}_E$ satisfying:

$$\boldsymbol{j}_E \times \boldsymbol{B}_E = \nabla p_E. \tag{4.6}$$

$\boldsymbol{B}_E$ may have tangential discontinuities, and is not necessarily unique. This equilibrium is more general than that of a force-free field, either globally ($\boldsymbol{j} = \alpha_0 \boldsymbol{B}$), this being also called a linear fff, or locally ($\boldsymbol{j} = \alpha(r)\,\boldsymbol{B}$). The constraint (4.6), as the Beltrami one (3.12), leads to chaotic field lines when $\nabla p_E \equiv 0$ in some subdomain of the flow and $\nabla\alpha(r) \equiv 0$. Note that here three-dimensionality is essential; e.g., the ABC flow is not chaotic when $ABC = 0$. The implication for MHD fluids is that it may consist of large blobs, labeled by i, of force-free fields, $\boldsymbol{j} = \alpha_i \boldsymbol{b}$, α_i = constant with $\alpha_j \neq \alpha_i$, between which there are localized current sheets, where all the dissipation is concentrated (see fig. 11 in Moffatt (1985) and adapt it to the MHD case). Now, here $\boldsymbol{v} \equiv 0$; but we know that, if initially $E^C = \langle \boldsymbol{v} \cdot \boldsymbol{b} \rangle$ is non-zero, i.e. if there is a net overall linkage between velocity and magnetic field lines, then this also is likely to be preserved (this point is discussed in section 7; recall that E^C is an invariant). One possibility, not magnetostatic, is to have either equipartition solutions $\boldsymbol{v} = \pm \boldsymbol{b}$ (but the fff condition needs not necessarily be fulfilled then) or parallel solutions $\boldsymbol{v} = \lambda \boldsymbol{b}$, with $\lambda(\boldsymbol{r})$ dependent on space. An example of such a solution is given in Tsinganos (1981), the magnetic analog of the spherical Hill vortex (Hill 1894). But then angular momentum breaks the Beltramization of flows, according to the analysis of Woltjer (1958), as shown in eq. (3.14a). So what is the end state? This question seems a good candidate for numerical investigation, but will require usage of many CPU and interactive graphic resources. Similar questions concerning the Euler flow (are they large blobs of helical flow separated by vorticity sheets? Are helicity and dissipation anti-correlated? Does reconnection of vortex lines occur?) are being investigated presently by several authors, and there is no general agreement, partly because they are at the border of what can be done today with computers; and remember that they are less computationally intensive than their MHD counterparts.

Finally note that, were this conjecture to be correct, the large-scale coherent structures, long-lived because the non-linear terms cancel almost exactly and also because the flow is at high kinetic and magnetic Reynolds number, are also the site of chaos in the sense that their field lines are extremely complex. There are a few examples in the literature showing magnetic field lines which indeed are complex. On the other hand, the small scales are spatially intermittent, as well as being presumably temporally chaotic.

4.3.2. Stability properties

The stability of the magnetostatic equilibrium (4.6) is analyzed by Moffatt (1986): one uses an energy principle, which will not be detailed here, and can conclude to the stability of the field for the MHD problem in some cases. As for force-free fields, the situation is somewhat confusing. The ABC flow (see eq. (3.11)) seems unstable, in the inviscid case for long-wavelength perturbations (Moffatt 1986) as well as in the viscous case, this being shown mostly numerically (Galloway and Frisch 1987). One of the first papers concerning the eventual instability of fff is that of Voslamber and Callebaut (1962). There may be some fff configurations, on the other hand, that are stable, both in Cartesian and in spherical geometry (Low 1988a, b).

The topological stability, now, of the magnetostatic equilibrium, i.e. that concerned with whether an equilibrium configuration will preserve its topological nature when perturbed, was examined in the context of Hamiltonian systems by Tsinganos et al. (1984). They conclude that in the symmetrical case (one ignorable coordinate), such states are unstable, and that the velocity plays a role in the equilibrium configuration: hence, magnetic fields are correlated to "activity" of astrophysical systems, as first pointed out by Parker (1979). But, as emphasized by the authors, there is not as yet proof that MHD equilibrium must necessarily be symmetric.

4.4. Where does the energy go?

In evolving towards a minimum-energy configuration, energy is indeed lost to the surroundings; these phenomena have thus been implicated by several authors to heat the corona (Heyvaerts and Priest 1984), or to power the radio jets (Königl 1987), or in the fusion community, to heat the plasma, taking into account the incomplete relaxation to a minimal-energy state (Turner and Christiansen 1981). However, the rate of dissipation of magnetic helicity itself is too slow, in the context of coronal loops, to be of any use (Berger 1984).

4.5. Topological solitons

Topological solitons, or t-solitons, are invoked, mainly in the Soviet literature (Kamchatnov 1982, Moiseev et al. 1982, Sagdeev et al. 1986, and references therein), by analogy with field theory. The ideas involved are not unrelated to what has been discussed up to now, but the technical means to write an exact solution of the incompressible MHD equations are different. In a classical soliton, described e.g. by the Korteweg de Vries equation, non-linearities (which would lead to the formation of a shock) are exactly balanced by dispersive terms, so that stable solutions arise, with particularly spectacular properties (Zabusky 1981), due in part

to the infinite number of invariants of the equations and to the related property of integrability (Ablowitz et al. 1980, Weiss et al. 1983).

By analogy, a topological soliton is a localized structure that arises through balance between the steepening effect of the non-linearities of the primitive MHD (or other) equations and the topological constraints on the dynamic evolution of the flow, stemming from the linkage of field lines on the one hand, and the frozen-in flux-conserving property on the other hand. The latter reads:

$$\frac{\partial \boldsymbol{F}}{\partial t} + \boldsymbol{v} \cdot \nabla \boldsymbol{F} = \boldsymbol{F} \cdot \nabla \boldsymbol{v}, \tag{4.7}$$

where $\boldsymbol{F}$ is some field, not necessarily the magnetic field. These frozen-in fields are related to the Lagrangian invariants, I, defined, as usual, as:

$$\left(\frac{\partial}{\partial t} + \boldsymbol{v} \cdot \nabla\right) I = \frac{\mathrm{D}I}{\mathrm{D}t} = 0, \tag{4.8}$$

meaning that I (e.g., the density in an incompressible fluid) is simply carried along by the fluid. Frozen-in invariants can be constructed from a set of two (or more) Lagrangian invariants.

The spatial localization of these t-solitons arises from the high degree of entanglement of their field lines. Using techniques of differential geometry, and in particular mapping $\mathcal{R}^3$ into the sphere $\mathcal{S}^3$ embedded in $\mathcal{R}^4$ via stereographic projection, these authors arrive at a solution whose field lines lie on stratified tori and wind around them with rotation frequencies ω_1 and ω_2. The magnetic field reads:

$$\boldsymbol{B} = \frac{-2B_0R^4}{(R^2+r^2)^3}[2(\omega_1 Ry + \omega_2 xz), -2(\omega_1 Rx - \omega_2 yz), \omega_2(R^2 - r^2 + 2z^2)], \tag{4.9}$$

where R is the characteristic size of the vortex solution and where $r^2 = x^2+y^2+z^2$. Further, writing $\boldsymbol{v} = \pm\boldsymbol{B}$ does provide a solution. When $\omega_1 = m$ and $\omega_2 = n$, one recovers the toric-knot solution, this time not magnetostatic but fully correlated.

The expression (Sagdeev et al. 1986) for the magnetic energy

$$E^{\mathrm{M}} = \frac{\pi(\omega_1^2 + \omega_2^2)}{16} B_0^2 R^2 \tag{4.10a}$$

and that for the magnetic helicity

$$H^{\mathrm{M}} = \frac{\pi\omega_1\omega_2 R^3}{2} B_0^2 \tag{4.10b}$$

show that the solutions with the same "topological charge" (or linkage), mn, have different energies; in this sense, the solution $\omega_1 = 1, \omega_2 = mn$ is less favorable than the one with $\omega_1 = m, \omega_2 = n$. Assuming that all the energy is concentrated at scale R, one can see that the magnetic helicity is maximal for $\omega_1 \sim \omega_2$.

The winding frequencies are not necessarily constant; e.g. (Sagdeev et al. 1986):

$$\omega_1 = f(1 + r^2 - 2\sqrt{x^2 + y^2}),$$

with f an arbitrary function would represent a solution whose lines of force are more complex than the simple toric knots.

The present author must confess to her inability to fully understand by which means these solutions have been obtained. More important is to determine whether this original approach does lead to new solutions or is yet another way to obtain some toric-knot solutions, such as those already unraveled by Moffatt (1969) and by Tsinganos (1981), except for the important, but in some sense trivial, extension to the dynamic case through the Alfvén wave condition, $\boldsymbol{v} = \pm\boldsymbol{b}$. Do they relate at all to the helical version of the Hill vortex, as described in Moffatt (1969)?

Furthermore, are such solutions stable? Topologically stable? And are they attractive? What role does dissipation, viscous or resistive, play in their evolution and stability? How to reconcile such concepts with traditional reconnection processes? Work along these lines is presently in progress. Several numerical experiments on 3D neutral fluids may also shed some light on such processes. They show a strong tendency of vortex filaments to become anti-parallel (Siggia 1985), including the trefoil knot (Kida and Takaoka 1987), which starts out with non-zero helicity.

It does seem, at the present time, that the simple vortex knotted solutions, axisymmetric or 3D, studied in the astrophysical context (Tsinganos 1981, 1982a, b, c, and references therein), in the fusion context (Taylor 1986, and references therein), or in a more theoretical context (Sagdeev et al. 1986, and references therein), are plausible attainable solutions. In that light, it would be of interest to look for actual observations of such structures in experimental flows in plasma fusion, or in astrophysics; in the latter case, the Sun is the most likely candidate. Indeed, braided loops in flares have been documented and are being studied in this context (Berger 1987); also, direct measurements of the three components of photospheric fields (Lites and Skumanich, private communication) indicate that indeed three-dimensionality is important.

4.6. The emerging dynamical picture

The opposing views of turbulence – either chaotic small scales, to be dealt with by statistical techniques, or large-scale long-lived coherent structures, which can be

modeled in a simple way – may in fact be reconciled: in the presence of more than one invariant, as noted in section 3.7, energy (in general) will cascade to small scales, scales which will likely be temporally chaotic and spatially intermittent, and the other invariant – the magnetic helicity, in three dimensions – will cascade to large scales, plausibly forming those coherent structures that may, e.g., be observed in the Sun (braids on solar flares). The added feature here is that this description of turbulence is energetically feasible, seems stable in some MHD cases, and corresponds to a fluid organized in large blobs in which the flow is Beltrami and/or force-free, with different large blobs having different constants of proportionality between the fields and their curl; in between, current and/or vorticity sheets form, which account for the intermittency of the small scales. This is the basis of the conjecture described by Moffatt (1985).

Taking the pure-fluid case, numerical experiments have not been able yet to disprove or support this picture, and this in fact represents a very active field of research. In MHD, one should also look at the equivalent conjecture; powerful graphics may well be essential, however.

4.7. Change of topology

Magnetic diffusivity has not played an essential part in the preceding analysis.

When non-zero, the current sheets, which are likely to form in establishing the equilibrium configurations, will be unstable, e.g., to the tearing-mode (Furth et al. 1963). However, current numerical results indicate that, in the presence of either a non-zero and turbulent velocity field, or non-zero viscosity, or both, the sheets, at least in two-dimensions, are much more stable than expected, for reasons not entirely understood. The three-dimensional reconnection problem, on the other hand, is almost unknown and open to much research. Reconnection is too vast a topic to be treated here. In section 6.7 the role of turbulence on reconnection will be briefly discussed.

5. Transport coefficients

5.1. Introduction

In view of the difficulty to deal either analytically or numerically with the full-blown, non-linear problem, several schemes have been devised to write simple models, using various techniques, e.g. that with short correlation time (Fitremann and Frisch 1969, Hoyng 1987) or one of many variants of the Heisenberg turbulent viscosity. These models are particularly useful in astrophysics, where there is no hope to be able to integrate numerically the flow at the required Reynolds number.

Therefore, an accurate description of the small-scale flow, that can be incorporated in a broader description of the fluid, is needed. In this section, we will describe mainly one such possible algorithm, providing the transport coefficients in the MHD case through two-point closures.

5.2. The closure equations in MHD

Let us now write the three-dimensional MHD equations in the following compact form:

$$\frac{\partial \mathcal{X}_a}{\partial t} = \mathcal{L}_0 \mathcal{X}_a + \mathcal{L}_{abc} \mathcal{X}_b \mathcal{X}_c \,. \tag{5.1}$$

where $\mathcal{L}_0$ is a linear operator that need not be detailed and where $\mathcal{X}$ is the six-dimensional vector $\mathcal{X} = (\hat{\boldsymbol{v}}, \hat{\boldsymbol{b}})$; the subscript a is shorthand for three indices: $a = (\alpha, i, k)$, where $\alpha = (v, b)$, $i = (1, 2, 3)$ and $\boldsymbol{k}$ is the wavevector, $\hat{v}_i(\boldsymbol{k})$, and $\hat{b}_i(\boldsymbol{k})$ being the Fourier components of the velocity and magnetic field. We assume that the non-linear operator $\mathcal{L}_{abc}$ is written in a symmetrical form with respect to the last two summation indices:

$$\mathcal{L}_{abc} = \mathcal{L}_{acb}\,; \tag{5.2}$$

when the magnetic field is identically zero, this operator reduces to:

$$\mathcal{L}\begin{pmatrix} v & v & v \\ i & j & l \\ k & p & q \end{pmatrix} = -\frac{\mathrm{i}}{2} P_{ijl}(\boldsymbol{k})\, \delta(\boldsymbol{k} - \boldsymbol{p} - \boldsymbol{q}), \tag{5.3}$$

with

$$P_{ijl}(\boldsymbol{k}) = k_j P_{il}(\boldsymbol{k}) + k_l P_{ij}(\boldsymbol{k}), \tag{5.4a}$$

and

$$P_{ij}(\boldsymbol{k}) = \delta_{ij} - \frac{k_i k_j}{k^2} \tag{5.4b}$$

being the projection operator ensuing incompressibility. In MHD, the operator arising from the Lorentz force has the same form as eq. (5.3); in the induction equation, after symmetrization of the equation in Fourier space, the corresponding operator reads:

$$\mathcal{L}\begin{pmatrix} b & b & v \\ i & j & l \\ k & p & q \end{pmatrix} = \frac{\mathrm{i}}{2} \delta_{ijl}(\boldsymbol{k})\, \delta(\boldsymbol{k} - \boldsymbol{p} - \boldsymbol{q}). \tag{5.5}$$

where

$$\delta_{ijl}(\boldsymbol{k}) = k_j \delta_{il} - k_l \delta_{ij}. \tag{5.6}$$

and where δ_{ij} is the Kronecker symbol. The symmetrical MHD equations thus read:

$$\left(\frac{\partial}{\partial t} + \nu k^2\right) \hat{v}_i(\boldsymbol{k}) = -\frac{\mathrm{i}}{2} P_{ijl}(\boldsymbol{k})[\hat{v}_j(\boldsymbol{p})\hat{v}_l(\boldsymbol{q}) - \hat{b}_j(\boldsymbol{p})\hat{b}_l(\boldsymbol{q})], \tag{5.7a}$$

$$\left(\frac{\partial}{\partial t} + \eta k^2\right) \hat{b}_i(\boldsymbol{k}) = \frac{\mathrm{i}}{2} \delta_{ijl}(\boldsymbol{k})[\hat{v}_j(\boldsymbol{p})\hat{b}_l(\boldsymbol{q}) - \hat{b}_j(\boldsymbol{p})\hat{v}_l(\boldsymbol{q})], \tag{5.7b}$$

where the temporal dependence of the fields is understood. From eqs. (5.7a, b) follows straightforwardly the definition of $\mathcal{L}_{abc}$. We now define the various covariances that are needed to describe MHD turbulence. Assuming homogeneity and isotropy, we can decompose the one-time covariances into their symmetrical and their helical part; they read:

$$2\langle \hat{v}_i(\boldsymbol{k})\hat{v}_j^*(\boldsymbol{k})\rangle = P_{ij}(\boldsymbol{k})U^{\mathrm{V}}(k) - \mathrm{i}\epsilon_{ijl}k_l\widetilde{U}^{\mathrm{V}}(k), \tag{5.8a}$$

$$2\langle \hat{v}_i(\boldsymbol{k})\hat{b}_j^*(\boldsymbol{k})\rangle = P_{ij}(\boldsymbol{k})\widetilde{U}^{\mathrm{C}}(k) - \mathrm{i}\epsilon_{ijl}k_l U^{\mathrm{C}}(k), \tag{5.8b}$$

$$2\langle \hat{b}_i(\boldsymbol{k})\hat{b}_j^*(\boldsymbol{k})\rangle = P_{ij}(\boldsymbol{k})U^{\mathrm{M}}(k) - \mathrm{i}\epsilon_{ijl}k_l\widetilde{U}^{\mathrm{M}}(k), \tag{5.8c}$$

with $k = [\boldsymbol{k}]$ and where $\widetilde{U}$ indicates a pseudo-scalar. In three dimensions, the energy spectra are:

$$E^{\mathrm{V}}(k) = 2\pi k^2 U^{\mathrm{V}}(k) \quad \text{and} \quad E^{\mathrm{M}}(k) = 2\pi k^2 U^{\mathrm{M}}(k);$$

the correlation spectrum – a pseudo-scalar, like the helicities – is:

$$E^{\mathrm{C}}(k) = 2\pi k^2 \widetilde{U}^{\mathrm{C}}(k);$$

the kinetic and magnetic helicity spectra are:

$$H^{\mathrm{V}}(k) = 2\pi k^4 \widetilde{U}^{\mathrm{V}}(k) \quad \text{and} \quad H^{\mathrm{M}}(k) = 2\pi k^2 \widetilde{U}^{\mathrm{M}}(k).$$

The relationships between the U spectra and the E spectra in d dimensions can be found in Fournier (1983). The realizability conditions yield:

$$|H^{\mathrm{V}}(k)| \leqslant kE^{\mathrm{V}}(k). \tag{5.9a}$$

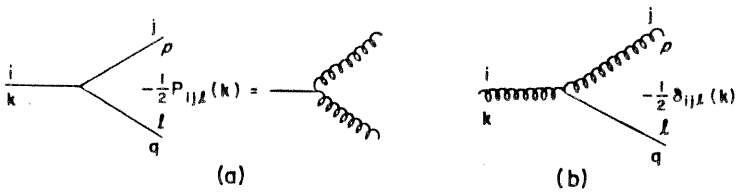

Fig. 5. Basic diagrams showing the quadratic non-linearities of the MHD equations: the straight line represents the i-th component of the velocity field at wavevector $\boldsymbol{k}$ and the wavy line the magnetic field $b_i(\boldsymbol{k})$; the two vertices appear in the momentum equation (a) and the induction equation (b).

$$|H^{\mathrm{M}}(k)| \leqslant E^{\mathrm{M}}(k)/k, \tag{5.9b}$$

$$|E^{\mathrm{C}}(k)| \leqslant [E^{\mathrm{V}}(k)\, E^{\mathrm{M}}(k)]^{1/2}; \tag{5.9c}$$

when the equality is fulfilled at all wavenumbers for one spectrum (V, M, or C), this is called a state of maximal (V or M) helicity or maximal correlation.

The two-point closures can be calculated from the following lemma (Frisch et al. 1974):

$$\frac{\partial\langle\mathcal{X}\otimes\mathcal{X}\rangle}{\partial t} = \theta\{\mathcal{L}(\mathcal{X}_E,\mathcal{X}_I)\otimes\mathcal{L}(\mathcal{X}_I,\mathcal{X}_E) + \mathcal{L}[\mathcal{L}(\mathcal{X}_E,\mathcal{X}_I),\mathcal{X}_I]\otimes\mathcal{X}_E + \mathcal{X}_E\otimes\mathcal{L}[\mathcal{X}_I,\mathcal{L}(\mathcal{X}_I,\mathcal{X}_E)]\}, \tag{5.10}$$

where θ is a characteristic correlation time, $\otimes$ indicates a tensor product, within which correlated variables are denoted here by the same subscript (either E or I). The algebra to get from eq. (5.10) to the closure equations found in the literature, is lengthy. However, the structure of these equations can be conveniently and easily written a priori when using a graphical representation, which is now given. Although it is directly inspired by the diagrammatic techniques arising in the renormalization-group (RG) approach, it is here meant only as a way to intuitively represent the various second-order interactions that take part in the time evolution of the covariances $\langle\mathcal{X}\otimes\mathcal{X}\rangle$. Let us then represent $v_i(\boldsymbol{k})$ by a straight line labeled by i and $\boldsymbol{k}$, and $b_i(\boldsymbol{k})$ by a solenoidal line, labeled in the same way; the graphical representations of the vertices appearing in eqs. (5.3) and (5.5) are given in fig. 5.

The diagrams are consistent with eqs. (5.7a, b). Now, in the equations for the covariances, it is clear from inspection of eq. (5.10) that there are two basic structures: the first term on the right-hand side of eq. (5.10) has a symmetrical form, shown in fig. 6b, whereas the second form is asymmetrical, and is shown in fig. 6a; fields pertaining to the same covariance are now linked by vertical bars; the third

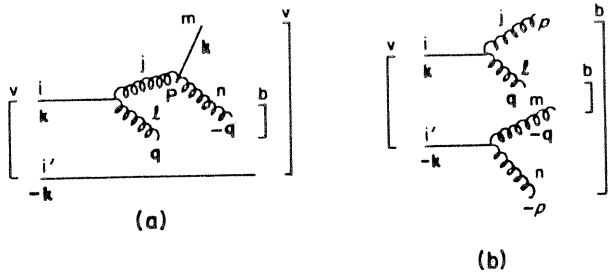

Fig. 6. Diagrams for the master equation (5.4) for the velocity covariance, U^{V} (see text). (a) Absorption term, (b) emission term. Here, homogeneity is taken into account.

term is equivalent to the second one, with the long line on top of the diagram instead of at the bottom.

In these two figures, the diagrams are labeled for the equation for the covariance $U^{\mathrm{V}}_{ii'}(\boldsymbol{k})$, so that we obtain:

$$\frac{\partial U^{\mathrm{V}}_{ii'}(\boldsymbol{k})}{\partial t} = \frac{\mathrm{i}}{2} P_{ijl}(\boldsymbol{k}) \frac{\mathrm{i}}{2} \delta_{jmn}(\boldsymbol{p}) U^{\mathrm{V}}_{mi'}(\boldsymbol{k}) U^{\mathrm{M}}_{nl}(\boldsymbol{q}) + \frac{\mathrm{i}}{2} P_{ijl}(\boldsymbol{k}) \frac{\mathrm{i}}{2} P_{i'mn}(-\boldsymbol{k}) U^{\mathrm{M}}_{jn}(\boldsymbol{p}) U^{\mathrm{M}}_{lm}(\boldsymbol{q}) + \cdots . \tag{5.11}$$

The first term on the right-hand side involves the velocity covariance at wavevector $\boldsymbol{k}$, and it can be interpreted as an eddy viscosity: looking at the diagram in fig. 6a, it means that the interaction of a velocity mode at wavevector $\boldsymbol{k}$ and a magnetic mode through Ohm's law produces a magnetic mode which interacts with another magnetic mode through the Lorentz force, and this double interaction (remember, the expansion here is second-order in the non-linear vertices) modifies the velocity mode at $\boldsymbol{k}$. On the other hand, the second term in eq. (5.11) represents the combined effect of magnetic modes at wavevectors $\pm\boldsymbol{p}$ and $\pm\boldsymbol{q}$ through Lorentz forces on the velocity mode at $\boldsymbol{k}$.

At this stage, a branching point appears in the procedure, according to how much or how little structure is put in the covariances. In the simplest case, the isotropic, homogeneous, fully symmetric one, each covariance gives rise to only one spectrum, the energy spectrum. If now the non-mirrorsymmetric part of the correlation tensor is included, to take into account the helicity, as defined in eq. (5.8), eq. (5.11) becomes two equations (real and imaginary part) and each product of covariances gives rise to four terms. This is where the bulk of the work lies, and it might better be done with the help of a program performing the algebra. Note that in computing the helical diagrams which involve products of the anti-symmetric tensor, the

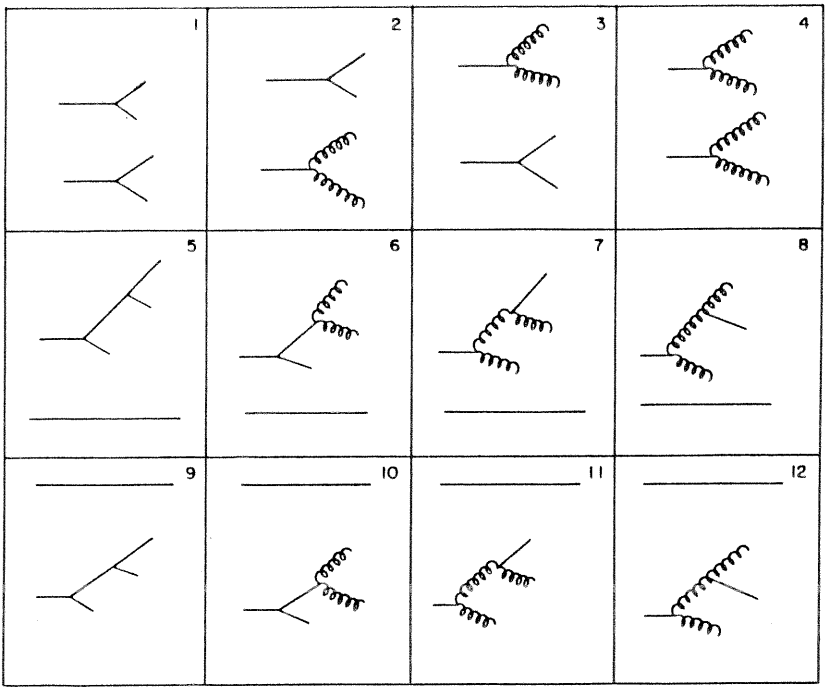

Fig. 7. Graphical representation of the second-order evolution equation for the velocity covariance $U^{V}_{ii'}(\boldsymbol{k})$.

following identity is of use:

$$\epsilon_{abc}\,\epsilon_{ijl} = \delta_{ai}\,\delta_{bj}\,\delta_{cl} + \delta_{aj}\,\delta_{bl}\,\delta_{ci} + \delta_{al}\,\delta_{bi}\,\delta_{cj} - \delta_{ai}\,\delta_{bl}\,\delta_{cj} - \delta_{aj}\,\delta_{bi}\,\delta_{cl} - \delta_{al}\,\delta_{bj}\,\delta_{ci}.$$

Of importance here is to remember that in fact only one vertex appears in eqs. (1.33a, b), the vertex in the second equation being deduced from the first one by interchanging + and −, so that the algebra can be reduced by a factor two. This algebra consists in computing geometrical coupling coefficients depending on the three wavevectors $\boldsymbol{k}$, $\boldsymbol{p}$, and $\boldsymbol{q}$, but the structure of the equations can be directly obtained by simple inspection of the diagrammatic representation of the master equations for the various covariances, given in fig. 7 for the velocity covariance and in fig. 8 for the magnetic covariance.

Some of the diagrams shown in either fig. 7 or in fig. 8 are equal, and can be accounted for by multiplicity factors. To further reduce the number of coefficients appearing in the closure equations, for analytical simplicity, and for numerical

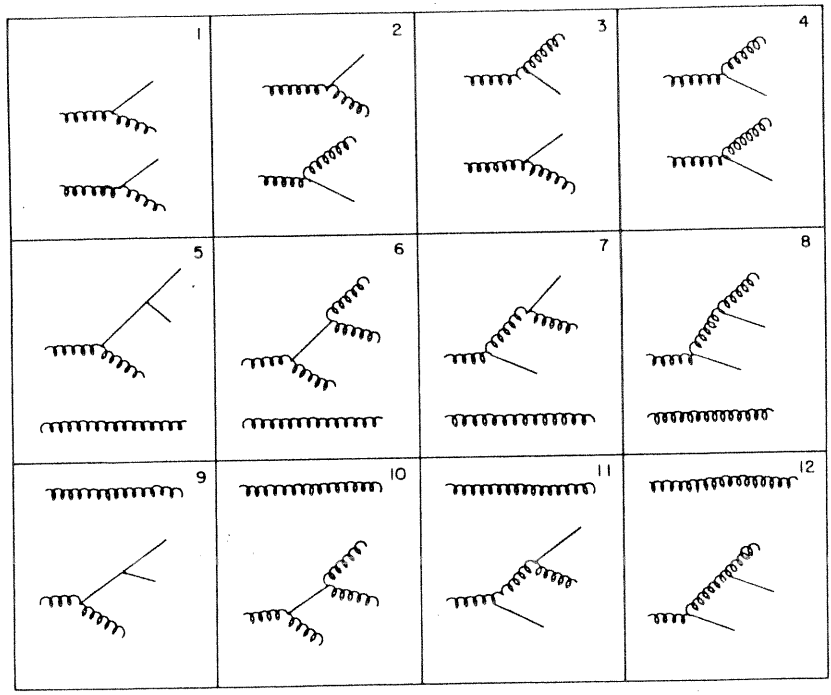

Fig. 8. Same as fig. 7 for the magnetic covariance $U^{M}_{ii'}(\boldsymbol{k})$.

convenience because of storage, and also to check the algebra in doing so, one makes use of the conservation laws eqs. (3.1) to (3.5), written in a detailed way: a useful remark is that *each* class of non-linear terms VV, VM, MM, $V\tilde{V}$, ..., following the notation in table 1 of Pouquet et al. (1976), conserves *separately* the invariants. For example, the conservation of total energy when $\nu \equiv 0$, $\eta \equiv 0$, written in Fourier space with integrating over all three wavenumbers $\boldsymbol{k}$, $\boldsymbol{p}$, and $\boldsymbol{q}$, implies, among other things, that there is a relationship between the geometrical coefficient stemming from diagram 4 in fig. 7 and those stemming from diagrams 6 and 10 in fig. 8, these two being equal. Omitting a lot of algebra, it reads:

$$2k^2\, a(k, p, q) = p^2\, j(p, k, q) + q^2\, j(q, k, p),$$

with

$$a(k, p, q) = \tfrac{1}{2}(1 - xyz - 2y^2 z^2)$$

and

$$j(k, p, q) = \frac{p}{k}\, z(1 - x^2);$$

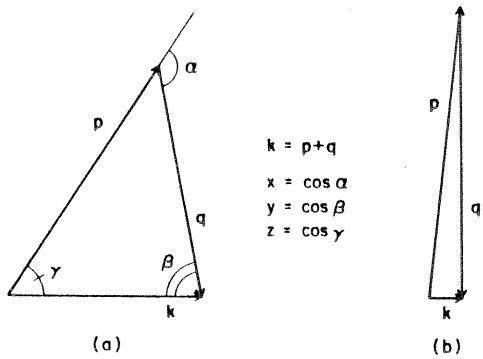

Fig. 9. Non-linear interactions between a triad of modes with (a) comparable scales (local interactions) and (b) widely different scales (non-local interactions).

here, k, p, and q are the sides of the triangle formed by the triad interaction of the wavevectors $\boldsymbol{k}$, $\boldsymbol{p}$, and $\boldsymbol{q}$, and x, y, and z are the cosines of the angles they form, as shown in fig. 9a.

The 3D, non-helical, non-correlated closure equations for MHD were first given by Kraichnan and Nagarajan (1967). For homogeneous and isotropic turbulence, the *EDQNM* equations for MHD in variable dimension for zero correlation and zero helicity can be found in Pouquet (1984), those for zero correlation but 3D helical flows can be found in Pouquet et al. (1976), those for correlated, non-helical flows in Grappin et al. (1983), and those for helical, correlated flows in Grappin (1986). There also exist in the literature different sets of closure equations, using e.g. the DIA (Lerche 1971, Vainshtein and Zeldovich 1978, Vainshtein 1982, Veltri et al. 1982; with no claim of completeness). In recent papers Yoshizawa (1985, 1987) tackles the MHD closure problem in the presence of shear and uses such a description in a large-eddy simulation (LES) for MHD.

The choice of the characteristic correlation time, $\theta(k, p, q)$, appearing in eq. (5.10), is somewhat arbitrary, contrary to the DIA case. In MHD, besides the dissipative times $(\nu k^2)^{-1}$ and $(\eta k^2)^{-1}$ and the eddy turn-over time, τ_{NL}, one can also introduce the Alfvén rate, $(kb_0)^{1/2}$, with b_0 the rms large-scale fluctuating magnetic field; we have seen in section 2 that this is an essential ingredient of the phenomenology of turbulence slowed down by a mixture of Alfvén waves. Thus, one writes:

$$\theta(k, p, q) = \frac{1 - \exp[-t\mu(k, p, q)]}{\mu(k, p, q)}, \tag{5.12a}$$

with

$$\mu(k, p, q) = \mu(k) + \mu(p) + \mu(q) \tag{5.12b}$$

and

$$\mu(k) = (\nu + \eta)k^2 + C_K \left[\int_0^k q^2 [E^V(q) + E^M(q)] \, dq \right]^{1/2} + k \left[\int_0^k E^M(q) \, dq \right]^{1/2}, \tag{5.12c}$$

where the constant C_K is adjusted so as to give the proper Kolmogorov constant.

The kinematic case (velocity field given) is obtained when: (i) one ignores the equations for the velocity covariance and (ii) one discards in the two remaining equations for the magnetic energy and helicity the terms quadratic in the magnetic covariance.

5.3. *Turbulent transport coefficients as non-local expansion of closures*

Closure equations are a set of coupled, non-linear integro-differential equations for the various spectra. They are intricate enough that they are best studied using a computer. However, these equations can be greatly simplified in the case of non-local interactions, i.e. interactions at widely different scales, as depicted in fig. 9b: in that case, a small expansion parameter – here k/p – can be used to obtain a simplified set of equations. For small k, as in fig. 9b, one looks at the integrated effect of small scales (large wavenumbers p and q) on large scales $\mathcal{O}(k^{-1})$; one such effect is that of eddy-viscosity. In other words, some of the non-local contributions from the closure equations can be written as:

$$\frac{\partial E^\iota(k_0, t)}{\partial t} = -\nu^\iota_{\text{turb}} k_0^2 E^\iota(k_0, t),$$

where ν^ι_{turb} is the turbulent eddy viscosity (ι = V) or eddy diffusivity (ι = M), obtained by averaging over small scales.

In this way, expanding the many terms of the closure equations, one derives a wealth of transport coefficients (Pouquet et al. 1976). Such coefficients can be used as a means of parameterizing the small scales of the flow not treated explicitly in a numerical simulation, as has been done (Chollet and Lesieur 1981) for the pure-fluid case and by Yoshizawa (1987) for an MHD fluid in the presence of shear. However, some care must be taken because these transport coefficients can sometimes be destabilizing, e.g. through a negative viscosity (see section 6.6), leading to an inverse cascade, or the destabilization can be first-order in the wavenumbers, as we will see below.

Transport coefficients can be given a more sound basis in the framework of the renormalization-group (RG) technique (Ma and Mazenko 1975, Forster et al.

1976, De Dominicis and Martin 1979, Fournier and Frisch 1978). For a conducting fluid, the direct-interaction approximation and the RG truncated to second order, do not agree anymore (Sulem et al. 1979), since the Ohm's law vertex, unlike the advection term, is renormalized, no Galilean invariance (operating on the magnetic field) preventing this from happening (in other words, a large-scale magnetic field has a non-trivial effect on the dynamics of the flow: Alfvén waves). One advantage is that the coefficient in front of the power law obeyed by the energy spectrum, can be computed, if one is ready to assume what that power law is (as, e.g., for the Kolmogorov range). If this constant were to be different in the Kolmogorov case and in the MHD case, that might provide a further test of what spectra actually arise, e.g. in the solar wind.

Note, however, that when small scales have a destabilizing effect on large scales, the RG procedure is self-defeating, and one must resort to other techniques.

5.4. Destabilization effect of small-scale magnetic helicity

5.4.1. A phenomenological argument

Take initially a small-scale turbulent magnetic field $\boldsymbol{b}$ with non-zero magnetic helicity and with $\langle \boldsymbol{b} \rangle = 0$, a strong, quasi-uniform, large-scale, time-independent magnetic field $\boldsymbol{B}$, and no velocity. The Lorentz force is the only relevant term in the momentum equation for small times:

$$\frac{\partial \boldsymbol{v}}{\partial t} \sim \boldsymbol{B} \cdot \nabla \boldsymbol{b},$$

so that

$$\boldsymbol{v}(t) \sim \boldsymbol{B} \cdot \nabla \int_0^t \boldsymbol{b}(\tau)\, \mathrm{d}\tau.$$

Ohm's law for infinite conductivity then gives us the induced electrical field, $\boldsymbol{E}(t)$, which becomes, when averaged over the small-scale turbulence (an operation which we indicate by SS):

$$\langle \boldsymbol{E} \rangle_{\mathrm{SS}} = \int_0^t \langle \boldsymbol{b}(t) \times \boldsymbol{B} \cdot \nabla \boldsymbol{b}(\tau) \rangle_{\mathrm{SS}}\, \mathrm{d}\tau.$$

which, assuming isotropy, reduces to

$$\langle \boldsymbol{E} \rangle_{\mathrm{SS}} \sim \tfrac{1}{3} \tau \langle \boldsymbol{b} \cdot (\nabla \times \boldsymbol{b}) \rangle_{\mathrm{SS}} \boldsymbol{B}.$$

where τ is a typical coherence time of the small-scale magnetic turbulence. Using now this expression for the mean electrical field in the induction equation for the

large-scale magnetic field, and performing an average over the large scales, we obtain:

$$\frac{\partial \langle \boldsymbol{B} \rangle}{\partial t} = -\alpha_{\mathrm{ph}}^{\mathrm{M}} \boldsymbol{\nabla} \times \langle \boldsymbol{B} \rangle, \tag{5.13a}$$

where

$$\alpha_{\mathrm{ph}}^{\mathrm{M}} = \tfrac{1}{3} \tau \langle \boldsymbol{b} \cdot \boldsymbol{j} \rangle_{\mathrm{SS}} \tag{5.13b}$$

is the phenomenological destabilization coefficient involving the small-scale averaged magnetic helicity. In deriving eqs. (5.13a, b), we followed the interaction of a large-scale (k) and a small-scale (p) magnetic field through the Lorentz force, giving rise to a small-scale velocity (p) which in turn interacted with a small-scale magnetic field (q) through Ohm's law to finally modify the large-scale (k) magnetic field.

5.4.2. Closure results

This information in fact is contained in the two diagrams 6 and 10 in fig. 8. When computing these diagrams for small wavenumbers, k_0, to first order in the non-local expansion, one obtains the closure-based relation

$$\frac{\partial E^{\mathrm{M}}(k_0, t)}{\partial t} = -\alpha_{k_0}^{\mathrm{M}} k_0^2 H^{\mathrm{M}}(k_0, t), \tag{5.14a}$$

$$\frac{\partial H^{\mathrm{M}}(k_0, t)}{\partial t} = -\alpha_{k_0}^{\mathrm{M}} E^{\mathrm{M}}(k_0, t), \tag{5.14b}$$

with

$$\alpha_{k_0}^{\mathrm{M}} = -\tfrac{4}{3} \int_a^{\infty} \theta(k, q, q)\, q^2 H^{\mathrm{M}}(q, t)\, \mathrm{d}q \tag{5.14c}$$

being the "magnetic torsality" and a being the low cutoff wavenumber, typically four times k_0. This expression for α^{M} is very similar to the one obtained from the phenomenological argument detailed above, as it should be, except that it acts on both the symmetrical (energetic) and anti-symmetrical (helical) part of the magnetic-field correlation. A similar expression can be found for the "kinetic torsality", α^{V}, both through phenomenology and through a non-local expansion of the relevant diagrams; in the latter case, it reads:

$$\alpha_{k_0}^{\mathrm{V}} = -\tfrac{4}{3} \int_a^{\infty} \theta(k, q, q)\, H^{\mathrm{V}}(q, t)\, \mathrm{d}q.$$

Now, taking all diagrams into account and doing some algebra, one finds (Pouquet et al. 1976) that the non-local terms acting on large scales are, to lowest order:

$$\frac{\partial E^{\mathrm{V}}(k_0, t)}{\partial t} = 0, \qquad \frac{\partial H^{\mathrm{V}}(k_0, t)}{\partial t} = 0, \tag{5.15}$$

and equations for the large-scale magnetic energy and helicity similar to eqs. (5.14 a–c) with α^{M} replaced by α^{R}, the residual torsality, defined as,

$$\alpha^{\mathrm{R}}_{k_0} = \alpha^{\mathrm{V}}_{k_0} - \alpha^{\mathrm{M}}_{k_0}. \tag{5.16}$$

In other words, it is the residual helicity of the small scales that destabilizes the large magnetic scales. When initially the small-scale magnetic field is weak, $\alpha^{\mathrm{R}} \sim \alpha^{\mathrm{V}}$ and one recovers the "alpha effect" due to kinetic helicity (Steenbeck et al. 1966). In the non-linear case, taking into account the reaction of the Lorentz force on the velocity field, it is the combination of kinetic and magnetic helicity that is the agent of large-scale magnetic instability. Note that the growth rate is proportional to $|\alpha^{\mathrm{R}}|k_0$ and thus this instability can be called "first order" in k, as opposed to a negative viscosity which would lead to a second order in k instability. Another remark is that the growth rate, in the limit of large kinetic and magnetic Reynolds number, becomes independent of viscosity and magnetic diffusivity.

5.5. The inverse cascade of magnetic helicity

5.5.1. Characteristic times

Now assume that the small-scale kinetic and magnetic turbulence is continuously fed at some wavenumber through an unspecificied mechanism. Does a steady state occur, and if so, which one?

Let us here follow the analysis of Norman and Heyvaerts (1983) to evaluate the characteristic dynamical time of evolution of magnetic energy, τ_E, compared to that of magnetic helicity, τ_H. To do so, write the evolution equations of the average magnetic energy:

$$\frac{\partial \langle b^2 \rangle}{\partial t} = -\eta \langle j^2 \rangle,$$

and the average magnetic helicity:

$$\frac{\partial \langle \boldsymbol{a} \cdot \boldsymbol{b} \rangle}{\partial t} = -\eta \langle \boldsymbol{b} \cdot \boldsymbol{j} \rangle.$$

Assume now that the magnetic energy obeys a power law:

$$E^{\mathrm{M}}(k) \sim k^{-m};$$

one then obtains:

$$\tau_E = \frac{\int k^{-m}\,\mathrm{d}k}{\eta \int k^{2-m}\,\mathrm{d}k} \tag{5.17}$$

and

$$\tau_H = \frac{\int k^{-1-m}\,\mathrm{d}k}{\eta \int k^{1-m}\,\mathrm{d}k}, \tag{5.18}$$

where the integrals are taken from the energy-containing wavenumber, k_E, to the dissipation wavenumber, k_D. For $1 < m < 2$, one obtains:

$$\frac{\tau_H}{\tau_E} \sim \frac{k_\mathrm{D}}{k_\mathrm{E}}, \tag{5.19}$$

and for $2 \leqslant m < 3$, this relationship becomes $\tau_H/\tau_E \sim (k_\mathrm{D}/k_\mathrm{E})^{3-m}$.

In both cases the characteristic time of evolution of magnetic helicity is considerably larger than that of energy, with a ratio whose order of magnitude is comparable to the Reynolds number. This tells us that the magnetic helicity can be considered quasi-static on the time-scale of the evolving magnetic energy, and this justifies in a phenomenological way the minimal-energy assumption made by Woltjer (1958) and followers.

5.5.2. Numerical evidence for large-scale self-organization of MHD flows

The reason may be simply dimensional: magnetic helicity, unlike kinetic helicity, stresses the large scales of the flow since it contains the magnetic potential. This is the basis of the preceding argument. More important is the fact that large magnetic scales are evolving through their interaction with the small-scale kinetic and magnetic helicity, eqs. (5.13a, b) and (5.14a–c). This gives rise to an inverse cascade of magnetic helicity, as shown in fig. 10. It is obtained using the EDQNM closure presented before.

The different curves are labeled with the time, measured in units of the eddy turnover time at $k_\mathrm{E} = 1$, at which energy is being injected together with helicity in a narrow band of wavenumbers. The spectrum achieves a steady state at scales smaller than k_E^{-1}, and also at scales progressively larger than it, as time proceeds, stationarity being achieved in a time that scales roughly as k^{-1}.

We can conclude that a steady state is obtained on the small scales, and a quasi-steady state on the large scales, with ever-larger scales being excited as time proceeds. Experimental evidence of this phenomenon from direct numerical simulations is shown in fig. 11 for periodic boundary conditions (Pouquet and Patterson 1978, Meneguzzi et al. 1981).

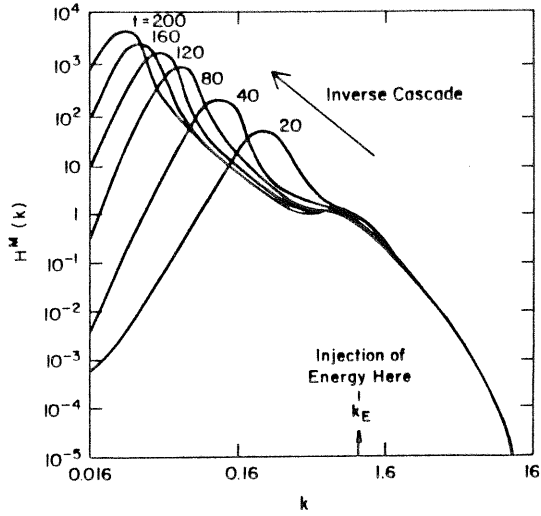

Fig. 10. Inverse cascade to large scales of the magnetic helicity; the curves are labeled with the time, in units of the eddy turn-over time at $k_E = 1$; closure calculation (Pouquet et al. 1976).

Whereas the kinetic energy on the large scales always decreases with time (solid line), the magnetic energy grows (dotted line) in the helical case (b), whereas it does not when helicity is forced to be zero, as in case (a). Injecting now energy at $k_E = 5$, an inverse cascade is indeed obtained (fig. 12) as well in direct, 3D numerical simulations of homogeneous flows.

Recall here that the measured typical scale of magnetic helicity in the solar wind is one order of magnitude larger than that for the energy (eqs. (2.3a, b)). Recent numerical simulations with more realistic boundary conditions in the RFP regime, indicate the same type of behavior.

5.6. Two-scale analysis of non-linear MHD

Closures provide an ideal framework to work at high Reynolds number, but contain the original defect of being some approximation to what is actually going on. Another type of approximation to the MHD flow is to perform two-scale or multiple-scale analysis. The drawback here is the assumption that the small-scale flow, over which one averages, is a laminar, low Reynolds number flow (unless one uses the short correlation time approximation). Many work has been performed along this line, either for the kinematic case or for the fully non-linear one.

In this way, the destabilizations of large magnetic excitation by the small-scale relative helicity can again be recovered (Chen and Montgomery 1987). Using

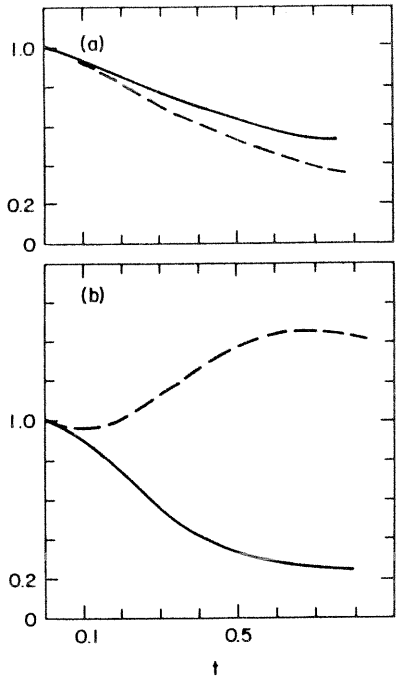

Fig. 11. Kinetic (solid line) and magnetic (dashed line) energy as a function of time in a 3D numerical decay run; (a) initially no helicity, (b) initially maximal magnetic helicity (Pouquet and Patterson 1978).

such techniques one can also obtain non-helical dynamos, by simply expanding to the next non-zero order (Gilbert et al. 1987). Note that a similar instability of large scales in the pure hydrodynamical case is precluded by reasons of symmetry (Krause and Rüdiger 1974), and in fact happens at the next order: it is a bi-Laplacian type of instability (Pouquet et al. 1978). However, several recent works show that breaking the symmetry through compressibility effects (Moiseev et al. 1983) or through anisotropy of the small scales (Frisch et al. 1987) yields again instability. Similarly, the quadrupole far-field emission of sound, found by Lighthill (1954), becomes dipolar when inhomogeneities are introduced (Kumar 1987).

5.7. *The non-linear dynamo*

The dynamo problem is dealt with in the lectures of Roberts (this volume); for an extensive account of mean-field theory see, e.g., Krause and Rädler (1980). Let me just mention briefly here the picture that emerges from closure phenomenology, about the way a non-linear dynamo works in a simple homogeneous flow: it is the residual small-scale helicity which is the true motor of the large-scale instability

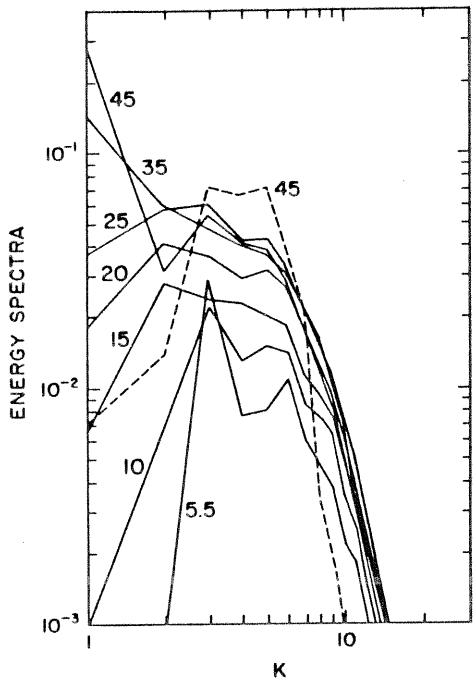

Fig. 12. Magnetic-energy spectrum for various times in units of the eddy turn-over time at $k_E = 5$; the dashed line is the steady-state kinetic-energy spectrum during the interval of time. Note the piling-up of magnetic excitation at the minimum wavenumber, due to an inverse cascade of magnetic helicity (Meneguzzi et al. 1981).

in the non-linear case; the saturation mechanism is provided by Alfvén waves: in the presence of a large scale rms magnetic field B_0, both the small-scale kinetic and magnetic energies and helicities become equal at scale l in a time l/B_0, so that

$$\alpha^{\mathrm{R}}_{k_0} \sim \int_{\alpha(k_0)}^{\infty} \theta[H^{\mathrm{V}}(q) - q^2 H^{\mathrm{M}}(q)]\,\mathrm{d}q \tag{5.20}$$

vanishes for some wavenumber k_0; however, the inverse cascade may still proceed for wavenumbers smaller than k_0, as long as the Alfvén effect has not had time to act. It will eventually have to stop, because of the finite size of the system.

6. Low-dimensional MHD

The approach described above is that of a numerical wind tunnel: the computed flows are, to within the accuracy of the spatial and temporal discretization

schemes, those in an experiment with a given set of parameters. It is worth noting that three-dimensional computations of MHD flows at a magnetic Reynolds number of 10^3 or of compressible flows at fluctuating Mach numbers of four have not been done in the laboratory, and may not be feasible with present-day techniques. Hence, numerical experimentation is a unique tool for MHD and/or compressible flows.

However, the solar, stellar, galactic, and extra-galactic physicist may be unhappy. To reasonably describe realistic conditions within a star, one must resort to drastic choices: lower the dimension (e.g. by assuming spherical symmetry), simplify the physics (by studying one problem at a time: convection, rotation, ...), and model the small-scale flow which will not be treated explicitly by the method, by an appropriate sub-grid scale parameterization. This is no longer an experiment, using computers, on fluid flows, but modeling of realistic flows, an approach widely used in the aeronautical industry for example. Let us then look at models of MHD.

6.1. The scalar model

The simplest models of turbulence are zero-dimensional, i.e. one deals with a system of non-linearly coupled ordinary differential equations. Such systems have been studied at length, if only for their chaotic behavior. In MHD, several low-dimensional models have been proposed, in particular in the context of the dynamo problem, in order to explain the chaotic reversal of the magnetic axis of the Earth's dipole, or the irregular disappearance of sunspots and of the magnetic cycle altogether (Maunder minimum). The chaotic evolution of the mean magnetic field can be described by the Lorenz system, or by extended versions of it to complex variables or to more modes (see, e.g., Zeldovich et al. (1983) or Jones et al. (1985)). However, such drastically truncated versions of fluid flows can but only capture some features of turbulent flows, namely the temporal chaotic behavior. On the other hand, the spatial distribution of modes is absent. To introduce it, one can proceed from a different point of view, with models in which the number of modes is a parameter that can be changed easily. For example, Obukhov (1971) and Desnianski and Novikov (1974) have proposed to truncate for a non-conducting fluid the non-linear interactions to a small range of wavenumbers. We will now follow-up on this idea and extend such models to the coupling to a magnetic field. The derivation and detailed description can be found in Gloaguen (1983) and Gloaguen et al. (1985).

We now construct a model of MHD turbulence from first principles; first define an average wavenumber, k_n, as sole representative of the n-shell, as:

$$\frac{k_n}{\sqrt{h}} < |k| < k_n \sqrt{h},$$

with $k_{n+1}/k_n = h$. For the sake of simplicity, assume that $h = 2$, although this is not essential. The one-dimensional system of partial differential equations that is obtained by letting $h \to 0$ is found in Gloaguen et al. (1985) and is reminiscent of Burgers' equation. In each shell represented by wavenumber $k_n = 2^{n-1}$, two fields, U_n for the velocity and b_n for the Alfvén speed, are defined. The dynamical evolution of $(U_n, b_n) = X_n$ is obtained by assuming that:

(i) the non-linear interactions are quadratic in the fields,

(ii) the characteristic time of the non-linear interactions must scale as $(k_n U_n)^{-1}$,

(iii) the non-linear interactions are restricted to nearest neighbors, i.e. only terms $X_i X_j$ with $(i, j = n, n \pm 1)$, and $X_n X_{n\pm1}$ appear in $\dot{X}_n$, where the dot on top means, as usual, the time differential,

(iv) furthermore, in $z_n^{\pm} = U_n \pm b_n$ variables, only $(z^+ z^-)$ interactions are included, following the structure of the primitive eqs. (1.33a, b),

(v) when summed over all shells, the energy $E^T = 0.5(\langle U_n^2 \rangle + \langle b_n^2 \rangle)$ and the correlation $E^C = 0.5\langle U_n b_n \rangle$ must be conserved by the non-linear interactions.

Taking for the dissipative terms their usual form, the model reads:

$$\left(\frac{\mathrm{d}}{\mathrm{d}t} + \nu k_n^2\right) U_n = \alpha(k_n U_{n-1}^2 - k_{n+1} U_n U_{n+1}) + \alpha(-k_n b_{n-1}^2 + k_{n+1} b_n b_{n+1}) + \beta(k_n U_{n-1} U_n - k_{n+1} U_{n+1}^2 - k_n b_n b_{n-1} + k_{n+1} b_{n+1}^2) + C_n \tag{6.1a}$$

and

$$\left(\frac{\mathrm{d}}{\mathrm{d}t} + \eta k_n^2\right) b_n = \alpha k_{n+1}(U_{n+1} b_n - U_n b_{n+1}) + \beta k_n (U_n b_{n-1} - U_{n-1} b_n), \tag{6.1b}$$

where $C_n = C\,\delta_{n1}$ is a forcing term so that the system may reach a steady state. The variables X_n are not constrained to be positive, they are viewed as mean fluctuating fields in shell n. Let us discuss the first term appearing in eq. (6.1a), assuming $\alpha > 0$. The mode U_n evolves due to positive input of energy from mode $n-1$ through the term U_{n-1}^2, i.e. from the large scale, and is likely to loose energy to the mode U_{n+1}. Note that this last term, linear in U_n can be interpreted as an eddy-viscosity, or an absorption term, whereas the former is a (positive) emission term. It is easily checked that these two interactions conserve the kinetic energy $\sum_{n=1}^{N} U_n^2$. Equations (6.1a, b) depend on five parameters: the kinetic and magnetic Reynolds numbers, defined here as $U_0/\nu k_0$ and $U_0/\eta k_0$, the ratio α/β, which appears in deriving the model, the forcing parameter C, and the number of shells, N.

Besides the conservation of E^T and E^C, when $C \equiv 0, \nu \equiv 0, \eta \equiv 0$, the system (6.1a, b) obeys the Liouville theorem; in the dissipative case, a volume in phase space shrinks as:

$$\sum_n \frac{\partial}{\partial U_n}\frac{dU_n}{dt} + \frac{\partial}{\partial b_n}\frac{db_n}{dt} = -(\nu+\eta)\sum_n k_n^2. \tag{6.2}$$

Furthermore, $U_n \sim k_n^{-1/3}$ and, similarly, $b_n \sim k_n^{-1/3}$ are solutions of the equations (which is not too surprising since the eddy turn-over time scale was imposed), but this solution is not necessarily attractive, as numerical computations show.

Taking $N = 3$, one has a six-mode dynamical system whose bifurcations from fixed point to limit cycle to chaos back to limit cycle back to chaos through period doubling, are not too surprising; a detailed description of the fixed points and of their stability can be found in Gloaguen (1983). At low Reynolds number, the steady state is non-magnetic ($b_n \equiv 0$ for all n), and the transition to a magnetic steady state ($U_n \neq 0$, $b_n \neq 0$) occurs at the same value of the parameter (here ν, with C, α/β, and η kept constant) as the transition to chaos, to within a few percent. Thus, this system exhibits a transition to magnetic behavior above a critical magnetic Reynolds number of the order of 40. As the number of modes is increased, the temporal evolution becomes intermittent at high wavenumber, with long periods of calm where the variable is close to zero, and high narrow bursts, of excursion of order one, probably accompanying the transfer of energy to that mode. This temporal intermittency increases with the wavenumber; the corresponding energy spectra are close to a $-\frac{5}{3}$ range, but the flatness factor:

$$\mathcal{F}^V = \frac{\langle U_n^4 \rangle}{\langle U_n^2 \rangle^2} \tag{6.3}$$

(with a similar definition for $\mathcal{F}^M$), when averaged over time in the span [0; 1,600] in units of the large-scale ($k_1 = 1$) eddy turn-over time, increases significantly with wavenumber, from 2.0 to 8.0 (for a Gaussian it should be 3.0), whereas the mean fields $\langle U_n \rangle / \sqrt{\langle U_n^2 \rangle}$ and $\langle b_n \rangle / \sqrt{\langle b_n^2 \rangle}$ tend to zero with increasing n: they are, respectively, 0.6 and 0.008 for the velocity and 1.0 and 0.002 for the magnetic field (values given for $k_n = 1$ and $k_n = 2^7$, respectively). Thus this model, which displays temporal chaotic behavior, also captures some of the spatial properties of a turbulent fluid, with scaling-law inertial ranges and intermittency effects (see also Kerr and Siggia (1978) for a non-magnetic model). It should be noted that with an exponential discretization, $k_n \sim 2^n$, a system of nine modes allows to simulate a Reynolds number of $(2^8/2^0)^{4/3} \sim 2 \times 10^3$; on the other hand, to follow correctly the temporal intermittency of the small scales, the temporal scheme chosen here is explicit and thus the system (6.1a, b) is stiff and costly to integrate.

6.2. *Dimensionality of the flow*

The scalar system (6.1a, b) is a model of MHD turbulence in which it is simple to vary the Reynolds number, R. It is then possible to look at the dimension of the underlying attractor and see how it varies with Reynolds number (Grappin et al. 1986): does it saturate, thereby indicating that only a small number of modes would be sufficient to describe the simple flow, or does it continue growing with R? There are several ways to define a dimension; the simplest one is the point-wise dimension: take a representative point on the attractor, i_0, and count the number of points N_p that are within a distance $\sim l$ of it; look how this number varies with $\sim l$: for a surface $N_p \sim l^2$, for a sphere $N_p \sim l^3$, and for an object with dimension d, embedded into the $2N$-dimensional phase space of the dynamical system, $N_p \sim l^d$. More precisely, one looks at the correlation function:

$$C_0(l) = \frac{1}{N} \sum_{i=1}^{N} \mathcal{H}(l - d_{i_0 j}), \tag{6.4}$$

where $d_{i_0 j} = |X_{i_0} - X_j|$ is the Euclidean distance between the i_0-th and j-th point in phase space and where $\mathcal{H}$ is the Heaviside function. If $C_0(l) \sim l^{d_0}$, then d_0 will be the point-wise dimension of the attractor. A more general correlation function (Grassberger and Procaccia 1983, Mandelbrot 1974), which averages over the whole attractor, is:

$$C(l) \sim \frac{1}{N^2} \sum_{i,j=1}^{N} \mathcal{H}(l - d_{ij}) \sim l^d, \tag{6.5}$$

where d is now the correlation dimension; its computation requires $\mathcal{O}(N^2)$ operations, as opposed to $\mathcal{O}(N)$ for $C_0(l)$, but it converges more rapidly. It also requires the storage of an array with size N^2, containing the distances between points in phase space sampled every ΔT, with $dt < \Delta T < \tau_{NL}$, where dt is the time-step of the computation and τ_{NL} the eddy turn-over time, as usual.

In fig. 13 is shown the dimension using eq. (6.5) for two computations at the same Reynolds number and all other parameters equal except that in run A, indicated by crosses, 2×3 modes are used whereas in run B, indicated by circles, 2×4 modes are used; for run A, the Kolmogorov dissipation wavenumber is close to the maximum wavenumber of the computation, whereas for run B, it is an octave below. The agreement between the two curves indicates that the dimension computed with such algorithms can indeed be linked to the Reynolds number of the flow, and not to the actual number of modes used in the computation, provided it is large enough to resolve the dissipation range as well as the inertial range.

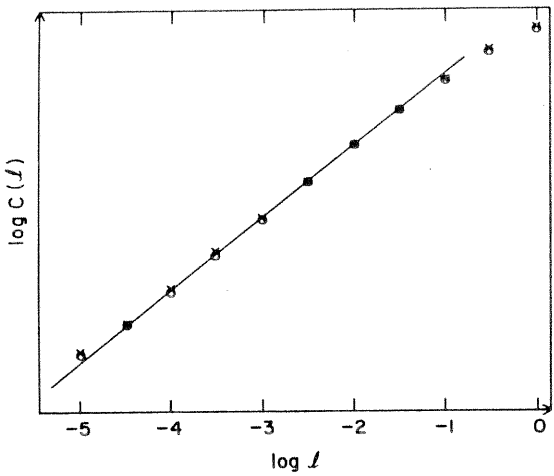

Fig. 13. Correlation index as a function of distance for the scalar model with all parameters equal except the number of modes. Crosses: 6 modes; circles: 8 modes. The two curves are indistinguishable; when 20×10^3 points are used, the correlation dimension is 3.31, whereas it is 3.26 with half as many points.

Finally, the dimension of the attractor can be computed using a conjecture of Kaplan and Yorke (1979), by evaluating the spectrum of Liapunov exponents, λ_j, which looks at how a j-dimensional parallelepiped expands (or eventually shrinks) under the dynamics of the system of ordinairy differential equations. It is a generalization of the concept of eigenvalues to a non-linear system.

The first Liapunov exponent indicates the divergence (if positive) of nearby trajectories, and thus is a measure of chaos; up to N_* the N_*-dimensional volume still expands:

$$\sum_{j=1}^{N_*} \lambda_j > 0,$$

and beyond N_* it shrinks:

$$\sum_{j=1}^{N_*+1} \lambda_j < 0$$

note that eventually this sum must become negative since $\sum_{j=1}^{N} \lambda_j = -(\nu + \eta) \sum_{j=1}^{N} k_j^2$ because of Liouville's theorem, so that at least $\lambda_N < 0$. Then the Liapunov dimension is:

$$d_{\mathrm{Lya}} = N_* + \sum_{j=1}^{N_*} \lambda_j / \lambda_{N_*+1} \,. \tag{6.6}$$

All three algorithms agree at low dimension (up to five), and all three indicate that the dimension of the turbulent attractor increases with Reynolds number, but the increase is markedly less with the counting algorithms. This can be attributed to a geometrical effect (Atten et al. 1986), since in a sphere with high dimension most of the points lie in the outer shells. The Liapunov dimension grows as

$$d_{\mathrm{Lya}} \sim -\tfrac{3}{2} \log_2 \nu, \tag{6.7}$$

which is in fact the number of degrees of freedom in the inertial range, since $(k_{\mathrm{D}}/k_0) \sim R^{3/4}$, $k_n/k_0 \sim 2^n$ and there are two modes per shell. It was also shown by Grappin et al. (1986) that the first Liapunov exponent scales as $1/\sqrt{\nu}$, since $\tau_{\mathrm{D}} \sim 1/\nu k_{\mathrm{D}}^2 \sim \nu^{1/2}$. It is tempting to conjecture that turbulent flows scale in the same way, and computations of the Liapunov dimension of shear flows have now been undertaken (Grappin and Léorat 1987) to verify this point.

6.3. One-dimensional Burgers' equation extended to MHD

An extension of Burgers' equation to coupling with a magnetic field was proposed by Thomas (1968); it reads:

$$\frac{\partial u}{\partial t} + u\frac{\partial u}{\partial x} = b\frac{\partial b}{\partial x} + \nu\frac{\partial^2 u}{\partial x^2}, \tag{6.8a}$$

$$\frac{\partial b}{\partial t} + u\frac{\partial b}{\partial x} = b\frac{\partial u}{\partial x} + \eta\frac{\partial^2 b}{\partial x^2}. \tag{6.8b}$$

Thomas wrote this model in the context of the dynamo effect. A recent study (Passot 1987), both analytical using the Painlevé test, and numerical, shows that these equations are not integrable, contrary to the $b \equiv 0$ Burgers case. A dominant-balance analysis, more conveniently performed with the Elsässer variables $z^{\pm} = u \pm b$, shows that, when writing $z^{+} \sim x^{\alpha}$ and $z^{-} \sim x^{\beta}$, one obtains $\beta = -1$ (a simple pole) and, for $P^{\mathrm{M}} = \nu/\eta > 1$, $\alpha = (1+P^{\mathrm{M}})/(1-P^{\mathrm{M}})$, i.e. $\alpha < -1$; in fact z^{β} is subdominant, whereas the (u,b) variables both behave as simple poles. This underlying structure appears very clearly in Fourier spectra of the velocity and the magnetic field. It can be shown using the Laplace method, that for wavenumbers $k \to \infty$, the largest contribution to the Fourier spectrum of a field $V(\boldsymbol{r})$ comes from the complex singularity closest to the real axis; writing

$$V(z) \sim (z - z_*)^{\rho},$$

the spectrum of $V(z)$ for large k behaves as (Carrier et al. 1966):

$$\widehat{V}(k) \sim k^{-(\rho+1)} \exp[-\mathrm{Im}(z_*)k]. \tag{6.9}$$

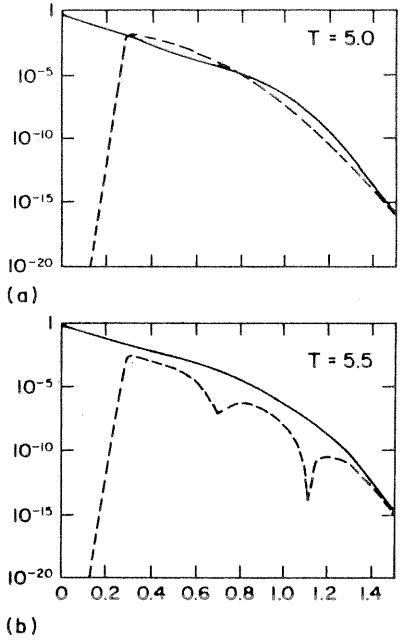

Fig. 14. Kinetic (solid line) and magnetic (dashed line) energy spectra at $t = 5.0$ (a) and $t = 5.5$ (b), in units of the eddy turn-over time, for the one-dimensional MHD model. Note the crests in the magnetic spectra (Passot 1987).

For $\rho_R = -1$, i.e. in the case of a simple pole, the prefactor in eq. (6.9) disappears and one simply obtains an exponential decay, as in the case of Burgers' equation. But when $\rho_R \neq -1$, the function $\widehat{V}(k)$ is not decreasing monotonically and can present crests that are the signature of poles with non-unity multiplicity.

Figure 14 shows the spectra of the velocity and magnetic field at t = 5.0 and 5.5 (in units of the large-scale turn-over time), and fig. 15 the profiles of the velocity and magnetic field at the same two times; although no difference is apparent in the profiles, the crests in the magnetic spectrum are due to a singularity approaching the real axis. This computation is done using 128 points with a pseudo-spectral code with initial conditions $u(x) = \sin x$ and $b(x) = 0.2 \sin x$ and with $\nu/\eta = 4$. Such crests have also been observed in direct numerical simulations of two-dimensional compressible flows. For a recent study of one-dimensional MHD, including the density equation, see Wu (1987).

6.4. Lack of singularity in two-dimensional inviscid MHD

Dissipative processes smooth the flow at small scales and very likely prevent the

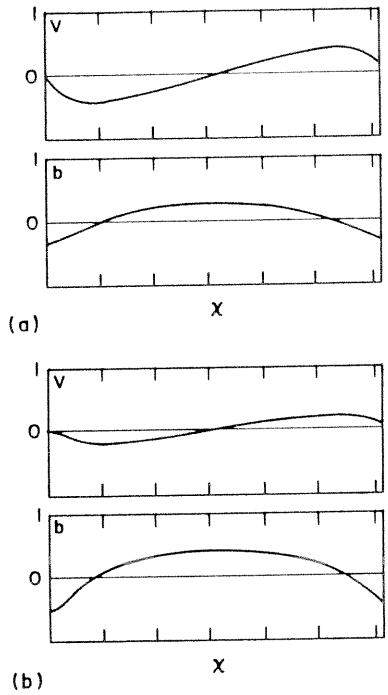

Fig. 15. Kinetic (solid line) and magnetic (dashed line) profiles at the same times in fig. 14.

formation of discontinuities in the flow variables or their derivatives. It has been demonstrated (see Sulem (1986) for a review) that for 3D, Navier–Stokes, incompressible flows with $\nu \neq 0$, singularities, if they exist, have a very small spatial and temporal dimension. In the inviscid case, however, the answer is not known. Closure models predict an enstrophy blow-up in a finite time. In two dimensions, for an Euler flow, because of the additional conservation of vorticity, singularities are prevented for all times (Wolibner 1933). When coupling to a magnetic field is switched on, what will happen? The Lorentz force breaks the conservation of vorticity, which may therefore blow up again; on the other hand, a mixture of Alfvén waves produces a possible equilibration mechanism by exchanging kinetic and magnetic energy on the time scale l/B_0, where B_0 is the uniform or large-scale field. When B_0 is sufficiently large, this time-scale is shorter than the eddy turnover time, and an eventual blow-up of enstrophy may be prevented because the dynamics reduce mostly to that of waves (Bardos et al. 1987). On the other hand, when B_0 is weak, the Lorentz force is negligible, and conservation of vorticity again prevents the formation of singularities. As time elapses, the magnetic field

grows and may remain of order one, for a velocity field of order one, for times long compared to the eddy turn-over time (although for even longer times Cowling's theorem applies and the 2D magnetic field eventually dies out). Closures indicate that the total enstrophy, defined as

$$\Omega^{\mathrm{T}} = \Omega^{\mathrm{V}} + \Omega^{\mathrm{M}}, \tag{6.10}$$

with

$$\Omega^{\iota} = \int_0^{\infty} k^2 E^{\iota}(k)\,\mathrm{d}k, \tag{6.11}$$

where $\iota = (\mathrm{V}, \mathrm{M})$, blows up in a finite time. However, numerical simulations at high resolution indicate the contrary (Frisch et al. 1983). Starting with initial conditions that are random and narrowly peaked on the large scales, or with the Orszag–Tang (OT in brief) vortex, defined as (Orszag and Tang 1979):

$$\psi(x, y) = 2\cos x + 2\cos y, \tag{6.12a}$$

$$a(x, y) = 2\cos x + \cos 2y, \tag{6.12b}$$

where ψ is the stream function ($\boldsymbol{v} = \mathrm{curl}\,\psi$), one lets the MHD equations evolve with $\nu \equiv 0$, $\eta \equiv 0$; the energy spectrum that develops with time is then fitted with the following functional form:

$$E(k, t) = C(t)\exp[-2\delta(t)k]\,k^{-m(t)}. \tag{6.13}$$

For the spectral index in the inviscid phase, one finds:

$$m(t) \sim 2.0 \pm 0.4, \tag{6.14}$$

which would ideally lead to a -2 spectrum.

When a uniform magnetic field $\boldsymbol{B}_0$ is added to the fluctuating field, strong enough to suppress neutral points (points at which the total field would be equal to zero), $\delta(t)$ saturates at a value δ_B substantially higher than the grid spacing, Δx, and there is an effective loss of computer resources if one were to continue with such a computation. These results indicate that the magnetic field, in the absence of neutral points, provides an effective cutoff in wavenumber space, through dispersive effects, just as dispersive effects prevent the formation of shocks in the 1D Korteweg–de Vries equation, leading in fact to well-behaved solitonic solutions. This may suggest some solitonic-like behavior in 2D MHD. In three dimensions,

however, it is not clear whether the dispersion will be sufficient to balance steepening (B.C. Low, private communication). However, when $B_0 \equiv 0$, $\delta(t)$ decays inexorably, but exponentially; the 2D data is consistent with:

$$\delta(t) \sim \exp(-at), \tag{6.15}$$

so that only for $t \to \infty$ will it reach 0; thus, numerical simulations indicate that no singularity will occur in a 2D MHD flow in a finite time.

6.5. *The inverse cascade of the magnetic potential*

Another feature of two-dimensional flows concerns their structure on large scales. As mentioned earlier, in two dimensions the magnetic helicity invariant is replaced by the magnetic anastrophy (quadratic in the field):

$$E^{\mathrm{a}} = \int a^2 \, \mathrm{d}^2 \boldsymbol{r}. \tag{6.16}$$

The same argumentations as in the 3D case can be given to justify the inverse cascade towards large scales of E^{a}; they will simply be enumerated here. The magnetic potential is a large-scale quantity, as compared to the magnetic energy. Its characteristic time of dissipation can be evaluated as:

$$\tau_{\mathrm{a}} \sim \left(\int a^2 \, \mathrm{d}^2 \boldsymbol{r} \right) \Big/ \left(\eta \int a j \, \mathrm{d}^2 \boldsymbol{r} \right);$$

assuming again $E^{\mathrm{M}}(k) \sim k^{-m}$, we have for the ratio τ_{a}/τ_E, where τ_E was defined in section 5.5.1, eq. (5.17):

$$\tau_{\mathrm{a}}/\tau_E \sim (k_{\mathrm{D}}/k_0)^2 \sim (R^{\mathrm{M}})^{4/3}. \tag{6.17}$$

So the time scale of the magnetic potential decay is of the order of $(R^{\mathrm{M}})^{2/3}$ times larger than that of the magnetic helicity in 3D. Again, minimization of energy on the one hand (section 3.4), and statistical mechanics of truncated systems (Fyfe and Montgomery 1976) on the other, all point in the same direction. Direct numerical simulations (Matthaeus and Montgomery 1980) confirm the existence of such an ordering of large-scale 2D MHD flows.

Let us close this section by indicating a simple phenomenological argument which shows that the turbulent magnetic diffusivity, η^{M}, due to small-scale magnetic excitation, is negative and thus destabilizing. Take at time t = 0, small-scale random b and j, a large scale A and no velocity at all. The velocity field grows

under the action of the Lorentz force, so that $\boldsymbol{V} \sim \theta j \nabla A$, where θ is the coherence time of the small-scale velocity field; this field now reacts on the small-scale magnetic potential through:

$$\frac{\partial a}{\partial t} = -\operatorname{div}(\boldsymbol{V} a). \tag{6.18}$$

Averaging now over small scales (an operation indicated as $\langle \cdot \rangle_{SS}$), we have:

$$\langle \boldsymbol{V} a \rangle_{SS} = \theta \nabla A \langle j a \rangle_{SS} = \theta \nabla A \langle b^2 \rangle_{SS},$$

so that the flux $\langle \boldsymbol{V} a \rangle$ is in the *same* direction as ∇A. Equation (6.18) for the large-scale magnetic potential now becomes:

$$\frac{\partial A}{\partial t} = -\operatorname{div}\langle \boldsymbol{V} a \rangle = -\theta \langle b^2 \rangle_{SS} \nabla^2 A. \tag{6.19}$$

Thus $\eta^M = -\theta \langle b^2 \rangle_{SS}$ is negative. On the other hand, it was shown by Krause and Rüdiger (1975) that the turbulent magnetic diffusivity due to the small-scale velocity, η^V, is positive, and the sign of the resulting transport coefficient, $\eta^T = \eta^M + \eta^V$, needs to be determined by a more sophisticated treatment. Two-point closures indicate that η^T is proportional to the relative energy $\langle E^V(k) - E^M(k) \rangle_{SS}$ on the small scales, and thus is indeed negative, since an excess of magnetic energy has been systematically found on the small scales, with few exceptions, in the solar wind, in closure calculations, and in direct numerical simulations.

6.6. *The development of current sheets*

The dissipation of energy occurs, e.g., through the formation of a current sheet. In fact, returning to $\boldsymbol{z}^{\pm} = \boldsymbol{v} \pm \boldsymbol{b}$ variables, and taking as initial conditions the OT vortex (6.12), both $\boldsymbol{z}^{\pm}$ variables have a neutral X-point and both develop a sheet, the angle between the two closing up as time elapses (Sulem et al. 1985). Assume that, at the common neutral point, the vorticities $\boldsymbol{\omega}^{\pm} = \operatorname{curl}(\boldsymbol{z}^{\pm})$ are of equal intensity. Since it is at k_D that the $E^{\pm}$ spectra cross (see section 7.2 on this point, eq. (7.7)), we see that the resulting structure at the X-point is also a sheet for the current $\boldsymbol{\omega}^+ + \boldsymbol{\omega}^-$, but is of higher order for the vorticity $\boldsymbol{\omega}^+ - \boldsymbol{\omega}^-$; it is in fact a quadrupole, as first shown numerically by Matthaeus (1982). The reconnection that takes place in the vicinity of the neutral region, when interacting with a turbulent flow, has been but rarely studied (see, however, Matthaeus and Lamkin (1986)).

7. The growth of velocity–magnetic field correlations

7.1. Introduction

We spent some time in the preceding sections looking at the steady states that arise when minimizing the energy while keeping constant either the magnetic helicity or the magnetic anastrophy. By doing this, we consciously forget the role that other invariants of the primitive MHD equations play. We will here concentrate on the complementary problem, neglecting the invariants arising purely from the induction equation and looking at the problem of minimizing the energy, keeping constant the correlation $E^{\mathrm{C}} = \langle \boldsymbol{v} \cdot \boldsymbol{b} \rangle$ between the velocity and the magnetic field. The statement of this problem is not dimension dependent and we will take advantage of this point by studying it in greater detail in the two-dimensional framework, which will prove very useful in the numerical context. Two dimensionless measures of correlation can be defined, one is:

$$\gamma = \frac{\langle \boldsymbol{v} \cdot \boldsymbol{b} \rangle}{\sqrt{\langle v^2 \rangle \langle b^2 \rangle}} = \frac{E^{\mathrm{C}}}{\sqrt{E^{\mathrm{V}} E^{\mathrm{M}}}}, \tag{7.1}$$

and the other:

$$\rho_{\mathrm{C}} = \frac{2\langle \boldsymbol{v} \cdot \boldsymbol{b} \rangle}{\langle v^2 \rangle + \langle b^2 \rangle} = \frac{2E^{\mathrm{C}}}{E^{\mathrm{T}}}. \tag{7.2}$$

The factor 2 in ρ_{C} is introduced so that $|\rho_{\mathrm{C}}| \leqslant 1$. In the context of turbulent flows, the latter coefficient is preferable since it is the ratio of two invariants of the non-dissipative MHD equations. Contrary to the case of magnetic helicity or magnetic potential, here the two invariants E^{C} and E^{T} have the same dimension and one cannot argue that the characteristic time scale of one is shorter than that of the other one, as was done in the helical case. What can then happen when the nonlinear coupling of modes sets in and the energy flows to small scales? Is the time evolution of ρ_{C} in any way predictable, or is it random?

7.2. Phenomenology of correlated flows

When dealing with the eventual fate of the correlation between the velocity and the magnetic field, the most convenient variables are those introduced by Elsässer, $z^{\pm} = \boldsymbol{v} \pm \boldsymbol{b}$. The invariants are then $E^{\pm} = \frac{1}{2}\langle (z^{\pm})^2 \rangle$, and the following relations are useful in transforming from one set of variables to the other:

$$E^{\pm} = E^{\mathrm{V}} + E^{\mathrm{M}} \pm 2E^{\mathrm{C}}, \tag{7.3a}$$

$$E^{\mathrm{T}} = E^{\mathrm{V}} + E^{\mathrm{M}} = \tfrac{1}{2}(E^{+} + E^{-}). \tag{7.3b}$$

$$E^{\mathrm{C}} = \tfrac{1}{4}(E^{+} - E^{-}). \tag{7.3c}$$

Thus the correlation coefficient ρ_{C} is just the normalized difference between the E^{+} and the E^{-} energy. Let us assume hereafter that $E_0^{+} > E_0^{-}$ (where the subscript 0 refers to initial conditions), hence the initial correlation ρ_{C}^0 is positive. As noted in the first section, the MHD equations are symmetrical under exchanging + and − and the same evolution as that described below would occur were we to start with $E_0^{+}/E_0^{-} < 1$ or, equivalently, $\rho_{\mathrm{C}}^0 < 0$.

Let us now restate the phenomenology of the interaction between non-linear turbulent transfer to small scales and propagation of Alfvén waves. Now we want to take into account the asymmetry of the initial conditions for which $\rho_{\mathrm{C}}^0 \neq 0$. We will again write the characteristic time for turbulent transfer to small scales as $\tau_{\mathrm{tr}} = \tau_{\mathrm{NL}}^2/\tau_{\mathrm{A}}$, as defined in eq. (2.8), but now take into account the fact that in the time evolution of the z^{+}-field the time scale τ_{NL}^{+} is scaled by the z^{-}-field and vice versa:

$$\tau_{\mathrm{NL}}^{+} \sim \frac{l}{z_l^{-}} \sim \frac{1}{\sqrt{k^3 E^{-}(k)}};$$

thus

$$\tau_{\mathrm{tr}}^{+} = \frac{B_0}{k^2 E^{-}(k)}.$$

Writing now that the transfer rate ϵ^{+} of z^{+} is:

$$\epsilon^{+} = \frac{E^{+}}{\tau_{\mathrm{tr}}^{+}},$$

we obtain the symmetrical relationship (Dobrovolny et al. 1980):

$$\epsilon^{+} = \epsilon^{-} = \frac{k^3 E^{+}(k) E^{-}(k)}{B_0}. \tag{7.4}$$

This immediately tells us two things. One is that by requiring that the transfer rate ϵ^{+} is independent of the wavenumber, and writing

$$E^{+}(k) \sim k^{-m^{+}}$$

and

$$E^{-}(k) \sim k^{-m^{-}}.$$

we have one (sole) constraint on the inertial range spectral indices m^+ and m^- of the $E^{\pm}(k)$ spectra:

$$m^+ + m^- = 3. \tag{7.5}$$

Note that, when $m^+ = m^- = \frac{3}{2}$, one recovers the solution derived by Iroshnikov and by Kraichnan in the uncorrelated case, since when $E^+ = E^-$, the correlation is zero.

In the correlated case, however, it is likely to have $m^+ \neq m^-$, and one relationship is lacking to close the problem. We can, however, bound the values that $m^{\pm}$ can take by noting that the transfer integrals diverge when $m^{\pm} \to 3$. We thus a priori expect the spectral indices of the $E^{\pm}(k)$ spectra to vary between 0 and 3. When they are markedly different, the total energy, E^{T}, is strictly speaking no longer a power law, but the dominant contribution of E^+ in the positively correlated case (and E^- otherwise) will make it appear so, with the index of E^+ (respectively E^-).

The other important consequence of eq. (7.4) is that, since $\epsilon^+ = \epsilon^-$, the rate of transfer of correlation, $\epsilon^{\mathrm{C}} \sim (\epsilon^+ - \epsilon^-)$, is zero. Thus, in the framework of this simple phenomenological analysis, correlation is not transferred to small scales and ρ_{C} grows with time. In fact, a more detailed analysis can be done to show that correlation is being transferred to small scale by non-linear interactions, as one expects a priori, but in smaller amounts than energy, although at the same temporal rate. The argument is as follows (Grappin et al. 1983): in a steady state there is balance at every wavenumber k between injection rate ϵ_k^+ and dissipation, which we model by a turbulent viscosity, viz.:

$$\epsilon^+(k) = \nu^+_{\mathrm{turb}}(k) k^2 E^+(k),$$

with

$$\nu^+_{\mathrm{turb}}(k) = \int_k^{\infty} \tau_{\mathrm{A}} E^-(p)\, \mathrm{d}p,$$

having averaged over small-scale turbulence, where $\tau_{\mathrm{A}} = (pB_0)^{-1}$. Supposing that the integral converges, it can be evaluated locally:

$$\nu^+_{\mathrm{turb}}(k) \sim \frac{kE^-(k)}{m^- B_0}.$$

This allows to break the symmetry between the $\pm$ injection rates and yields:

$$\epsilon^+/\epsilon^- \sim m^+/m^-; \tag{7.6}$$

again $\epsilon^+ = \epsilon^-$, with $m^+ = m^-$, in the uncorrelated case. This relation will hold provided m^- does not become too close to zero; otherwise, non-local contributions in wavenumber space must be taken into account in evaluating the eddy viscosity, ν^+_{turb}.

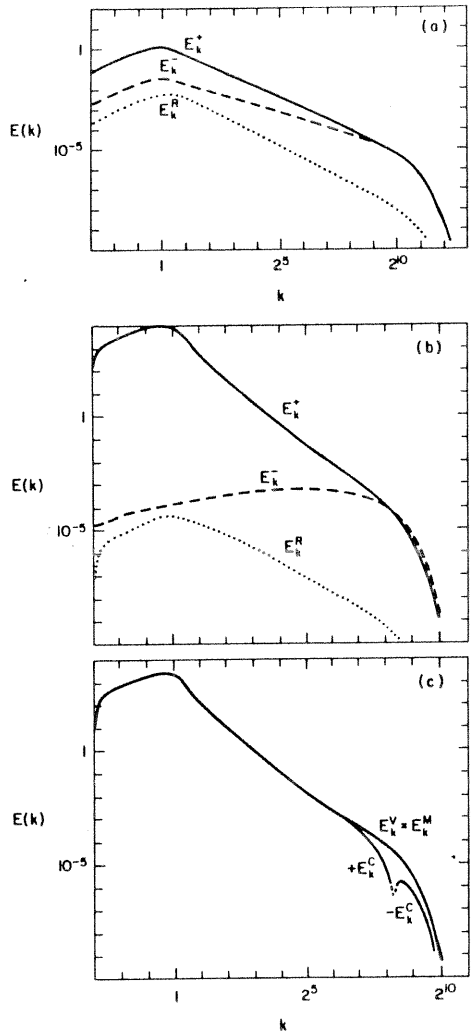

Fig. 16. Steady-state energy spectra $E^{\pm}(k)$, using the EDQNM closure, for injection rates with a correlation of (a) 10% and (b) 80%; (c) the corresponding kinetic energy spectrum $E^{V}(k)$ and correlation spectrum $E^{C}(k)$ (Grappin et al. 1983).

Figure 16 shows the steady-state $E^{\pm}(k)$ spectra for two values of the relative rate of injection $(\epsilon^+ - \epsilon^-)/(\epsilon^+ + \epsilon^-)$, respectively equal to 10% (a) and 80% (b), using the EDQNM closure with reduced equations for which one as-

sumes $E^V(k) \equiv E^M(k)$ for all k; in fig. 16c is shown the corresponding kinetic (or magnetic) energy spectrum $E^V(k)$ and the correlation spectrum $E^C(k)$, with a change of sign in the latter around $k = 2^8$. For details on the computation see Grappin et al. (1983). The Reynolds number here is of the order of 10^3. The steady-state correlation coefficient ρ_C is, respectively, 88% and 99.998%, and the corresponding spectral indices are $m^+ = 1.8$ and $m^- = 1.2$ in case (a) and $m^+ \simeq 2.99$ and $m^- \simeq 0$ in the highly correlated run (b); in the latter case, the spectral indices of the energy $E^V(k)$ and the correlation $E^C(k)$ are also very nearly equal to 3. Note that in case (a) $\epsilon^+/\epsilon^- = 1.22$ and $E^+/E^- = (1 + \rho_C)/(1 - \rho_C) = 15.7$, whereas in case (b) we have $\epsilon^+/\epsilon^- = 9$ and $E^+/E^- \sim 10^5$.

The other striking feature of the spectra displayed in fig. 16 is that the $\pm$ inertial ranges become equal at approximately the same wavenumber at which they also yield the dissipative range, hence the only change of sign of the correlation spectrum is at that same wavenumber. This result can again be recovered by a phenomenological argument. Indeed, we have equilibration between injection and dissipation of energy, and thus:

$$\epsilon^+ = 2\nu \int_0^\infty p^2 E^+(p)\,\mathrm{d}p \approx 2\nu \int_{k_0}^{k^+} p^2 E^+(p)\,\mathrm{d}p,$$

where we suppose $\nu = \eta$ (magnetic Prandtl number of unity), and where k_0 and k^+ (respectively k^-) are the characteristic wavenumbers of the energy-containing range and of the dissipation range of E^+ and E^-. Evaluating the latter is done as usual by stating that, at $k^\pm$, the dissipation time and the transfer time are equal. This yields:

$$E^-(k^+) = E^+(k^-) = \nu B_0.$$

Moreover, $k^+ = k^-$ to within a numerical factor. If this were not the case, take an intermediate wavenumber $k^- < k_i < k^+$; irrespective of the sign of the correlation, $E^-(k_i)$ is negligible due to the exponential decay setting in at k^-, and the transfer time τ_{tr}^+ is thus longer than the dissipation time $(\nu(k^+)^{-2})$, contrary to the hypothesis. We therefore conclude that the $\pm$ energy spectra become equal at the wavenumber:

$$k^+ = k^- = k_D, \tag{7.7}$$

at which dissipation sets in, hence the change of sign of the correlation spectrum at that wavenumber. However, this does not explain why the correlation spectrum has such a simple form, with only one change of sign. This point is treated in the next section.

7.3. *Does the correlation coefficient really grow and why?*

The organization of the correlation spectrum in two lobes of opposite signs, with a cross over at k_D, provides a posteriori a simple explanation of why ρ_C might grow. There is one important difference between the energy E^T and the correlation E^C, and that is the fact that the correlation spectrum is not positive definite, contrary to the energy. Think now in terms of an eddy viscosity which models the non-linear transfer of correlation and governs the temporal evolution of its large scales.

Its functional dependence, which may be obtained, e.g., from non-local expansion of the closure equations, is rather complicated. It contains averages over the small scales, $\mathcal{O}(q^{-1})$, of the total energy, of the relative energy $E^R(q) = E^V(q) - E^M(q)$, and of the correlation $E^C(q)$. Concentrating on this latter term, we can argue that a negative tail of the correlation in the dissipation range (assuming that the large-scale correlation is positive) is likely to act as a negative viscosity; however, destabilization of the large-scale correlation does not occur, since other terms in the evaluation of the transport coefficients modeling the non-linear transfer of correlation counteract it, and it therefore produces a marginal effect, consisting simply in slowing down the depletion of the large-scale correlation.

Let us now turn to the problem of growth with time of the correlation coefficient. One can show that, for short times, ρ_C indeed grows, at least in 2D. Write the two-dimensional MHD equations in Fourier space, with $\nu \equiv 0$, $\eta \equiv 0$, for the vorticities $\omega^+ = \mathrm{curl}(\boldsymbol{v} + \boldsymbol{b})$ and $\omega^- = \mathrm{curl}(\boldsymbol{v} - \boldsymbol{b})$, for a fluid embedded in a uniform magnetic field $\boldsymbol{B}_0$:

$$\left(\frac{\partial}{\partial t} - \mathrm{i}\boldsymbol{k}\cdot\boldsymbol{B}_0\right)\omega^{\pm}(\boldsymbol{k}) = \iint M(\boldsymbol{k},\boldsymbol{p},\boldsymbol{q})\,\omega^{\pm}(\boldsymbol{p})\,\omega^{-}(\boldsymbol{q})\,\mathrm{d}^2\boldsymbol{p}\,\mathrm{d}^2\boldsymbol{q}, \tag{7.8a}$$

$$M(\boldsymbol{k},\boldsymbol{p},\boldsymbol{q}) = \delta(\boldsymbol{k}-\boldsymbol{p}-\boldsymbol{q})\,(p_x q_y - p_y q_x)\,(\boldsymbol{k}\cdot\boldsymbol{p})/p^2 q^2. \tag{7.8b}$$

Following the analysis of Grappin (1986), let us first integrate eq. (7.8a) formally:

$$\omega^{\pm}(\boldsymbol{k},t) = \mathrm{e}^{\pm\mathrm{i}\boldsymbol{k}\cdot\boldsymbol{B}_0 t}\;\Omega^{\pm}(\boldsymbol{k}) + \int_{t_0}^{t} \mathrm{d}\,\mathrm{e}^{\pm\mathrm{i}\boldsymbol{k}\cdot\boldsymbol{B}}_{0(t-u)}$$
$$\times \int M(\boldsymbol{k},\boldsymbol{p},\boldsymbol{q})\,\omega^{\pm}(\boldsymbol{p},u)\,\omega^{\pm}(\boldsymbol{q},u)\,\mathrm{d}^2\boldsymbol{p}\,\mathrm{d}^2\boldsymbol{q},$$

where $\Omega^{\pm}(\boldsymbol{k})$ is the initial $+/-$ vorticity up to a phase factor. Let us iterate the above equation once and expand the result in powers of $\Omega^{\pm}(\boldsymbol{k})$, letting $t_0 \to -\infty$ and $t \to \infty$; first, writing formally:

$$\omega^{+} = G^{+}\Omega^{+} + g^{+}(\omega^{+};\,\omega^{-})$$

and iterating once, one obtains:

$$\omega^+ = G^+\Omega^+ + g^+[G^+\Omega^+ + g^+(\omega^+;\,\omega^-);\,G^-\Omega^- + g^-(\omega^-;\,\omega^+)]\,;$$

writing now, to first order, that the fluctuating fields are equal to their linear value $G^+\Omega^+$ (and here the expansion parameter is $z^\pm/B_0$, so that to lowest order the solution is that of Alfvén waves) and rearranging factors:

$$\omega^+ = G^+\Omega^+ + g^+(G^+\Omega^+;\,G^-\Omega^-) + g^+[G^+\Omega^+;\,g^-(G^-\Omega^-;\,G^+\Omega^+)] + g^+[g^+(G^+\Omega^+;\,G^-\Omega^-);\,G^-\Omega^-] + \mathcal{O}(\Omega^4).$$

The algebra becomes lengthy (see Grappin (1986) for details), so we will concentrate only on a further simplification of the resulting equations for the $\omega^\pm$ vorticity, by looking at the dominant non-local terms in it; writing the non-linear kernel as:

$$M(\boldsymbol{k},\boldsymbol{p},\boldsymbol{q}) = \frac{k}{p}\,\sin\alpha\,\cos\gamma, \tag{7.9}$$

where α and γ are the angles $(\boldsymbol{p},\boldsymbol{q})$ and $(\boldsymbol{k},\boldsymbol{p})$, respectively, and denoting by a the extra expansion parameter which is the small ratio of two of the three wavenumbers in the interaction, three cases arise: when $q \ll k \sim p$ (here, $a = q/k$), then $\gamma \simeq 0$ and the kernel reduces to:

$$M(\boldsymbol{k},\boldsymbol{p},\boldsymbol{q}) \sim \frac{k}{q}\,\sin\alpha$$

and is of order a^{-1}; on the other hand, when $p \ll k \sim q$ (here, $a = p/k$), the kernel is of order unity, and when $k \ll p \sim q$ (here, $a = k/p$), the kernel is of order a^2. Therefore, if we neglect mode coupling between comparable scales, the resultant temporal evolution for scales of disparate sizes is that the small-scale $\omega^+(\boldsymbol{k})$ vorticity evolves mainly under the combined action of small-scale ω^+ and large-scale ω^- vortices, namely:

$$\left.\frac{\partial\omega^+(\boldsymbol{k})}{\partial t}\right|_{\mathrm{SS}} \simeq \omega^+(\boldsymbol{k})\,\omega^-_{\mathrm{LS}}\,, \tag{7.10}$$

where SS and LS stand, respectively, for small scale and large scale (on which we have averaged). Naturally, we can recover eq. (7.10) from a phenomenological argument and it is also obtained in the context of closures (Grappin et al. 1983). Suppose initially that on the large scales $E^+_{\mathrm{LS}} > E^-_{\mathrm{LS}}$, and suppose that on the small scales both $e^\pm$ are identically zero. Then:

$$\frac{\mathrm{d}e^\pm}{\mathrm{d}t} = \frac{k}{B_0}E^\mp e^\pm$$

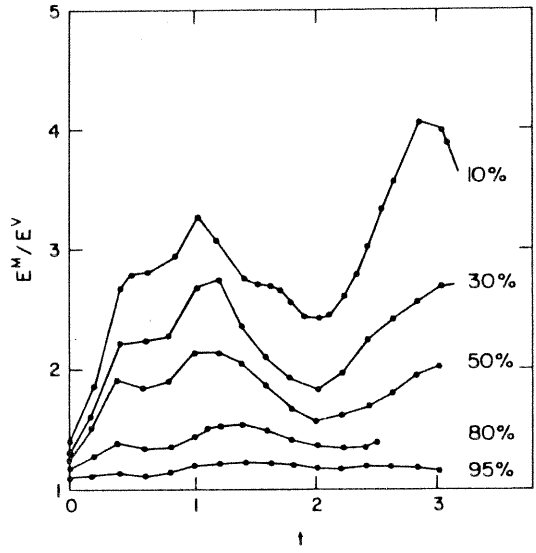

Fig. 17. Temporal evolution of the ratio of magnetic to kinetic energy for different initial correlations (Pouquet et al. 1986).

and e^- grows faster than e^+, so that correlation of the opposite sign (here negative) is created on the small scales by the non-linear interactions. This argument can be iterated and one thus constructs for short times a correlation spectrum with many lobes with alternating sign if initially it is narrowly peaked on the large scales.

There are now several numerical simulations that have shown that the correlation coefficient grows with time in two-dimensional flows (Léorat et al. 1982, Matthaeus and Montgomery 1984, Grappin 1986) as well as in three-dimensional flows (Pouquet et al. 1986), and they show a two-lobe structure (see below) in the correlation spectrum, with a change of sign at approximately the wavenumber at which dissipation sets in. When the correlations are strong, the non-linear transfer is inhibited, since its amplitude is greatly reduced relative to the uncorrelated case; this is visible, e.g., in fig. 17, in which is displayed as a function of time the ratio of magnetic to kinetic energy, E^M/E^V, for different initial correlations.

The unit of time is the eddy turn-over time of the large scale, also equal to the Alfvén time, ($E^M(t = 0) \simeq E^V(t = 0)$). When the correlation increases, the oscillations between E^M and E^V are strongly damped, but their characteristic frequency (corresponding to the rate of energy transfer, τ_{tr}^{-1}) is approximately the same.

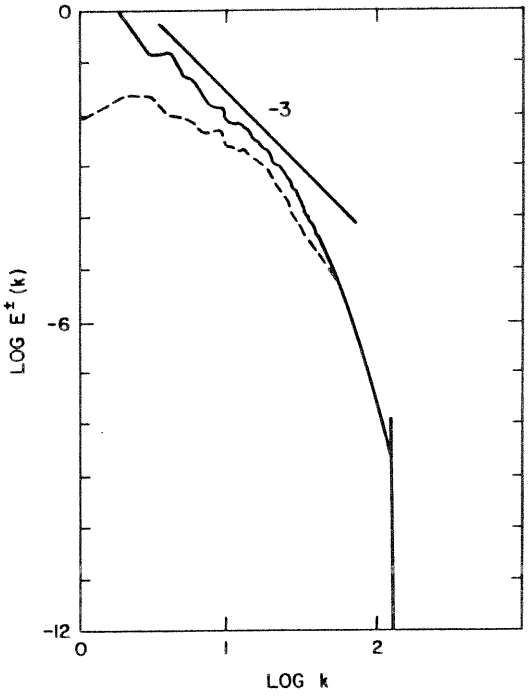

Fig. 18. $E^{\pm}(k)$ spectra at $t = 5\pi/2$, from a two-dimensional, direct, numerical simulation (Grappin 1986).

7.4. Lack of universality of the inertial ranges of correlated MHD flows

One may use numerical simulations to measure the inertial ranges that establish in correlated MHD flows. However, such problems require a high resolution, so that the eddy-containing range, the inertial range, and the dissipation range are reasonably well separated. Otherwise, each range is contaminated by the neighboring one, and in particular the inertial range is no longer a simple power-law. However, simple visual inspection of the spectra obtained in Grappin (1986) for a flow which is 80% correlated, initially clearly shows that the $E^{\pm}(k)$ spectra have different slopes.

Figure 18 is extracted from this paper and shows the spectra at $t = 5\pi/2$, with E^{-} the dotted line and E^{+} the solid line. The straight line drawn above the spectra has a -3 slope, and the results are clearly consistent with the prediction (7.5) for a strongly correlated flow: the $E^{-}(k)$ spectrum is flat for a small interval of wavenumbers.

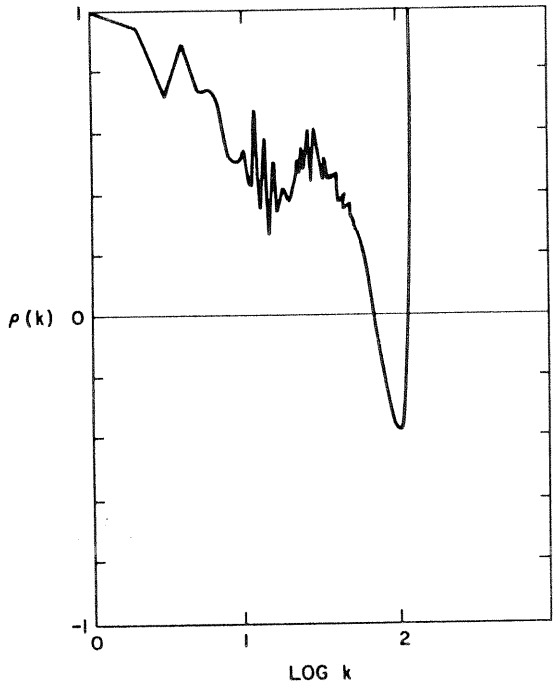

Fig. 19. $\rho(k)$, for the run as in fig. 18.

Figure 19 shows the correlation spectrum in lin–log coordinates, at the same time; it changes sign only once, around $k = 80$, in the dissipation part of the energy spectrum.

In order to get a systematic evaluation of the inertial indices, one may again resort to fitting the spectra with the functional form already mentioned in section 6.3, namely:

$$E(k,t) = C(t)\exp[-2\delta(t)k]\,k^{-m(t)},$$

for the constant $C(t)$, the logarithmic decrement $\delta(t)$, and the spectral indices $m(t)$. Here, we concentrate on the determination of $m^{\pm}(t)$ as a function of the initial correlation. The computations were performed on a Cray-1 with a uniform 512×512 grid and periodic boundary conditions. The code occupies more than three times the available memory of the central processor of the computer and thus makes heavy use of transfer of data between CPU and peripheral memory, only roughly 50% of it being used by computations. A typical run takes 20 h. The variation of the spectral indices with correlation is shown in fig. 20, for the m^+ (curve a) and m^- (curve b) indices as a function of ρ_C.

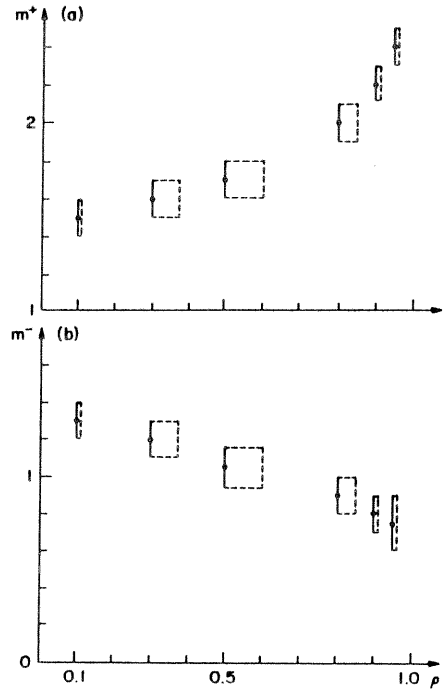

Fig. 20. Temporal evolution of the spectral indices $m^{\pm}(t)$ of the energy spectra $E^{\pm}(k)$, for a run with an initial correlation of 80% (Pouquet et al. 1988).

The horizontal extent of the curve represents the growth with time of the correlation coefficient. Thus these numerical 2D experiments (Pouquet et al. 1987) confirm the predictions of two-point closures of 3D MHD turbulence and of phenomenology on the variation of the spectral index of MHD flows with the amount of correlation between velocity and magnetic field, at least for this parameter regime ($P^{M} = 1$, $E^{M}/E^{V} = 1$). However, one should keep in mind that observations on the solar wind, where correlations are strong, seem consistent with a Kolmogorov spectrum; possibly they are taken at quiet times in the wind when MHD effects are damped? This point needs further investigation.

7.5. Selective decay

Restricting the discussion to two-dimensional flows, the simplest minimum-energy state is, when the correlation is conserved, $v = \pm b$, i.e. aligned equipartitioned fields with no constraint on scale, and when, on the other hand, the squared

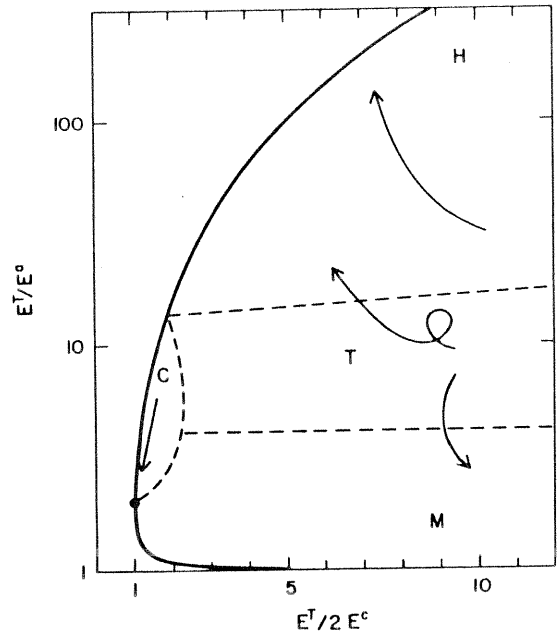

Fig. 21. Four regions of parameter space in two dimensions. H: hydrodynamic; M: magnetic; C: correlated; T: transitory (Ting et al. 1986).

magnetic potential is conserved, a zero-pressure ($v \equiv 0$) solution is obtained with the magnetic excitation concentrated in the largest scale available to the system. The general case, taking into account conservation of correlations. E^C, magnetic anastrophy, A^2, and of angular momentum (in the vertical direction), is given by eqs. (3.18) and (3.19). To determine to what state a given flow with random initial conditions evolves, one again can resort to numerical experimentation. Leaving aside angular momentum, the results (Ting et al. 1986) show that the long-time evolution seems to terminate on two branches in the $(E^T/A^2;\ 1/\rho_C)$ plane.

In fig. 21, redrawn from Ting et al. (1986), four regions of parameter space can be distinguished: region H (for hydro) corresponds to initial conditions with $v^2 \gg b^2$, and the ensuing evolution is one where the velocity field remains dominant throughout; similarly, region M (for magnetic) is one in which initially $b^2 \gg v^2$, which corresponds to regimes of magnetic confinement in the laboratory, and which terminates in a state where the magnetic potential is at the minimum wavenumber; region C (for correlated flows) is one in which v^2 and b^2 are of the same order of magnitude and the flow evolves towards a state of maximum correlation; finally, region T (for transitory behavior) is one in which sets of initial

conditions that are close in parameter space end up either in H or in M for reasons not determined, although they might be linked to the resolution.

Recalling that $j = -\nabla^2 a$ and using eq. (3.21) leads to, in Fourier space:

$$A(\boldsymbol{k}) = \delta(\boldsymbol{k} - \boldsymbol{k}_a), \tag{7.11a}$$

$$k_a^2 = \frac{\alpha}{1 - \beta^2}, \tag{7.11b}$$

except when $\beta^2 = 1$, in which case the fully correlated solution ($\boldsymbol{v} = \pm\boldsymbol{b}$) occurs. It follows that $\boldsymbol{b}(\boldsymbol{k}) = \mathrm{i}\boldsymbol{k}_a \times \boldsymbol{a}(\boldsymbol{k})$ and $\boldsymbol{v} = \beta\boldsymbol{b}$ both depend only on one the wavenumber, k_a. As shown in Ting et al. (1986), the wavenumber appearing in eq. (7.11) is not necessarily the minimum wavenumber of the truncated system (say $k_{\min} = 1$) in order to satisfy the minimal-energy condition. However, their numerical results seem to indicate that usually the system relaxes to a state dominated by $k_{\min}$, that is to say to a state not minimizing the energy. This may be an effect of numerical resolution; on the other hand, these states occur in the hydrodynamical regime (region H in fig. 21) and thus correspond to a minimum of the squared vorticity, keeping the energy constant, as is expected in order to explain the inverse cascade of energy in a two-dimensional, non-conducting, Navier–Stokes fluid.

The boundaries in the $(E^T/A^2;\ 1/\rho_C)$ plane can be found analytically (Ting et al. 1986) by simple manipulations of eqs. (3.21) and (7.11b). This yields:

$$\frac{E^T}{A^2} = 2\frac{k_a^2}{\rho_C^2}\left[1 \pm \left(1 - \rho_C^2\right)^{1/2}\right], \tag{7.12}$$

where the + (respectively −) sign corresponds to the upper (respectively lower) branch in fig. 21.

In the three-dimensional case, and dealing with high kinetic and magnetic Reynolds numbers, it is likely that the hydrodynamical region, H, will have a more limited extent because the dynamo can operate. Note also that taking into account the invariance of angular momentum breaks the force-free Beltramization of the flow, and more complex configurations may then arise. Angular momentum also plays a role in determining what size and energy of the topological configuration establish themselves, for given magnetic helicity (Kamchatnov 1982), as mentioned in section 4.

7.6. The emerging dynamical picture

We have given here a hopefully converging set of arguments that indicate that the likely equilibrium state of a 3D MHD fluid is one with large-scale, long-lived magnetic structures with maximal magnetic helicity, with possibly equipartitioned

velocity fields, or at least aligned; this equilibrium may not be magnetostatic, thus confirming the ideas of Parker on the dynamism and activity of magnetic fields in astrophysics. We arrived at this conclusion using statistical mechanics, by establishing topological constraints linked to the frozen-field condition (section 4.3 in the magnetostatic case, and section 4.5 for the Alfvén-type solution). Phenomenology indicates that the time-scale of the evolution of magnetic helicity indeed is slower than that of energy, and statistical closures, both numerically and analytically, show clear evidence of an inverse cascade of magnetic helicity; so does two-scale analysis. Experimental evidence in RFP and numerical evidence for the RFP and for homogeneous flows also indicate this self-ordering of MHD flows.

These results were obtained for the most part in the incompressible domain. But in fact they may well apply too in the compressible case, since the detailed equation of state, linking pressure and temperature, does not affect the frozen-in condition for the magnetic field. Hence large-scale helical entities may well form too, with small-scale structures now dominated by shocks. In fact, analytical results for the non-magnetic case using the diffusion approximation for the short correlation time of the small-scale turbulence, indicate that large-scale compressible flows are helically unstable (Moiseev et al. 1982). This result is presently being extended to the MHD case. In the interstellar medium, molecular clouds are the site of star formation, and these are known to be turbulent, with a scaling law in the inertial range between the Kolmogorov value of $-\frac{5}{3}$ and the shock-like value of -2 (Larson 1981, Perrault 1987). Moreover, magnetic fields are dynamically important (Heiles 1987, Scalo 1985). Is there any way to see whether large scales are helical?

The next step, aside from ample numerical exploration of parameter space, may be in the hand of astrophysicists, and in particular those able to derive multiple-scale information with instrumentation with a large dynamical range. This is the case for radio jets, thanks to VLA in particular, and evidently this is also the case with the Sun: can one determine, either at the photospheric level or in the loops of the corona, the three-dimensional nature of the fields? This is one of the fascinating results that may emerge in the next decade by sophisticated ground-based and airborne instrumentation.

7.7. Conclusion

Magnetic phenomena occur in many instances of astrophysical interest. For example, the Fermi acceleration of particles in magnetized shocks, the transfer of angular momentum and magnetic breaking of stars, the stochasticity of magnetic surfaces due to the underlying Hamiltonian structure, the interaction of a magnetic field with either rotation or convection, and all phenomena associated with reconnection, in particular solar flares and heating of the corona, have all been but

briefly mentioned at best. It is hoped that enough energy is left to the reader to at least browse through the various books and review papers that exist on these topics; a few of them are given in the list of references.

Finally, it is worth mentioning that with the advent of ever-larger computers, the "experiment via numerics" approach to MHD turbulence – unique and yet very expensive – will probably grow. Databases with some basic flows, stored on optical disks, are likely to be made available to the community of researchers for the most demanding computations, with the hope that the numerous parameters (R^{V}, R^{M}, P^{M}, M_{a}, β, P, R_{a}, ...) will be sufficiently representative of the problems at hand. Visualization of such flows with sophisticated equipment (large storage, rapid access to disk, on line manipulation of the 3D image, rotation, zooming, different perspective, bit shift, oblique sections, and also access to the temporal dimension, which gives an idea of the dynamical evolution of structures – how do they arise, how do they interact and possibly merge, where are the dissipative structures concentrated – and naturally color coding, to name a few requirements) is of primary importance and yet not widely available today. It is to be hoped that, as e.g. for dynamical systems and the discovery of chaos, and for one-dimensional flows and the understanding of solitons, such numerical experiments will help unravel the underlying structure of MHD turbulence, the description of which remains, somewhat frustrating, in the domain of phenomenology, and will help suggest the proper way to model the intricate and fascinating flows that arise in astrophysical and geophysical fluids.

Acknowledgements

I am thankful to Jean-Paul Zahn for having invited me to give these lectures. Part of the pleasure I took in preparing them came from using a database with the relevant literature, a subset of which is quoted here. This database has been developed by John S. Davis, it was a tremendous help.

Several persons have participated in the typing and editing of this text, on both sides of the Atlantic, and did a great job; so did the NCAR graphics group with my sketches.

R. Beck, R. Perley and Y. Sofue have kindly provided me with reproductions of their observations; they certainly are inspiring. In several sections of these lectures, I have drawn from published works, in particular from those of M. Berger, R. Grappin, A. Königl, H.K. Moffatt and M. Woltjer; and I hope my interpretations have not betrayed the intentions of the authors. In many places I have also used portions of works done in collaboration over the years with U. Frisch, A. Gilbert, C. Gloaguen, R. Grappin, J. Léorat, M. Meneguzzi, Th. Passot, G.S. Patterson and P.L. Sulem. May they be thanked here.

B.C. Low had the grueling job of reading this manuscript; his patience and co-operation are greatly appreciated.

Finally, I wish to express my gratitude to Andrew Gilbert, Thierry Passot and Pierre-Louis Sulem for their encouragement during this past year.

References

Ablowitz, M.J., A. Ramani and H. Segur, 1980, J. Math. Phys. **21**, 7.
Acheson, D.J. and R. Hide, 1973, Rep. Prog. Phys. **36**, 159.
Arnold, V.I., 1965, C. R. Acad. Sci. **261**, 17.
Atten, P., J.G. Caputo, B. Malraison and Y. Gagne, 1986, Preprint Laboratoire d' Electrostatique, 166x, 38042, Grenoble.
Bardos, C., C. Sulem and P.L. Sulem, 1987, preprint, Université Paris VII.
Beck, R., 1986, IEEE Trans. Plasma Sci. **14**, 740.
Belcher, J.W. and L. Davis, 1971, J. Geophys. Res. **76**, 3534.
Berger, M.A., 1984, Geophys. Astrophys. Fluid Dyn. **30**, 79.
Berger, M.A., 1987, Proc. Beer–Sheva Meeting, Jerusalem (ed. Branover).
Berger, M.A. and G. Field, 1984, J. Fluid Mech. **147**, 133.
Campos, L.M.B., 1987, Rev. Mod. Phys. **59**, 363.
Carrier, G.F., M. Krook and C.E. Pearson, 1966, Functions of a Complex Variable (McGraw-Hill, New York).
Chandrasekhar, S., 1956, Proc. Nat. Acad. Sci. U.S.A. **42**, 1.
Chandrasekhar, S., 1961, Hydrodynamic and Hydromagnetic Stability (Dover, New York).
Chen, H. and D. Montgomery, 1987, Plasma Phys. Controlled Fusion **29**, 205.
Chollet, J.-P. and M. Lesieur, 1981, J. Atmos. Sci. **38**, 2747.
Choudhuri, A.R. and A. Königl, 1986, Astrophys. J. **310**, 96.
Cram, L.E., 1983, IAU Symposium **102** (ed. J.O. Stenflo).
Crowell, R.H. and R.H. Fox, 1963, Introduction to Knot Theory (Springer).
Dahlburg, J.-P., D. Montgomery, G.O. Doolen and L. Turner, 1986, Phys. Rev. Lett. **57**, 428.
De Dominicis, C. and P.C. Martin, 1979, Phys. Rev. **A19**, 419.
Denianski, V.N. and E.A. Novikov, 1974, Prikl. Nat. Mech. **38**, 507.
Dobrovolny, M., A. Mangeney and P.-L. Veltri, 1980, Phys. Rev. Lett. **45**, 144.
Dombre, T., U. Frisch, J.M. Greene, M. Hénon, A. Mehr and A.M. Soward, 1986, J. Fluid Mech. **167**, 353.
Drury, C., 1987, Proc. Cargèse Workshop on Extragalactic Magnetic Fields (eds. E. Asseo, M. Dubois and R. Grésillon).
Elsässer, W.M., 1950, Phys. Rev. **79**, 183.
Elsässer, W.M., 1956, Rev. Mod. Phys. **28**, 135.
Fitremann, M. and U. Frisch, 1969, C. R. Acad. Sci., Série A **268**, 705.
Forster, D., D.R. Nelson and M.J. Stephen, 1976, Phys. Rev. Lett. **36**, 867.
Fournier, J.-D., 1983, Thèse d' Etat, Université de Nice.
Fournier, J.-D. and U. Frisch, 1978, Phys. Rev. **A17**, 747.
Fournier, J.-D., P.L. Sulem and A. Pouquet, 1982, J. Phys. **A15**, 1393.
Frank-Kamenetski, M.D. and A.V. Vologodski, 1981, Sov. Phys. Usp. **24**, 679.
Frisch, U., M. Lesieur and A. Brissaud, 1974, J. Fluid Mech. **65**, 145.
Frisch, U. and R. Morf, 1981, Phys. Rev. A. **23**, 2673.
Frisch, U., A. Pouquet, P.-L. Sulem and M. Meneguzzi, 1983, J. Mécanique Théor. Appliquée **2D**, 191.

Frisch, U., Z.S. She and P.L. Sulem, 1987, Physica **D 28**, 382.
Furth, H.P., J. Killeen and M.N. Rosenbluth, 1963, Phys. Fluids **6**, 459.
Fyfe, D. and D. Montgomery, 1976, J. Plasma Phys. **16**, 181.
Gaffet, B., 1985, J. Fluid Mech. **156**, 141.
Galloway, D. and U. Frisch, 1984, Geophys. Astrophys. Fluid Dyn. **29**, 13.
Galloway, D. and U. Frisch, 1986, Geophys. Astrophys. Fluid Dyn. **36**, 53.
Galloway, D. and U. Frisch, 1987, J. Fluid Mech. **180**, 557.
Gardner, F.F. and J.B. Whiteoak 1966, Annual Review Astron. Astrophys. **4**, 245.
Gilbert, A., U. Frisch and A. Pouquet, 1987, Geophys. Astrophys. Fluid Dyn. **42**, 151.
Gloaguen, C., 1983, Thèse de Troisième cycle Université Paris VII.
Gloaguen, C., J. Léorat, A. Pouquet and R. Grappin, 1985, Physica **17D**, 154.
Grappin, R., 1986, Phys. Fluids **29**, 2433.
Grappin, R., A. Pouquet and J. Léorat, 1983, Astron. Astrophys. **126**, 51.
Grappin, R., J. Léorat and A. Pouquet, 1986, J. Phys. **47**, 1127.
Grappin, R. and J. Léorat, 1987, Phys. Rev. Lett. **59**, 1100.
Grassberger, P. and I. Procaccia, 1983, Phys. Rev. Lett. **50**, 346.
Hameiri, E. and J.H. Hammer, 1982, Phys. Fluids **25**, 1855.
Hasegawa, A., 1985, Adv. Phys. **34**, 1.
Heiles, C., 1987, Summer School on Interstellar Processes Jackson Hole, Wyoming.
Hénon, M., 1966, C. R. Acad. Sci. **262**, 312.
Heyvaerts, J. and E.R. Priest, 1984, Astron. Astrophys. **137**, 63.
Hill, M.J.M., 1894, Phil. Trans. Roy. Soc. **A 185**, 213.
Hide, R., 1983, Ann. Geophys. **1**, 59.
Hoyng, P., 1987, Astron. Astrophys. **171**, 357.
Iroshnikov, P.S., 1963, Astron. J. SSSR **40**, 742; Soviet Astron. **7**, 566.
Jeffrey, A. and T. Taniuti, 1964, Nonlinear Wave Propagation (Academic Press, New York).
Jones, C.A., N.O. Weiss and F. Cattaneo, 1985, Physica **D14**, 161.
Jones, V., 1986, Science **231**, 1506.
Kamchatnov, A.M., 1982, Sov. Phys. JETP **55**, 69.
Kaplan, J.-L. and J.-A. Yorke, 1979, Lecture Notes in Mathematics, **730**, 228 (eds. Dietten and Walther; Springer).
Kerr, R.M. and E.D. Siggia, 1978, J. Stat. Phys. **19**, 543.
Kida, S. and M. Takaoka, 1987, Phys. Fluids Lett. **30**, 2911.
Königl, A. and A.R. Choudhuri, 1985, Astrophys. J. **289**, 173.
Königl, A., 1987, Proc. Cargèse Workshop on Extragalactic Magnetic Fields (eds. E. Asseo, M. Dubois and R. Grésillon).
Kraichnan, R.H., 1965, Phys. Fluids **8**, 1385.
Kraichnan, R.H. and S. Nagarajan, 1967, Phys. Fluids **10**, 859.
Kraichnan, R.H. and D. Montgomery, 1980, Rep. Prog. Phys. **43**, 547.
Krause, F. and G. Rüdiger, 1974, Astron. Nachr. **295**, 93.
Krause, F. and G. Rüdiger, 1975, Solar Phys. **42**, 107.
Krause, F. and K.H. Rädler, 1980, Mean-Field Magnetohydrodynamics and Dynamo Theory (Akademie-Verlag, Berlin).
Kumar, P. 1987, PhD Thesis, California Institute of Technology.
Landau, L.D. and E.N. Lifshitz, 1959, Fluid Dynamics (Pergamon Press).
Larson, R.B., 1981, Monthly Not. Roy. Astron. Soc. **194**, 809.
Léorat, J., R. Grappin, A. Pouquet and U. Frisch, 1982, J. Geophys. Astrophys. Fluid Dyn. **2**, 69.
Lerche, I., 1971, Astrophys. J. **166**, 627 and 639.
Lighthill, M.J., 1954, Proc. Roy. Soc. London **A222**, 1.

Low, B.C., 1988a, b. Preprint, HAO, NCAR.
Lundquist, S., 1952, Arkiv. Fys. **5**, 297.
Ma, S. and G.F. Mazenko, 1975, Phys. Rev. **B 11**, 4077.
Mandelbrot, B., 1974, J. Fluid Mech. **62**, 381.
Marcy, G.W., 1983, Solar and Stellar Magnetic Fields, IAU coll. 102 (ed. J.O. Stenflo), 3.
Matthaeus, W.H., 1982, J. Geophys. Res. Lett. **9**, 660.
Matthaeus, W.H. and D. Montgomery, 1980, Ann. N.Y. Acad. Sci. **357**, 203.
Matthaeus, W.H. and M.L. Goldstein, 1982, J. Geophys. Res. **87A**, 6011.
Matthaeus, W.H., M.L. Goldstein and D. Montgomery, 1983, Phys. Rev. Lett. **51**, 1484.
Matthaeus, W.H. and D. Montgomery, 1984, Statistical Physics and Chaos in Fusion Plasmas (eds. C.W. Horton and L.E. Reichl: Wiley, New York), 285.
Matthaeus, W.H. and S. Lamkin, 1986, Phys. Fluids **29**, 2513.
Meneguzzi, M., U. Frisch and A. Pouquet, 1981, Phys. Rev. Lett. **47**, 1060.
Mestel, L., 1983, Protostars and Planets II (eds. D.C. Black and M.S. Matthews; Univ. of Arizona Press).
Moffatt, K.H., 1969, J. Fluid Mech. **35**, 117.
Moffatt, K.H., 1978, Magnetic Field Generation in Electrically Conducting Fluids (Cambridge University Press).
Moffatt, K.H., 1985, J. Fluid Mech. **159**, 359.
Moffatt, K.H., 1986, J. Fluid Mech. **173**, 289.
Moiseev, S.S., R.Z. Sagdeev, A.V. Tur and V.V Yanovski, 1982, Sov. Phys. JETP **56**, 117.
Moiseev, S.S., R.Z. Sagdeev, A.V. Tur, G.A. Khomenko and V.V. Yanovski, 1983, Sov. Phys. JETP **58**, 1149.
Montgomery, D., 1985, Maximum Entropy and Bayesian Methods in Inverse Problems (eds. C.R. Smith and W.T. Grandy Jr.; Reidel), 455.
Montgomery, D., L. Turner and G. Vahala, 1979, J. Plasma Phys. **21**, 239.
Montmerle, T., L. Koch-Miramond, E. Falgarone and J. Grindlay, 1983, Astrophys. J. **269**, 182.
Mouschovias, T. Ch., 1980, IAU Symposium 93 (eds. D. Sugimoto, D.Q. Lamb and D.N. Schramm; Reidel).
Neuwirth, L., 1979, Scient. American, June, p. 84.
Nocera, L., E. Priest and J.V. Hollweg, 1986, Geophys. Astrophys. Fluid Dyn. **35**, 111.
Norman, C.A. and J. Heyvaerts, 1983, Astron. Astrophys. **124**, L1.
Obukhov, A.M., 1971, Izv. Akad. Nauk SSSR, Fiz. Atm. Okeana **7**, 471.
Onsager, L., 1949, Nuovo Cimento Suppl. **6**, 279.
Orszag, S.A., 1977, Les Houches Summer School (eds. J.L. Peube and R. Balian; Gordon and Breach).
Orszag, S.A. and C.M. Tang, 1979, J. Fluid Mech. **90**, 129.
Parker, E.N., 1979, Cosmical Magnetic Fields (Clarendon Press).
Passot, Th., 1987, Thèse, Université Paris VII.
Perley, R., 1987, Proc. Cargèse Workshop on Extragalactic Magnetic Fields (eds. E. Asseo, M. Dubois and R. Grésillon).
Perrault, M., 1987, Thèse d'Etat, Université Paris VII.
Polyakov, A. M., 1974, Sov. Phys. JETP Letters **20**, 194.
Pouquet, A., 1984, Statistical Methods in Turbulence, Langley Research Workshop (Springer-Verlag), Applied Math. Sci. **58**, 209.
Pouquet, A., U. Frisch and J. Léorat, 1976, J. Fluid Mech. **77**, 321.
Pouquet, A. and G.S. Patterson, 1978, J. Fluid Mech. **85**, 305.
Pouquet, A., J.D. Fournier and P.L. Sulem, 1978, J. Phys. Lettres **39**, 1199.
Pouquet, A., U. Frisch and M. Meneguzzi, 1986, Phys. Rev. **A33**, 4266.
Pouquet, A., P.L. Sulem and M. Meneguzzi, 1988, Phys. Fluids, **31**, 2635.

Prendergast, K., 1957, Astrophys. J. **123**, 498.
Priest, E.R., 1982, Solar Magnetohydrodynamics (Reidel; Dordrecht).
Reidel, K.H., 1986, Phys. Fluids **29**, 1093.
Roberts, B., 1984, 6th General Conf. European Phys. Soc., Prague.
Roberts, P.H., 1967, An Introduction to Magnetohydrodynamics (Longsman).
Sagdeev R.Z., S.S. Moiseev, A.V. Tur and V.V. Yanovski, 1986, Non Linear Phenomena in Plasma Physics and Hydrodynamics **6**, 137, (ed. R.Z. Sagdeev; Mir, Moscow).
Scalo, J.M., 1985, Protostars and Planets II (eds. D.C. Black and M.S. Mattews; U. of Arizona Press).
Shercliff, J.A., 1979, Liquid Metal Flows Beer-Sheva Meeting **2**, 3, (eds. F. Branover and A. Yakhot).
Siggia, E., 1985, Phys. Fluids **28**, 1985.
Smith C.W., M.L. Goldstein and W.H. Matthaeus, 1983, J. Geophys. Res. **88**, 5581.
Sofue Y., M. Fujimoto and R. Wielebinski, 1986, Ann. Rev. Astron. Astrophys. **24**, 459.
Spitzer, L., 1962, Physics of Fully-Ionised Gases (Interscience, New York).
Spruit, H.C., 1983, Max Planck Institut Report **96** "Magnetic Activity of Stars: Theoretical Aspects".
Steenbeck, M., F. Krause and K.-H. Rädler, 1966, Z. Naturforsch. **21 a**, 369.
Stenzel, R.L., W. Gekelman and N. Wild, 1983, J. Geophys. Res. **88**, 1245.
Strauss, H.R., 1976, Phys. Fluids **19**, 134.
Sulem, P.L., 1986, Ecole de Goutelas (eds. A. Baglin and M. Auvergne).
Sulem, P.L., J.D. Fournier and A. Pouquet, 1979, Lecture Notes in Physics **104**, 321, (ed. C.P. Enz; Springer- Verlag).
Sulem, P.L., U. Frisch, A. Pouquet and M. Meneguzzi, 1985, J. Plasma Phys. **33**, 191.
Taylor, J.B., 1974, Phys. Rev. Lett. **33**, 1139.
Taylor, J.B., 1986, Rev. Mod. Phys. **58**, 741.
Thomas, J.H., 1968, Phys. Fluids **11**, 1245.
't Hooft, G., 1974, Nucl. Phys. **B 79**, 276.
Ting, A.C., W.H. Matthaeus and D. Montgomery, 1986, Phys. Fluids **29**, 3261.
Trotter, H.F., 1963, Topology **2**, 341.
Tsinganos, K.C., 1981, Astrophys. J. **245**, 764.
Tsinganos, K.C., 1982a, Astrophys. J. **252**, 775.
Tsinganos, K.C., 1982b, Astrophys. J. **259**, 820.
Tsinganos, K.C., 1982c, Astrophys. J. **259**, 832.
Tsinganos, K.C., J. Distler and R. Rosner, 1984, Astrophys. J. **278**, 409.
Turner, L. and J.P. Christiansen, 1981, Phys. Fluids **24**, 893.
Vainshtein, S.A., 1982, Sov. Phys. JETP **56**, 86.
Vainshtein, S.A. and Ya. Zeldovich, 1982, Sov. Phys. JETP **56**, 86.
Van Kampen, N.G. and B.U. Felderhof, 1967, Theoretical Methods in Plasma Physics (North-Holland, Amsterdam).
Veltri, P.L., A. Mangeney and M. Dobrovolny, 1982, Il Nuovo Cimento, **68**, 235.
Voslamber D. and D.K. Callebaut, 1962, Phys. Rev. **128**, 2016.
Weiss, J., M. Tabor and G. Carnavale, 1983, J. Math. Phys. **24**, 522.
Wilson, O.C., 1978, Astrophys. J. **226**, 379.
Wolibner, W., 1933, Math. Z. **37**, 668.
Woltjer L., 1958, Proc. Nat. Acad. Sci. **44**, 833.
Wu, C.C., 1987, Geophys. Res. Lett. **14**, 668.
Yoshizawa, A., 1985, Phys. Fluids **28**, 3313.
Yoshizawa, A., 1987, Phys. Fluids **30**, 1089.
Zabusky, N.J., 1981, J. Comp. Phys. **43**, 195.
Zeldovich, Ya, A.A. Ruzmaikin and D.D. Sokolov, 1983, Magnetic Fields in Astrophysics (Gordon and Breach, New York).